Earth-Science Reviews 236 (2023) 104242

Contents lists available at ScienceDirect

Earth-Science Reviews

journal homepage: www.elsevier.com/locate/earscirev

Back-arc basins: A global view from geophysical synthesis and analysis

Irina M. Artemieva [a,b,c,*]

[a] SinoProbe Laboratory, China Academy of Geological Sciences, Beijing 100037, China
[b] State Key Laboratory GPMR, School of Earth Sciences, China University of Geosciences, Wuhan 430074, China
[c] Section of Marine Geodynamics, GEOMAR Helmholtz Center for Ocean Research, Kiel 24148, Germany

ARTICLE INFO

Keywords:
Subduction
Lithosphere extension
Isostasy
Buoyancy
Crustal thickness
Magmatic underplating
Lower crust
Heat flow
Cooling plate model
Slab dip

ABSTRACT

This global study of 31 off-shore back-arc basins and subbasins (BABs) identifies their principal characteristics based on a broad spectrum of geophysical and subduction-related parameters. My synthesis is used to identify trends in the evolution of back-arc basins for improving our understanding of subduction systems in general. The analysis, based on the present plate configuration, demonstrates that geophysical characteristics and fate of the back-arc basins are essentially controlled by the tectonic type of the overriding plate, which controls the lithosphere thermo-compositional structure and rheology. The type of the plate governs the length of the extensional zone in back-arc settings along the trench, the efficiency of lithosphere stretching, and the crustal structure, buoyancy and bathymetry of the BABs. Subduction dip angle apparently controls the location of the slab melting zone and the efficiency of slab roll-back with feedback links to other parameters. By the tectonic nature of the overriding plate (the downgoing plate is always oceanic) the back-arc basins are split into active BABs formed by ocean-ocean, arc-ocean, and continent-ocean convergence, and extinct back-arc basins. By geophysical characteristics, BABs formed on continental plates are subdivided into active BABs with and without seafloor spreading, and extinct BABs are subdivided into the Pacific BABs, possibly formed on oceanic plates, and the non-Pacific BABs with reworked continental or arc fragments.

Six types of BABs are distinctly different. Extension of the overriding oceanic plate above a steeply dipping old oceanic plate, preferentially subducting nearly westwards, forms large deep back-arc basins with a thin oceanic-type crust. In contrast, BABs on the overriding continental or arc plates form at small opening rates and often by shallow subduction of younger oceanic plates with a random subduction orientation; these BABs have small sizes, shallow bathymetry, and hyperextended or transitional ~20 km thick arc- or continental-type crust typical of passive margins. The presence of a 2–5 km thick high-Vp lowermost crustal layer, characteristic of BABs in all settings, indicates the importance of magmatic underplating in the crustal growth.

Conditions required for the initiation of a back-arc basin and transition from stretching to seafloor opening depend on the nature of the overriding plate. BABs formed on oceanic plates always evolve to seafloor spreading. BABs formed on continental or arc plates require long spreading duration with large (>8 cm/y) opening rates and a large crustal thinning factor of 2.8–5.0 to progress from crustal extension to seafloor spreading. On the present Earth such transition does not happen in the back-arc basins formed behind a shallow subduction (<45°) of a young (<40 My) oceanic plate.

The nature of the overriding plate also determines the fate of back-arc basins after termination of lithosphere extension: the extinct Pacific back-arc basins with oceanic-type crust evolve towards deep old "normal" oceans, while the shallow non-Pacific BABs with low heat flow and thick crust are likely to preserve their continental or arc affinity. BABs do not follow the oceanic cooling plate model predictions. Distinctly different geophysical signatures for mid-ocean ridge spreading and for back-arc seafloor spreading are caused by principally different dynamics.

* Corresponding author at: State Key Laboratory GPMR, School of Earth Sciences, China University of Geosciences, Wuhan 430074, China.
E-mail address: iartemieva@geomar.de.

https://doi.org/10.1016/j.earscirev.2022.104242
Received 31 July 2022; Received in revised form 15 October 2022; Accepted 31 October 2022
Available online 15 November 2022

1. Introduction

The concept of back-arc basins (BABs) was originally proposed to describe geodynamics of marginal seas with active seafloor spreading behind subduction systems of the western Pacific (Karig, 1971). Later, back-arc basins were also recognized in the Indian ocean, the Atlantic ocean, in the Mediterranean Sea, and also in on-shore settings behind subduction zones. This review excludes on-shore BABs, and focuses only on the back-arc basins of the marginal seas (Fig. 1).

Back-arc basins form by lithosphere extension which may, or may not, lead to seafloor spreading. In this regard, there is certain similarity between back-arc extension and rifting which also may, or may not, initiate seafloor spreading. However, the geodynamic framework of continental rifting and back-arc extension is different because of a spatially limited length of extension zone in back-arc basins, controlled by the length of a subduction system and its part where back-arc basins develop. In contrast to the rift-to-drift mechanism, back-arc seafloor spreading apparently has never produced a new ocean (i.e. a global-scale marine basin split by a major plate tectonic boundary, in contrast to a limited-size oceanic microplate (Li et al., 2018)).

By the definition of a back-arc (Karig, 1971), *subduction is a necessary condition* for its identification, since a back-arc basin is defined as "any basin with seafloor spreading that forms over an active subduction zone" (Stern and Dickinson, 2010). Near-coastal ocean basins without subduction are termed marginal seas. However, *subduction is not a sufficient condition* for back-arc extension: there are subduction systems without associated back-arc basins and there are back-arc basins where back-arc extension ceased while subduction continued. Therefore, geodynamic links and casual relationships between subduction and back-arc extension remain controversial. The mechanisms of lithosphere extension in back-arc basins are not a part of the back-arc definition. Thus mechanisms with a subordinate (or no) role of subduction in back-arc extension were proposed for some back-arc basins formed behind subductions systems (Fig. 2g-i).

The most commonly proposed mechanism is slab roll-back. In this model, the vector sum of subducting slab pull and gravity force creates trench retreat (Fig. 2a). The overriding plate passively follows the retreating trench, thus producing passive lithosphere extension, which commonly occurs on the overriding plate behind the arc, where the back-arc basin forms. The process may also split the arc into extinct and active arc segments (Karig, 1974; Molnar and Atwater, 1978). In such cases, typically both the trench and the active arc segment will move towards the incoming plate (Allen et al., 2019); in rare cases (more common in continent-ocean subductions) arc migration may occur in both directions (Yang et al., 1996). Lithosphere rupture with onset of seafloor spreading may occur not only behind the magmatic arc, or along the magmatic arc, but it can also occur in front (trenchward) of the magmatic arc (Martinez and Taylor, 2006). Localization of lithosphere extension is primarily controlled by its rheology which, in turn, is strongly controlled by temperature and hydration (Kohlstedt et al., 1995). The weakest part of the lithosphere is expected to be above the region of melt generation (Van Keken et al., 2002), which in subduction settings is typically at depths of 65–170 km with a global average of around 100 km depth (cf. Mibe et al., 2011). This observation has led to a number of attempts to link the location of the spreading axis in back-arc basins to subduction dip angle. However, in the Mariana Trough and the East Scotia back-arc basins the axial parts of seafloor opening lie beyond the deepest limit of the seismogenic zone, interpreted as the slab (e.g. Taylor and Karner, 1983). Statistical analysis based on paleo-reconstructions suggests that subduction of an old, dense oceanic lithosphere with an age of >55 Ma may be important for formation of back-arc basins by slab roll-back (Sdrolias and Mueller, 2006), since the process is driven by the negative buoyancy of the subducting slab (slab pull) with respect to the underlying asthenosphere (Molnar and Atwater, 1978).

An alternative mechanism for back-arc extension assumes that a trench is stationary in an absolute reference frame and the associated slab is deeply anchored (Uyeda and Kanamori, 1979; Scholz and Campos, 1995). The overriding plate is being stretched if it moves landward (Fig. 2b) leading to formation of a back-arc basin. The mechanism was proposed to explain the extension in the Mariana Trough by subduction of the Philippine Sea Plate beneath the Philippines (Uyeda and Kanamori, 1979; Stern et al., 2003), while it has been recognized that the Mariana Trench is advancing (Carlson and Mortera-Gutiérrez, 1990) and thus the associated slab is not fully anchored.

Models of back-arc extension associated with an eastward horizontal

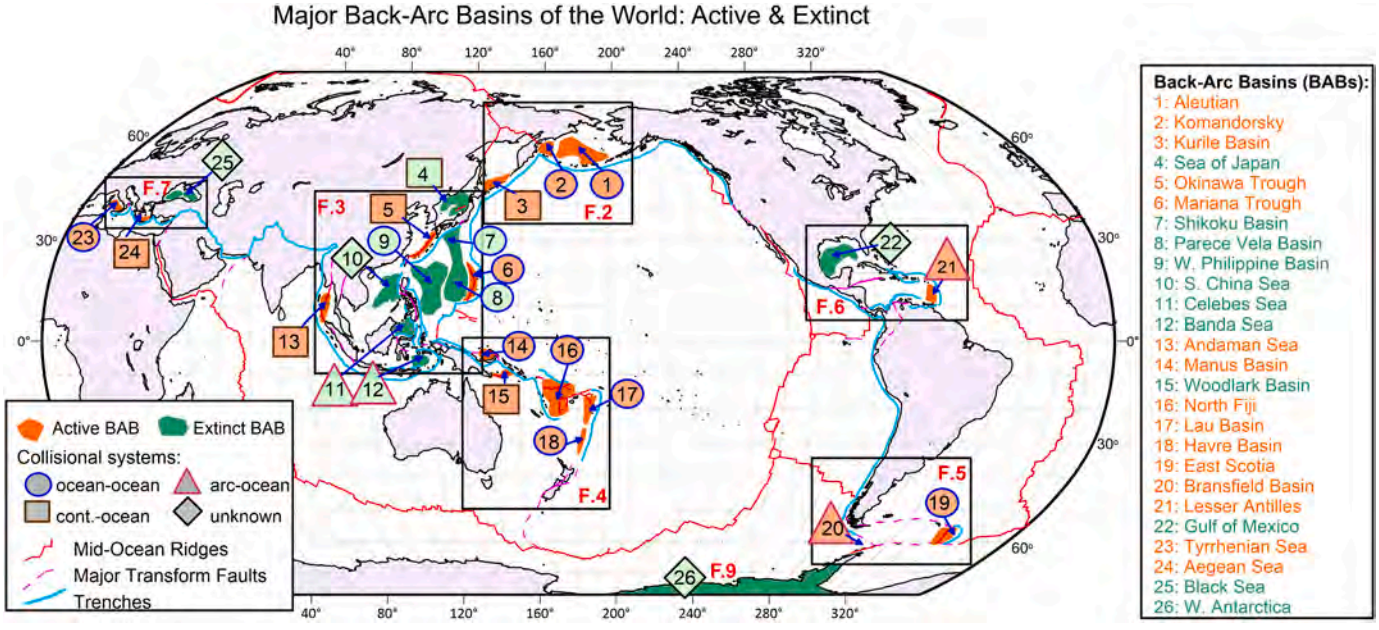

Fig. 1. Off-shore back-arc basins (BABs) included into the present overview. Seven regions are zoomed in Figs. 3-9. BABs numbers 1 to 26 are used in all other figures. See Section 2 and Table 1 for details. Active BABs are marked in orange and extinct BABs in green. Active BABs are further split into 3 types by the tectonic origin of converging plates (ocean-ocean, arc-ocean, and continent-ocean convergence).

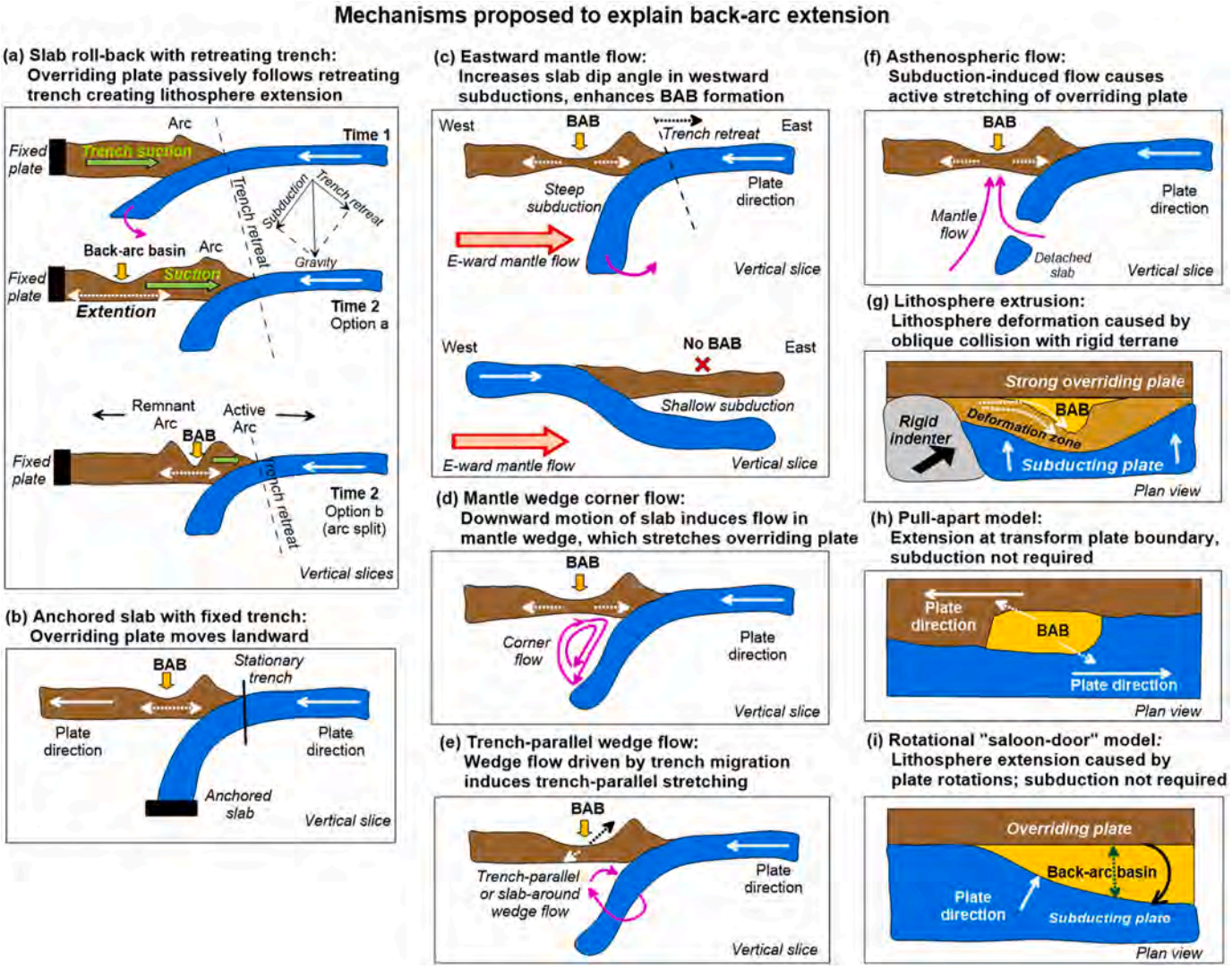

Fig. 2. Mechanisms proposed to explain back-arc extension. See text (Introduction) for discussion and references.

mantle "wind" (Fig. 2c), i.e. the westward drift of lithospheric plates with respect to the mantle (Uyeda and Kanamori, 1979; O'Connell and Hager, 1991; Ricard et al., 1991), make an independent group. In these models, supported by numerical modeling (Ficini et al., 2017) but still controversial (Schellart, 2007), back-arc basins form in case of west-dipping, steep and even near-vertical, subductions and lithosphere extension is associated with slab roll-back and eastwards migration of the slab hinge as it has been proposed for the Tyrrhenian Sea (Doglioni, 1991). In case of east-directed slabs, mantle flow would promote slab shallowing and hamper lithosphere stretching thus precluding formation of a back-arc basin (Doglioni et al., 2009; Ficini et al., 2017).

A separate class of models assumes an active role of mantle flow in back-arc extension (Fig. 2def), by analogy with the concept of active versus passive rifting in the sense of Sengör and Burke (1978). These models of active spreading explain lithosphere extension either by asthenosphere upwelling caused by slab subduction (Karig, 1971) or by secondary convection in the mantle wedge above a slab (Sleep and Toksöz, 1971; Billen and Gurnis, 2001; Kneller and van Keken, *2008*; Wirth and Korenaga, 2012; Lee and Wada, 2017). The uprising mantle flow which drags the bottom of the overriding plate seawards produces tensile deformation in the overriding plate and the consequent formation of a back-arc basin (Fig. 2d). Corner flow in mantle wedge (Fig. 2e) forms because subducting slab causes downward motion of mantle material, and coupling between mantle and slab material is important for the wedge flow dynamics (Shemenda, 1993). However, numerical models show that the expected velocities of mantle flow are inconsistent with the observed subduction rates, for example in the Mediterranean back-arc basins (Davies and Stevenson, 1992). A modified version of this model based on an analysis of seismic anisotropy styles in subduction systems (e.g. Long and Wirth, 2013) involves a trench-parallel or around-slab wedge flow (Fig. 2f), possibly caused by slab migration, which can create along-strike pressure gradients (Conder and Wiens, 2007) and induce local trench-parallel stretching in the mantle wedge for obliquely subducting slabs with complex shapes (Kneller and van Keken, 2008).

Several alternative models do not involve subduction as a primary mechanism of back-arc extension. The extrusion model (Fig. 2g) explains lithosphere deformation and extension along a convergent plate boundary by interaction of the incoming plate with a buoyant rigid lithospheric block (Tapponnier, 1977; Uyeda, 1986). This interaction may lead to deformation of the accretionary belt with its partial separation from the overriding plate (Fig. 2g). The mechanism, tested by analogue experiments (Fournier et al., 2004), was proposed to explain the Mediterranean back-arc basins (Mantovani et al., 2001). Two alternative mechanisms, where lithosphere extension does not result from subduction, were proposed to explain the back-arc basins of the Sea of Japan (Fig. 2 hi). They include a pull-apart extension along a transform plate boundary with a step-over release of deformation (Jolivet

et al., 1994) and lithosphere stretching by plate rotation (sometimes called a "saloon-door" model) (Kimura and Tamaki, 1986; Otofuji, 1996).

A review of published studies on the formation mechanisms of back-arc basins testifies that different mechanisms have been involved in their formation and evolution, and no universal global mechanism can possibly explain the multiplicity of global observations. This overview does not aim to reevaluate the roles of different mechanisms proposed to explain the formation of various back-arc basins (Fig. 2). Instead it invites to discussion: how much is known about back-arc basins from a geophysical point of view? how different are they? which geophysical features do they have in common? which parameters describing the structure of back-arc basins are correlated with parameters related to the subduction process? and what can we learn from this?

Back-arc basins largely remain in the focus of fundamental academic research. A vast amount of regional, mostly geological and geochemical, studies of back-arc basins has been summarized in a number of dedicated reviews. An extensive global overview of back-arc tectonics, geology, magmatism, and hydrothermal activity can be found in Taylor et al. (1995). A comprehensive summary of petrological characteristics of back-arc magmatism is presented by Wilson (2007), while a review of geological and environmental aspects of back-arc systems is given by Christie et al. (2006). There are also numerous extensive regional geophysical reviews, but an overall geophysical perspective is yet missing. This paper aims to fill this gap. The analysis starts with a geophysical overview of 26 active and extinct marine back-arc basins (Fig. 1) presented in *Section 2: Synthesis*. This is followed by a comparative analysis of typical geophysical and geodynamic characteristics and correlations between them for back-arc basins of different tectonic types *Section 3: Analysis*. Finally, *Section 4* presents a brief summary of the major findings.

2. Synthesis

2.1. Datasets

2.1.1. Types of back-arc basins (BABs)

This brief summary, in particular its geological part, should not be considered as a detailed overview for any particular back-arc region. Due to a large amount of publications, references are limited to selected most relevant studies to stay within a journal format. Back-arc basins are numbered from #1 to #26 in the text, the figures and tables as listed in Section 2. The numbering starts from the northern Pacifics and continues counter-clockwise to South America, the Caribbean and the Mediterranean region (Fig. 1). Several back-arc basins with essentially different extensional regimes and therefore geophysical characteristics in their different parts are subdivided into the sub-basins that are considered independently, giving in total 31 analyzed areas, specified in Tables 1 and 2.

Following a traditional approach, the back-arc basins are initially split into active and extinct (Fig. 1), and active basins are further classified by subduction type (ocean-ocean, arc-ocean, and continent-ocean) to make the following groups: (i) ocean - ocean subduction (OO-type, blue colors in all figures), (ii) island arc - ocean subduction (AO-type, magenta colors), (iii) continent - ocean subduction (CO-type, dark yellow colors), and (iv) extinct back-arc basins (Ext-type, purple colors). Extinct basins are further split into the Pacific (Ext-1) and non-Pacific (Ext-2) groups due to their principally different characteristics. The Sea of Japan (#4) located behind subduction systems associated with the active continent-ocean collisions is analyzed as part of the CO-type, essentially to increase the amount of data in this small group. Finally, tectonic setting associated with a continent - island arc subduction includes only the extinct back-arc basin of the Banda Sea (#12), which is analyzed with other extinct BABs. It is shown later (Sections 3, 4) that the originally adopted types are insufficient to describe the complexity of back-arc basins, since the CO-type BABs with and without seafloor spreading make different types (Table 3).

An overview of geodynamic and geophysical information follows a similar structure for each of 26 back-arc basins (with several sub-basins) (Figs. 3-9): geodynamic setting, history of extension, bathymetry (based on a global elevation ETOPO1 model), gravity anomalies, heat flow data, and seismic data on the crustal-scale structure where available. Additional data include duration of spreading, total opening rate, slab age (at present along the trench) and dip angle (at present, inferred from intermediate depth seismicity). The following data sources are used throughout the study as described below and without an additional referencing. Note that for many back-arc basins the existing geophysical information is scarce and often controversial.

2.1.2. Gravity anomalies

Free-air gravity anomalies are taken from a global EGM2008 model (Pavlis et al., 2012) and compared to regional high-resolution gravity data along ship tracks, where available. For the ice-covered Antarctica, a recent data compilation is used (Scheinert et al., 2016). Close-to-zero free-air anomalies are interpreted as diagnostic of regional isostatic equilibrium (Figs. 3-9). However, flexure of the elastic portion of the lithosphere, especially in small-size back-arc basins, produces the short-wavelength signal in free-air anomalies, so that free-air anomalies may still be non-zero even when topography is isostatically compensated (Burov and Gerya, 2014). It will be argued in Section 3.2 that isostasy is important in all back-arc basins, while non-zero free-air gravity anomalies are largely caused primarily by flexure of the elastic portion of the lithosphere. Interpretations of non-zero free-air anomalies in terms of mantle flow (dynamic) topographic support may adopt the following "rules of thumb" (McKenzie, 1994; Molnar et al., 2015): mantle convection flow associated with density contrasts near the lithosphere base (e.g. by temperature-induced lateral density variations as in the McKenzie's model with a constant chemistry) produces a ca. 30 mGal/km ratio of free-air gravity-anomaly to bathymetry-anomaly, and in submarine regions the ratio increases to 100 mGal/km if the density anomalies generating bathymetric uplift are located deep in the mantle (Molnar et al., 2015).

The extent of back-arc basins (shown by white lines in Figs. 3-9) is defined here by high gradient zones in Bouguer anomalies which mark transitions from smaller values in trenches and "normal" oceans to significantly higher values in back-arc basins. These gradient zones are obviously associated with large bathymetric changes associated with back-arc basins. In off-shore regions, crustal columns have a negative load at the surface because water is less dense than rock; therefore to maintain isostatic balance this density deficit requires the existence of excess compensating masses at depth, which produce high Bouguer anomalies in oceanic areas (Figs. 3-9). Geophysical characteristics of back-arc basins (BABs) discussed in text (e.g. bathymetry, gravity anomalies, heat flow, Table 1) are automatically averaged from the corresponding digital databases within the outlined BAB areas. Bouguer anomalies calculated at sea by replacing the seawater with rocks of average crustal density assume rock density of 2670 kg/m^3, water density of 1050 kg/m^3 and ice density of 919 kg/m^3 (Artemieva et al., 2016).

2.1.3. Magnetic anomalies and heat flow

Information on magnetic lineations and their interpretation in terms of ages of seafloor opening and total opening rates is based on regional high-resolution magnetic data along ship tracks, where available and as referenced in the text. Magnetic anomalies are marked in Figs. 3-9 where exist and are absent in many back-arc basins.

Off-shore heat flow is based on a recently updated compilation of the International Heat Flow Commission, IHFC (Fuchs et al., 2021). The analysis is limited to high quality data. Extreme values (<30 mW/m^2 and >130 mW/m^2) are excluded, since these anomalous values imply advective and transient thermal regime and as such they do not meet the key requirements to geothermal heat flow measurements which are

Table 1
Geophysical characteristics of back-arc basins (BABs).

#	Name of BABs	Associated island arc	Active or Extinct	Tectonic type[1]	Spreading age or extension age (Ma)[2]	Total opening rate (cm/y)[2]	Sea-floor spreading	Crustal type[3]	Thickness: total crust / basement / lower crust (km)[4]	Dimensionless crustal thinning [5]	Free air / Bouguer gravity anomalies (mGal)[6]	Bathymetry (km)[6]	Heat flow (mW/m^2)[7]
	Northern Pacific Ocean												
1.	Aleutian Basin	Aleutians	Active	OO	?	?	Yes	O	12/8/6.5	NA	-15/230	3.6	65 ± 16
2.	Komandorsky Basin	Aleutians	Active	OO	20–10	3	Yes	O	9/7/5	NA	0/240	3.5	91 ± 36
3.	Kuril Basin	Kuriles	Active	CO	30–15	1	Yes	O	15/11/8	0.73	10/225	3.2	89 ± 8
4.	a) Sea of Japan-N	*Extinct*	Extinct	CO	28–18	5	Yes	O	10/7/5	4.41	0/225	3.3	94 ± 16
	b) Sea of Japan-S	*Extinct*	Extinct	CO	28–18	5	No?	O?	17/13/9	2.31	10/160	2.2	91 ± 14
5.	a) Okinawa Trough-N	Ryukyu	Active	CO	10–0	1	No	C	22/18/11	1.67	30/85	0.8	80 ± 20
	b) Okinawa Trough-S	Ryukyu	Active	CO	1–0	4	Yes	O?	11.5/6.5/4.5	4.61	25/145	1.7	84 ± 28
6.	Mariana Trough	Marianas	Active	OO	10–0	4.3	Yes	O	5.5/4.5/3	NA	50/300	3.6	62 ± 23
7.	Shikoku Basin	Bonin	Extinct	OO?	26–15	3.5	Yes	O	6/4.5/3	1.78	15/330	4.6	82 ± 31
8.	Parece Vela Basin	*Extinct*	Extinct	OO?	28–15	?	Yes	O	5.5/4/2.5	1.95	15/340	4.8	74 ± 31
9.	W Philippine Basin	*Extinct*	Extinct	OO?	60–35	8.8	Yes	O	5.5/5/3	1.67	10/400	5.7	70 ± 25
10.	S China Sea	Manila	Extinct	?	32–16	4	Yes	O	5.5/5/1.5	1.60	10/270	3.9	89 ± 23
11.	Celebes Sea	Sangihe	Extinct	AA or AC?	47–42	4.7	Yes	O	9.5/7.5/5.5	1.07	35/345	4.6	58 ± 12
12.	Banda Sea	Banda	Extinct	AC	25?-3?	?	Yes	O?	10/9/7	2.78	25/290	3.9	81 ± 25
	Indian and Southern Pacific Oceans												
13.	Andaman Sea	Andaman	Active	CO	13–0	3.7	Yes	O	8.5/7/4	4.28	-5/150	2.3	88 ± 19
14.	Manus Basin	New Britain	Active	OO	3.5–0	13.2	Yes	O?	No seis. data	NA	65/190	1.9	73 ± 49
15.	Woodlark Basin	*Extinct*	Extinct	CO	45–35	7.2	Yes	O?	No seis. data	NA	35/260	3.3	52 ± 18
16.	North Fiji Basin	New Hebrides	Active	OO	10–0	7.0	Yes	O	4/4/3	NA	35/235	2.9	80 ± 32
17.	Lau Basin	Tonga	Active	OO	6–0	16	Yes	O	6/5.5/3.5** 7/7/5*	NA	45/200	2.3	45 ± 24
18.	Havre Basin	Kermadec	Active	OO	5.5–3.0	2	Yes?	O? C?	No seis. data	NA	70/240	2.5	No data
	Atlantic Ocean												
19.	East Scotia	S. Sandwich/ Scotia	Active	OO	15–0	6.8	Yes	O?	No seis. data	NA	40/250	3.0	115 ± 21
20.	Bransfield Basin	S. Shetlands	Active	AO	4–0	1	No	A?	14.5/10.5/9	2.28	40/90	0.8	102 ± 19
21.	a) Lesser Antilles-S	Lesser Antilles	Active	AO	25–0	?	Yes	O?	15.5/7.5/5	1.62	-40/145	2.7	69 ± 12
	b) Lesser Antilles-N	*Lesser Antilles*	Active	AO	25–0	?	No	A?	24.5/22.5/11.5	1.02	0/145	2.1	66 ± 14
	c) Aves Ridge	*Extinct*	Extinct	?	88–59	?	Yes	A	25.5/23.5/19	1.07	0/150	1.5	64 ± 13
22.	Gulf of Mexico	*Extinct*	Extinct	?	155–140?	2.2	Yes	O	13/6/6	1.29	-25/175	2.9	46 ± 16
	Mediterranean Sea												
23.	Tyrrhenian Sea	Calabrian	Active	OO	9–0	5	Yes	O	6.5/5.5/3.5	NA	5/210	3.0	95 ± 36
24.	Aegean Sea	Hellenic	Active	CO	13–4	3	No	C	30/27/14	1.11	130/135	1.0	62 ± 18
25.	a) W. Black Sea	*Extinct*	Extinct	CO?	Ca. 100?	?	?	O?	20/8/3	3.75	-25/115	2.0	42 ± 9
	b) E. Black Sea	*Extinct*	Extinct	CO?	60–50?	?	?	C? O?	16/7/0	4.28	−20/120	2.1	37 ± 11
	West Antarctica Seas												
26.	W. Antarctica	*Extinct*	Extinct	CO?	Pz-Mz	8	?	C	19/13/7.5	2.31	−20/20	0.6	>100

References are provided in the text.

[1] OO = ocean-ocean, AO = island arc-ocean, AA = arc-arc, CO = continent-ocean plates collision,? = debated or unknown.

[2] For spreading duration (start-end in Ma) most commonly accepted values are listed (see text for references). In BABs with no spreading, duration of major extensional phases is listed. Total opening rate is shown without decimals when the uncertainty in estimates is large.

[3] O = oceanic, C = (hyper)extended continental, and A = arc crust as interpreted in the original publications (see the text for details). Hybrid crust is not shown separately. In OC collisions with seafloor spreading, oceanic crust may be present only around the spreading axis, with continental crust elsewhere. Such BABs are marked as having oceanic crust, however sparse seismic profiles in most BABs and the absence or unclear patterns of magnetic lineations preclude conclusions on the areal extent of oceanic crust.

[4] Crustal structure (with thickness rounded to 0.5 km) corresponds to representative values along existing seismic profiles within the areas marked in Figs. 3-9 (for the Lau Basin: * at the spreading axis; ** at basin margins). Lower crust refers to layer with Vp > 6.8 km/s in continental crust and to Layers 3A + 3B in oceanic crust as identified in regional seismic interpretations.

[5] Crustal thinning factor = [pre-extensional basement thickness] divided by [present basement thickness]. Pre-extensional basement thickness is assumed to be 25 km for arc crust (AO-type), 30 km for extended continental crust (CO-type), 8 km as in "normal" oceans for extinct BABs #7–11 (assumed to be formed on oceanic plates, the OO-type), 25 km for extinct BABs formed by arc-ocean collisions (#12, 21AR) and 30 km for extinct BABs #4, 25, 26 (assumed to be formed on stretched continental plates). NA = non-available. The OO-type is excluded from the analysis, since the approach is invalid there. See section 3.3.3 for details.

[6] Gravity anomalies and bathymetry are averaged on 5 min grids within the areas marked in Figs. 2-8 and rounded to 5 mGal and 0.1 km. For West Antarctica the equivalent bathymetry compensated for ice load is given. Standard deviation is in the range of 0.2–0.9 km for bathymetry with larger values in small BABs, and typically 10–30 mGal for free air and 20–40 mGal for Bouguer anomalies.

[7] Heat flow is averaged within the areas marked in Figs. 3-9; values >130 and < 30 mW/m^2 are excluded as unreliable.

Table 2
Subduction slab characteristics of individual back-arc basins (BABs).

#	Name of BABs	Active or Extinct	Tectonic type[1]	EQ mid-depth range (km)[2]	Mid-depth dip angle (deg)[2]	Top-slab trench distance (km) at z = 100 km[2]	Trench-normal slab velocity (mm/y), S/M[3]	Age of subducting plate (My)[4]	Trench direction[5]	Axis of extension (deg)[6]	Direction of magnetic anomalies[5]	Major peculiarities (see section 2, Figs. 2-9)
	Northern Pacific Ocean											
1.	Aleutian Basin	A	OO	70–270	58	180	44/68	57	W-E	(W:20, E:-20)	NNW-SSE to NNE-SSW	Seafloor spreading. The subduction system may be irrelevant to the back-arc basin. Magnetic anomalies, roughly perpendicular to the front of the Aleutian arc, are interpreted as a trapped fragment of oceanic crust. The extension rates and the age of the basin basement are unknown.
2.	Komandorsky Basin	A	OO	100–340	52	220	?/43	60	WNW-ESE	(40)	NE-SW	Seafloor spreading. The subduction system may be irrelevant to the back-arc basin. Magnetic anomalies are roughly perpendicular to the front of the Aleutian arc as in #1. Old and sparse seismic data on the crustal structure.
3.	Kuril Basin	A	CO	50–320	31	260	70/88	125	NE-SW	(65)	Absent	Fan-shaped geometry may be caused by the Pacific subduction combined with the rotation of the continental plate. The extension rates and the basement age are unknown. Large number of seismic profiles with controversial interpretations.
4.	a) Sea of Japan-N	E	CO	50–310	31	320	80/104	135	NE-SW	75	NE-SW	Seafloor spreading is present in the Japan Basin and possibly absent in the Yamato Basin.
	b) Sea of Japan-S	E	CO	NA	NA	320	80/46	135	NE-SW	70	Uncertain	Complicated and incoherent magnetic lineations. The subduction system may be irrelevant to the back-arc origin of both basins. Rotational and pull-apart models for the opening of the Sea of Japan do not require subduction. Crustal profiles are mostly at the margins. Crustal origin of the Yamato Basin (S part) is debated. One of the densest coverages by heat flow measurements.
5.	a) Okinawa Trough-N	A	CO	50–250	60	190	31/69	57	NE-SW	30	Uncertain	Possible seafloor spreading in the southern part. Progressive extension from south to north. In the north, bathymetry is unusually shallow with small positive Bouguer anomalies, and the crust is possibly still continental.
	b) Okinawa Trough-S	A	CO	70–300	51	250	41/69	44	NE-SW	60	NE-SW	
6.	Mariana Trough-N	A	OO	120–700	77	220	68/107	150	N-S	−25	Absent	Seafloor spreading. A rare example of a near-vertical subduction system. Limited number of seismic profiles. Anomalous type of OO-subductions by many geophysical parameters.
	Mariana Trough-S	A	OO	120–700	87	220	68/107	150		15		
7.	Shikoku Basin	E	OO?	NA	NA	NA	80/93	NA	NW-SE	−20	N-S	Relict (early-middle Miocene) seafloor spreading. Thin crust, deep bathymetry, strong positive Bouguer anomalies. Similar evolution with #8.
8.	Parece Vela Basin	E	OO?	NA	NA	NA	?/?	NA	N-S?	5	N-S	Relict (Oligocene-middle Miocene) seafloor spreading. Strong E-W heat flow asymmetry. Thin crust, deep bathymetry, strong positive Bouguer anomalies. Similar evolution with #7.
9.	W Philippine Basin	E	OO?	NA	NA	NA	?/?	NA	N-S?	−60	NW-SE	Relict (Paleocene-Eocene) seafloor spreading. The basin may be a trapped oceanic fragment rather than a relict back-arc basin. The deepest (by ~1 km) BAB worldwide and extreme high positive Bouguer anomalies, both similar to very old oceans.

(*continued on next page*)

Table 2 (*continued*)

#	Name of BABs	Active or Extinct	Tectonic type[1]	EQ mid-depth range (km)[2]	Mid-depth dip angle (deg)[2]	Top-slab trench distance (km) at z = 100 km[2]	Trench-normal slab velocity (mm/y), S/M[3]	Age of subducting plate (My)[4]	Trench direction[5]	Axis of extension (deg)[6]	Direction of magnetic anomalies[5]	Major peculiarities (see section 2, Figs. 2-9)
10.	South China Sea	E	?	NA	NA	NA	?/58	NA	?	70	NE-SW	Relict (Oligocene-middle Miocene) seafloor spreading. Strong N-S asymmetry in free air anomalies. Thin crust and strong positive Bouguer anomalies typical of other OO-type BABs. The basin, possibly formed by CO collision, has poor resolution by conventional seismic profiles.
11.	Celebes Sea	E	AA/AC?	NA	NA	NA	?/?	NA	?	75	ENE-WSW	Relict (Eocene-middle Miocene) seafloor spreading. May also represent an entrapped oceanic fragment. Similar evolution with adjacent small-scale basins. Positive free air and Bouguer anomalies are among the largest among the extinct BABs, while heat flow is among the lowest. Conventional seismic profiles are sparse and old.
12.	Banda Sea	E	AC	NA	NA	NA	20/?	NA	?	70	ENE-WSW	Relict (Miocene to Pliocene, debated) seafloor spreading. A rare example of collision between an arc and continental margin. The basin has the greatest curvature of any active arc. Seismic profiles are limited and old.
	Indian and Southern Pacific Oceans											
13.	Andaman Sea	A	CO	80–200	39	300	41/?	78	N-S	25	NNE-SSW	Seafloor spreading, possibly caused by oblique subduction. Large variations in sediment thickness. Numerous reflection profiles, but refraction/wide-angle reflection studies are old and sparse.
14.	Manus Basin	A	OO	70–350	63	100	58/63	?	ENE-WSW	65	ENE-WSW	Seafloor spreading. Very high free air anomalies and shallow bathymetry. Low Bouguer anomalies suggest a low-density mantle. Only two heat flow measurements. No seismic data on the crustal structure.
15.	Woodlark Basin	E	CO or CA	NA	NA	NA	56/63	125	E-W?	E:65, W:105	E-W	Relict (Pliocene) seafloor spreading. Formed by collision between the Ontong-Java plateau and continental margin with westward propagation of stretching. Crustal seismic models are restricted to the westernmost and youngest extension of the basin
16.	North Fiji Basin	A	OO	50–320	69	110	40/24	57	N-S	N:-55, S:10	N-S	Seafloor spreading. Basin formation may be by block rotations and similar to the Sea of Japan, possibly with no link between the subduction and the BAB. Westward propagation of stretching is reflected in bathymetry and gravity. A very thin crust as imaged by low-resolution old seismic refraction studies.
17.	Lau Basin	A	OO	70–700	54	250	73/105	110	NNE-SSW	15	Complex	Controversial interpretations of complicated magnetic anomalies, with seafloor spreading. Extension caused by the Pacific rollback. The largest slab displacement from the trench in the OO-type, with a typical steep slab dip. Unusually low heat flow.
18.	Havre Basin	A	OO	70–600	64	200	61/93	105	NNE-SSW	(20)	No regular patter	Controversial interpretations of complicated magnetic anomalies. No spreading axis. Extension caused by the Pacific rollback, possibly still at rifting stage. Small slab displacement from the

(*continued on next page*)

Table 2 (*continued*)

#	Name of BABs	Active or Extinct	Tectonic type[1]	EQ mid-depth range (km)[2]	Mid-depth dip angle (deg)[2]	Top-slab trench distance (km) at z = 100 km[2]	Trench-normal slab velocity (mm/y), S/M[3]	Age of subducting plate (My)[4]	Trench direction[5]	Axis of extension (deg)[6]	Direction of magnetic anomalies[5]	Major peculiarities (see section 2, Figs. 2-9)
												trench. Very high free air anomalies. Seismic data on the crustal structure is absent. No heat flow data.
	Atlantic Ocean											
19.	East Scotia	A	OO	50–350	63	125	13/75	59	N-S	−15	N-S	Seafloor spreading caused by normal OO-type collision. Bathymetry and gravity anomalies typical of OO-type basins. Seismic data on the crustal structure is absent. Heat flow is known only in the eastern part.
20.	Bransfield Basin	A	AO	50–190	25	350	7/?	19	ENE-WSW	70	Possibly only an axial high	No seafloor spreading yet. The most shallow slab dip angle. Formed by NW-SE rifting propagation in a volcanic arc caused by a combination of transtension and roll-back of the Phoenix Plate. Most shallow BAB, the smallest Bouguer anomalies among all of BABs worldwide, high free air and high heat flow require a shallow hot mantle. High-quality seismic data.
21.	a) Lesser Antilles-S	A	AO	80–160	29	460	13/?	88	N-S	30	No regular pattern	a-b) Seafloor spreading may exist only in the southern part that has one of the most shallow slab dip angles and the largest negative free air anomaly values among all back-arc basins. The northern part has one of the thickest crust among all back-arc basins. c) Relict (Cretaceous-Paleocene) seafloor spreading. High-quality seismic data show one of the thickest crust among all back-arc basins.
	b) Lesser Antilles-N	A	AO	70–190	43	250	13/?	92		−10		
	c) Aves Ridge	E	?	NA	NA	NA	?/?	NA	N-S	(0)	N-S	
22.	Gulf of Mexico	E	?	NA	NA	NA	?/?	NA	?	W:30, C:60, E:110	Absent	Relict (Upper Jurassic) seafloor spreading. Spreading age and its duration are not well known. Relatively low Bouguer anomalies. Abundant heat flow measurements with equilibrated low values. High-quality but spatially restricted seismic data.
	Mediterranean Sea											
23.	Tyrrhenian Sea	A	OO	150–330	59	125	1/6	80	Semi-circular, NE-SW	20	N-S	Seafloor spreading. Oceanic crust is restricted to two small axial sub-basins. The age of subducted Mediterranean plate is debated. A rare example of a semi-circular subduction system with one of the largest trench curvatures. A localized near-vertical seismogenic zone at large depths. High-quality seismic data.
24.	Aegean Sea	A	CO	70–160	31	200	21/6	125	W-E	(−80)	Absent	No seafloor spreading. The age and extension rate are poorly known. Debated tectonic origin includes the Africa-Eurasia plate convergence and transtension associated with westward escape of Anatolia. One of the most shallow slab dip angles. Extremely shallow bathymetry and extremely high free air anomalies indicate a strong lithosphere deformation. Sparse and old classical seismic profiles image a ca. 30 km thick crust.

(*continued on next page*)

Table 2 (*continued*)

#	Name of BABs	Active or Extinct	Tectonic type[1]	EQ mid-depth range (km)[2]	Mid-depth dip angle (deg)[2]	Top-slab trench distance (km) at z = 100 km[2]	Trench-normal slab velocity (mm/y), S/M[3]	Age of subducting plate (My)[4]	Trench direction[5]	Axis of extension (deg)[6]	Direction of magnetic anomalies[5]	Major peculiarities (see section 2, Figs. 2-9)
25.	a) W. Black Sea	E	CO?	NA	NA	NA	?/?	NA	NNW-SSE?	(80)	Absent	No known seafloor spreading. The age and extension rate are debated. The nature of the crust is also debated. It may include trapped oceanic fragments or eclogitized crust. Heat flow is one of the lowest in the back-arc basins globally. Spatially restricted seismic refraction/wide-angle reflection profiles. Sediments exceed 10 km in thickness.
	b) E. Black Sea	E	CO?	NA	NA	NA	?/?	NA		(−70)	Absent	
	West Antarctica											
26.	W. Antarctica basins	E	CO?	NA	NA	NA	?/?	NA	NNW-SSE	(−50)	Absent	No known seafloor spreading. Extension rate is unknown. One of the shallowest marine BABs with the lowest Bouguer anomalies. Limited seismic profiles. Sediments may exceed 10 km in thickness. Controversial and limited heat flow measurements.

See text for references.

[1] OO = ocean-ocean, AO = island arc-ocean, AA = arc-arc, CO = continent-ocean plates collision,? = debated or unknown; NA = non-available.

[2] Constrained by intermediate depth seismicity (M > 5.0, depth range between 50-80 km and 200–300 km).

[3] Trench-normal slab velocity (mm/y): first values based on Schellart et al., 2011; second values based on Mantovani et al., 2001.

[4] Based on seafloor age map (Mueller et al., 2008).

[5] See references in Section 2 and patterns in Figs. 3-9.

[6] Determined from published maps and rounded to 10°. Numbers in brackets – inferred from trench direction. Zero corresponds to north.

based on mathematical assumptions on steady-state, conductive heat transfer. In some cases heat flow data for young active back-arc basins (<6 Ma of extension) are excluded as discussed in the text. Oceanic heat flow commonly requires correction for the effects of sedimentation and compaction (e.g. Hutchison, 1985). Such corrections are not introduced here because (i) seafloor spreading did not commence in a half of back-arc basins and the extent of similarity between back-arc spreading and ocean spreading is debated (see Section 3), and (ii) details on the structure of sedimentary cover are unavailable for many (most?) back-arc basins. The exclusion of extremely low and high heat flow values from the analysis essentially compensates for possible effects of sedimentation and compaction. Heat flow in Antarctica includes both borehole and ice-drilling measurements (cf. Artemieva, 2022). Similar to off-shore regions, extreme values >130 mW/m^2 (e.g. Fig. 9) are excluded from the analysis.

2.1.4. Subduction parameters

Ages of subducting oceanic plates along the trenches are taken for the present time from a global model of seafloor age (Mueller et al., 2008) and for some basins are averaged along the trench. The slab age at the time of extension is not used due to large uncertainties in such constraints, for the same reason the slab age averaged over the duration of extension is not used.

Subduction dip (Fig. 10) is calculated from the geometry of the seismogenic zone constrained by M > 5.0 seismicity derived from the USGS catalogue (Jacobsen, 2018). At shallow depth, slab dip angle is often unclear; therefore dip angle at intermediate depth (50–80 km to 200–300 km) is used. Some other published values are listed in the text as referenced, since there is a discrepancy in some published values.

Duration of extension (or seafloor) spreading and total opening rate are compiled from literature as referenced in the text. In case of several phases of extension, the values used in the analysis refer to the phase with the highest extension rate (or to the cumulative of several phases if extension rates were similar).

A number of parameters, potentially important for evolution of back-arc basins, is excluded from the present study. This includes, in particular, kinematic parameters related to subduction, such as convergence rate, plate descent rate, obliquity and direction of collision, direction of arc migration, curvature and length of subduction zone, and depth of slabs below back-arc basins, etc. Data on the age, distribution, volume and composition of extensional magmatism, and locations and sizes of volcanic arcs associated with subductions, are also excluded, and can be found elsewhere (Taylor, 1995; Christie et al., 2006; Wilson, 2007). While these parameters are closely related to the properties and processes discussed in this study and further specify dynamics of back-arc basins evolution, they are omitted to keep the overall length within a paper rather than a book format.

2.1.5. Seismic structure of the crust

Insufficient coverage by seismic reflection/refraction profiles of nearly all back-arc basins precludes estimates of the portion of oceanic, continental and hybrid (transitional) crust within basins. Therefore the analysis focuses on the tectonic nature of converging plates (oceanic, arc, and continental) and identification of basins where lithosphere stretching has led to seafloor spreading (Table 1).

Crustal structure (Fig. 11) is based on regional seismic studies referenced in the text, and only crustal-scale models are used with the preference given to seismic reflection/refraction profiles. In few regions where such profiles are lacking, tomographic models and receiver function studies are used instead. Global crustal models and gravity constraints on the crustal structure are not used due to unknown uncertainties in such models. Because of a small number of seismic profiles for nearly all back-arc basins, the presented cross-sections and further analysis refer to a typical crustal structure in each back-arc basin. In basins with a good seismic coverage, only crustal structure away from spreading axes but within a newly formed oceanic crust is used, unless

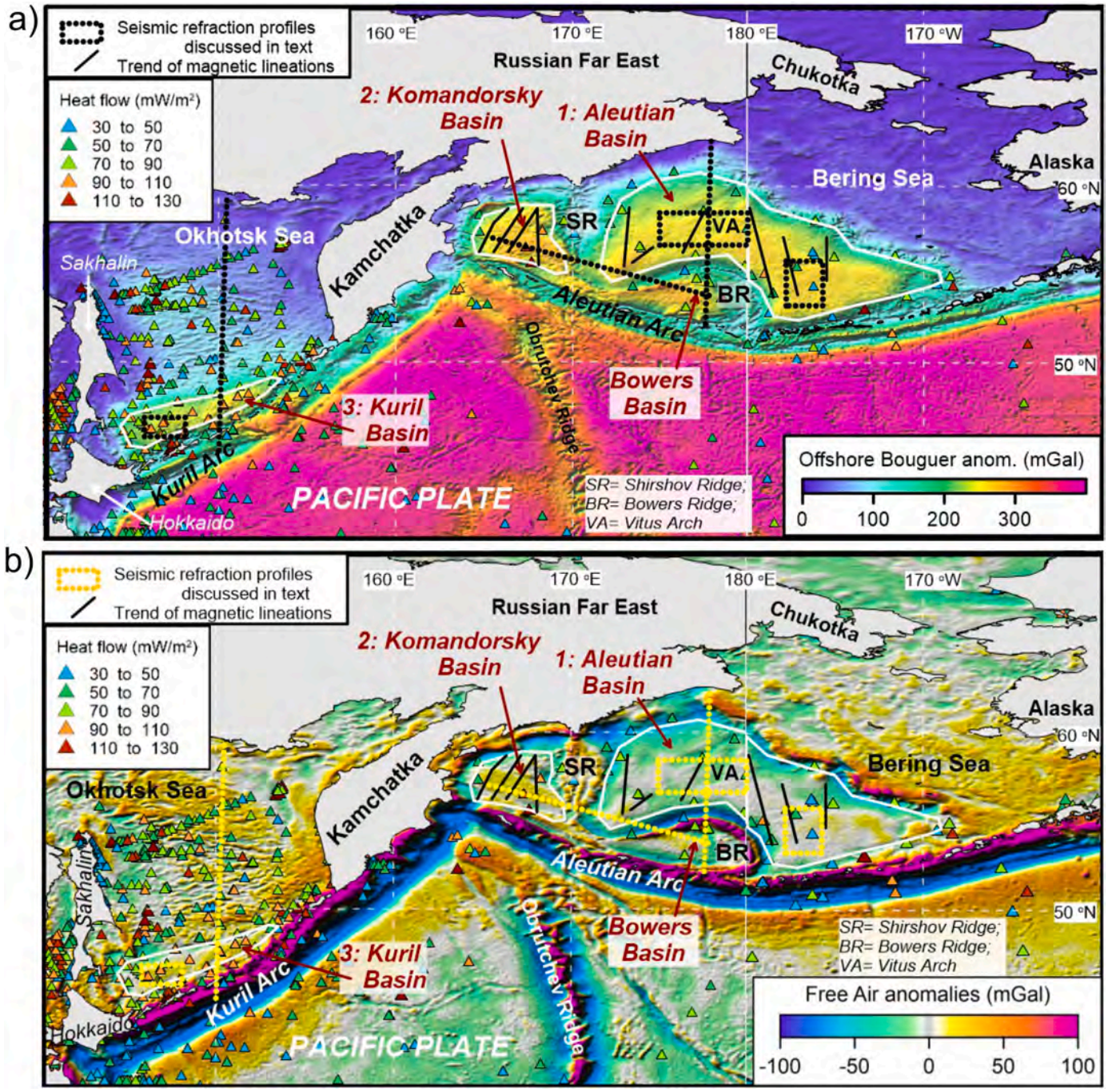

Fig. 3. Back-arc basins of the northern Pacific; BABs limits are shown by white outline; red text - BABs names and numbers (#1–3 in Fig. 1). Background: Bouguer (a) and free-air (b) gravity anomalies over shaded relief. Symbols - heat flow measurements. Color codes are the same in Fig. 3-9. Black (yellow in b) dotted lines - seismic reflection/refraction profiles discussed in the text (only offshore parts are shown); black solid lines - inferred major magnetic anomalies. For references see the text.

otherwise noted. For the Lau Basin (#17), seismic data from both the spreading axis and basin margins are included for comparison. Where lower crustal layer is discussed, its definition is adopted from the original seismic studies (Fig. 11).

Lithosphere thickness in convergent plates and in back-arc basins is excluded from the analysis. For most of basins, regional lithosphere-scale seismic models are absent, while global tomographic models have insufficient resolution with significant differences between the models. Indirect constraints used in numerical models and geochemical derivations on lithosphere thickness are excluded for the same reasons (e.g. Kerswell et al., 2021).

2.2. BABs of the north-western Pacific Ocean

#1. Aleutian Basin

The Bering Sea marginal basins formed behind the Aleutian arc include the Aleutian, Bowers, and Komandorsky Basins (Fig. 3). The Aleutian Basin (water depth 3.5–3.9 km) is part of the North America Plate underthrust by the subducting Pacific Plate with age of 56–58 Ma along the trench and ~ 53° intermediate depth (80 to 250 km) dip-angle at the basin (Jacobsen, 2018). The formation of the Aleutian subduction zone and related Aleutian island arc started in in the middle Eocene (50–47 Ma ago) when the direction of the Pacific Plate has changed,

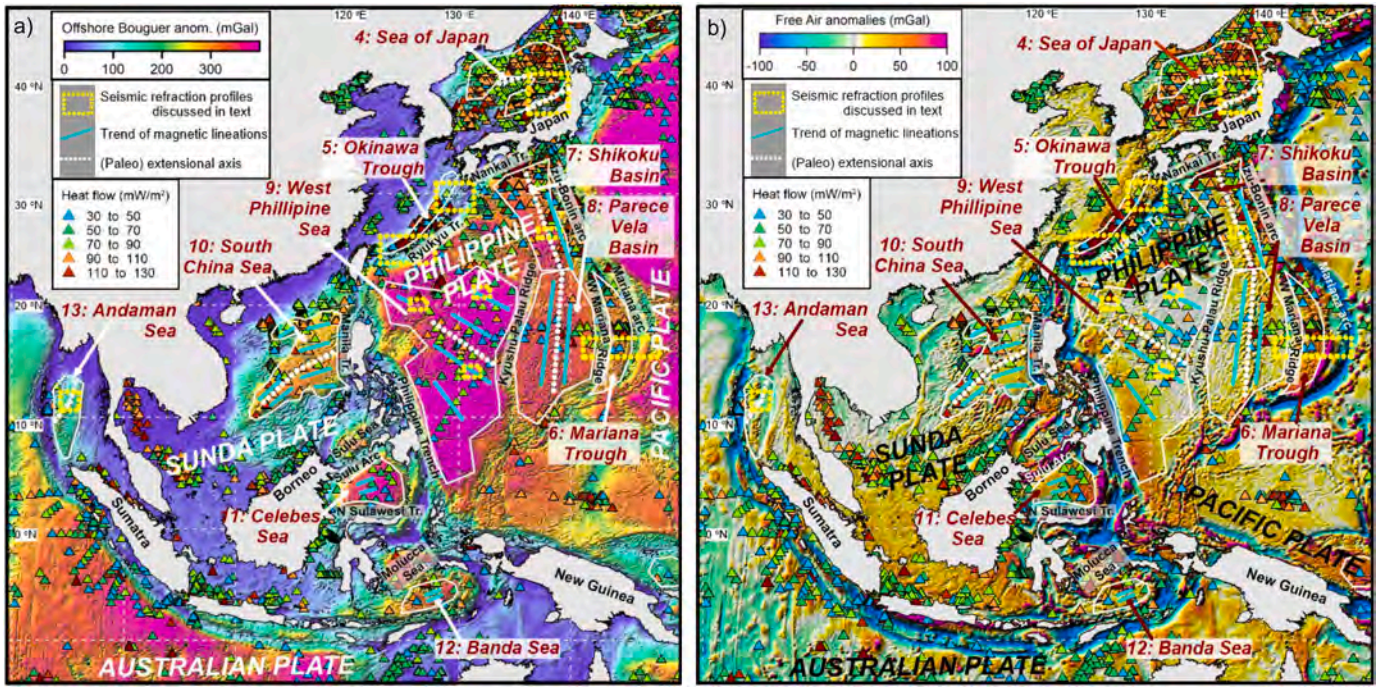

Fig. 4. Back-arc basins of the north-western Pacific and Indian oceans (#4–13 in Fig. 1); BABs limits are shown by white outline; red text - BABs names and numbers. Background: Bouguer (a) and free-air (b) gravity anomalies over shaded relief. Symbols - heat flow measurements. Color codes are the same in Fig. 3-9. Yellow dotted lines - seismic reflection/refraction profiles discussed in the text; cyan solid lines - inferred major magnetic anomalies, white dotted lines - inferred paleo- or active extensional axes. For references see the text.

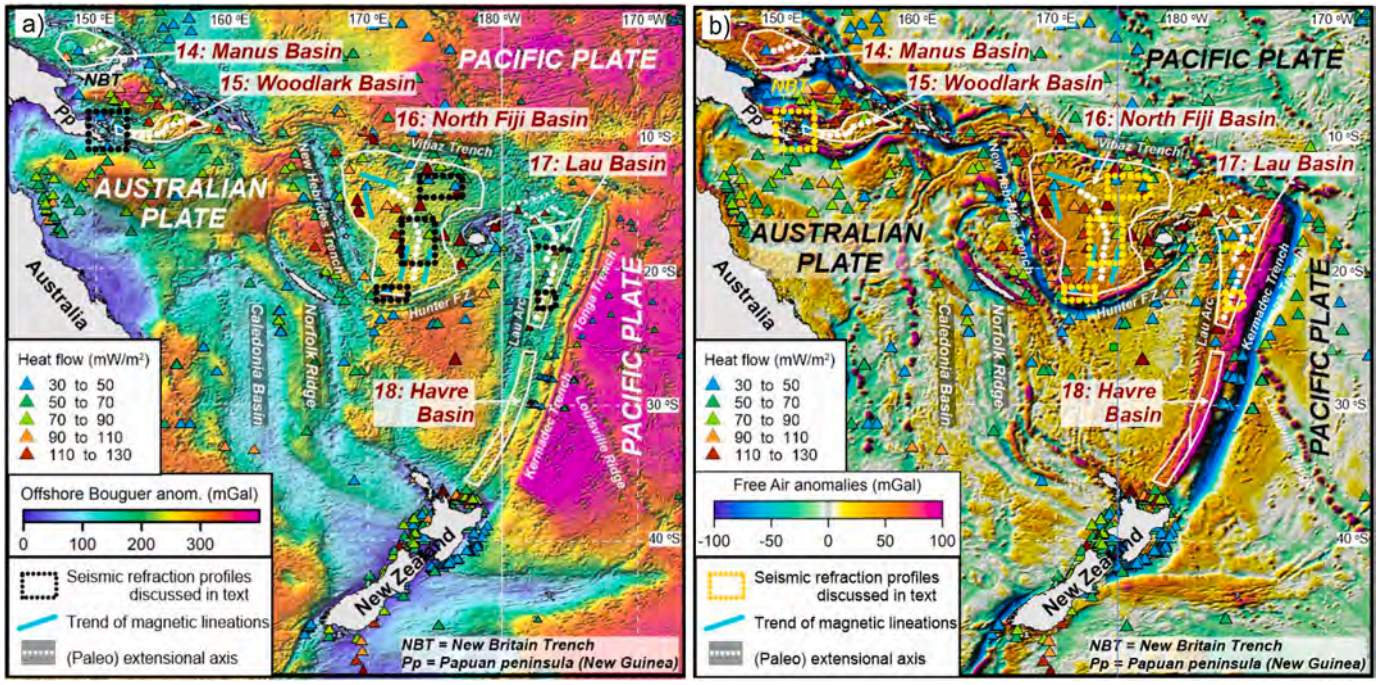

Fig. 5. Back-arc basins of the south-western Pacific (#14–18 in Fig. 1); BABs limits are shown by white outline; red text - BABs names and numbers. Background: Bouguer (a) and free-air (b) gravity anomalies over shaded relief. Symbols - heat flow measurements. Color codes are the same in Fig. 3-9. Black dotted boxes - regions with seismic reflection/refraction profiles discussed in the text; cyan solid lines - inferred major magnetic anomalies, white dotted lines - inferred paleo- or active extensional axes. For references see the text.

possibly as the result of the first Pacific subduction along the plate's western margins (Faccenna et al., 2012).

The Aleutian Basin has prominent magnetic anomalies, with crudely N-S and NNW-SSE lineation in the eastern part of the basin and with NE-SW lineation in its north-western part (Fig. 3). The pattern is unusual because magnetic lineations are roughly perpendicular to the front of the Aleutian arc (Table 2). They also lack symmetry with respect to a possible relict spreading axis (Cooper et al., 1992). Due to a complex pattern of the anomalies, links of magnetic lineaments to the geomagnetic polarity timescale remain controversial. Therefore, the extension

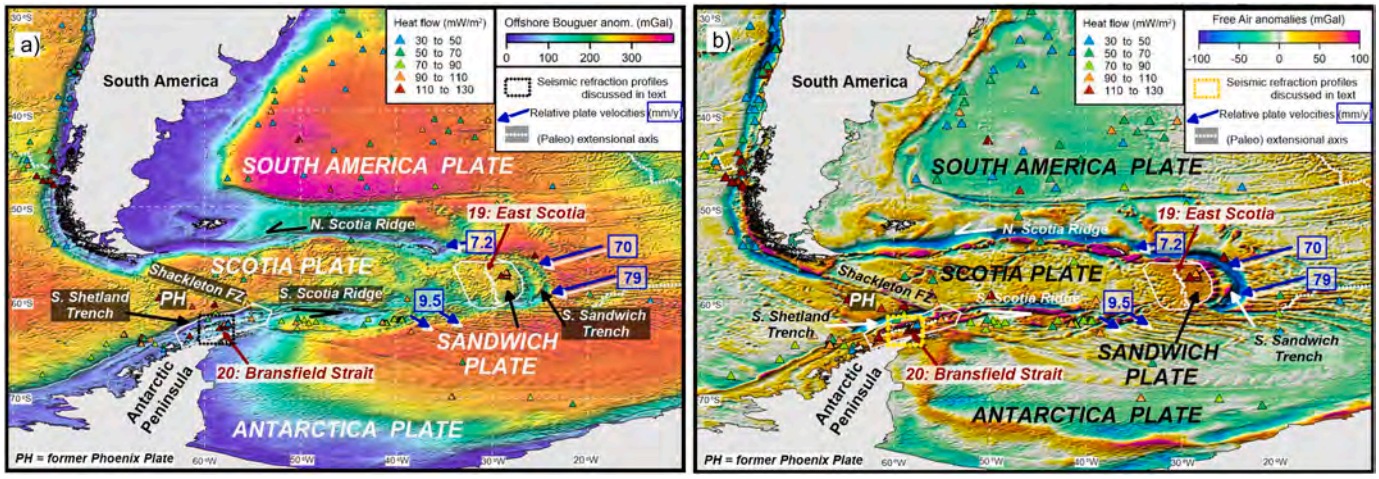

Fig. 6. Back-arc basins of the southern Atlantic (#19–20 in Fig. 1); BABs limits are shown by white outline; red text - BABs names and numbers. Background: Bouguer (a) and free-air (b) gravity anomalies over shaded relief. Symbols - heat flow measurements. Color codes are the same in Fig. 3-9. Black dotted box in the Bransfield Strait - region with seismic reflection/refraction profiles discussed in the text; white dotted line - inferred extensional axes in two BABs. For references see the text. Arrows with numbers in boxes - local rate of relative motion (in mm/y) of the major plate (South American or Antarctica) relative to the smaller plate (Scotia or Sandwich) (Thomas et al., 2003; Livermore, 2006). For locations of BABs 19 and 20 with respect to Antarctica see Fig. 9.

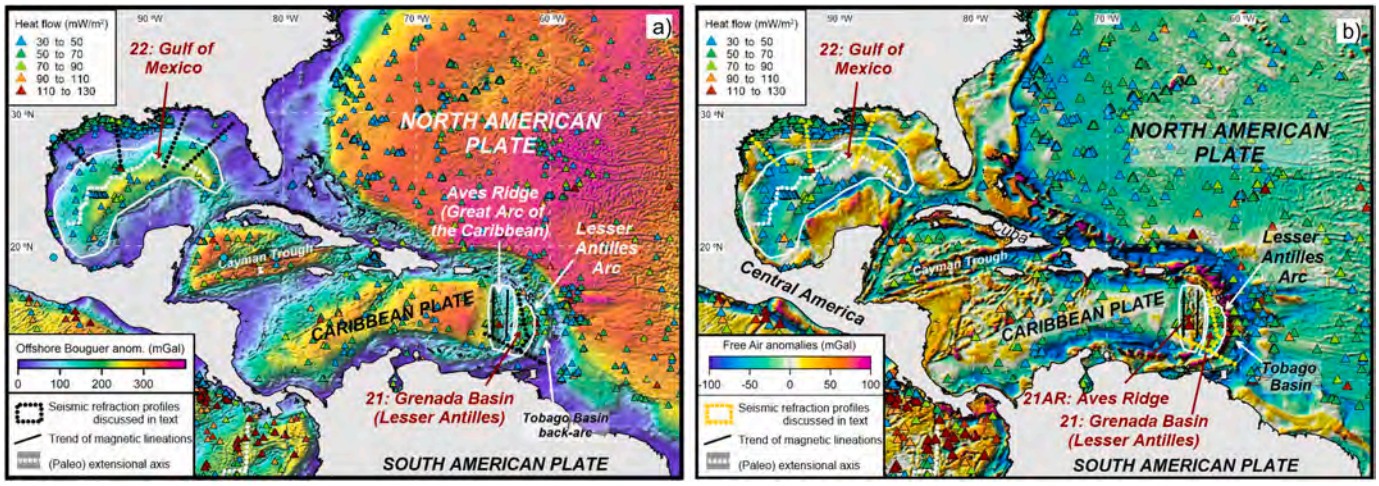

Fig. 7. Back-arc basins of the Caribbean (central Atlantics) (#21–22 in Fig. 1); BABs limits are shown by white outline; red text - BABs names and numbers. Background: Bouguer (a) and free-air (b) gravity anomalies over shaded relief. Symbols - heat flow measurements. Color codes are the same in Fig. 3-9. Black dotted lines - seismic reflection/refraction profiles discussed in the text; black solid lines - inferred major magnetic anomalies; white dotted lines - inferred paleo- or active extensional axes. For references see the text.

(spreading) rates in the Aleutian Basin cannot be constrained. The age of the basin basement is also still unknown.

Due to its remarkable N-S trend of magnetic lineations, common interpretations consider the Aleutian Basin as a fragment of oceanic crust trapped in the Paleogene by the Pacific subduction (Scholl et al., 1975; Cooper et al., 1992), and therefore this back-arc basin did not originate from lithosphere stretching behind the Pacific subduction. An alternative model regards the basin's oceanic crust as a Mesozoic Pacific oceanic terrane accreted to the North American Plate at 50–55 Ma (Scholl, 2016). Note that in these geodynamic models the Aleutian Basin is still a back-arc basin, because the mechanism of basin formation is not a part of the back-arc definition (see Introduction). These interpretations for the Aleutian Basin are in striking contrast to geodynamical models for other marginal basins of the north-northwest Pacific, which are conventionally explained by back-arc spreading behind a subduction-related volcanic arc. In line with these models, recent plate-kinematic reconstructions of the Pacific northwest since the Cretaceous suggest that the crust of the Aleutian Basin may have been formed 85–60 Ma in back-arc setting of the relict Olyutorsky intraoceanic arc (identified on-shore on Kamchatka, E. Sakhalin, and E. Hokkaido) (Vaes et al., 2019). Some recent interpretations argue for a possible Paleogene back-arc origin of the Aleutian Sea crust (Stern et al., 2012).

The Aleutian Basin is unusual in having negative free-air anomalies (ca. –15 mGal) since most other active back-arc basins have positive free-air anomalies (Table 1, Fig. 12a). This observation supports geodynamic interpretations that the basin may represent a trapped fragment of oceanic lithosphere, and the Aleutian Basin with an average oceanic bathymetry plots next to a ca. 100 Ma ocean and the extinct back-arc basins of the Pacific Ocean in a bathymetry–Bouguer anomalies correlation (Fig. 12b). Strong positive Bouguer anomalies (ca. +200 + 260 mGal) are typical of back-arc basins, but are significantly lower than in normal oceanic plates (Fig. 3). The basin has a relatively high heat flow of ca. 69 mW/m^2 after correction for the effects of sedimentation (Langseth et al., 1980), in overall agreement with later, still sparse, heat flow measurements which report slightly smaller values (Table 1).

The presence of oceanic crust below the Aleutian Basin with crustal

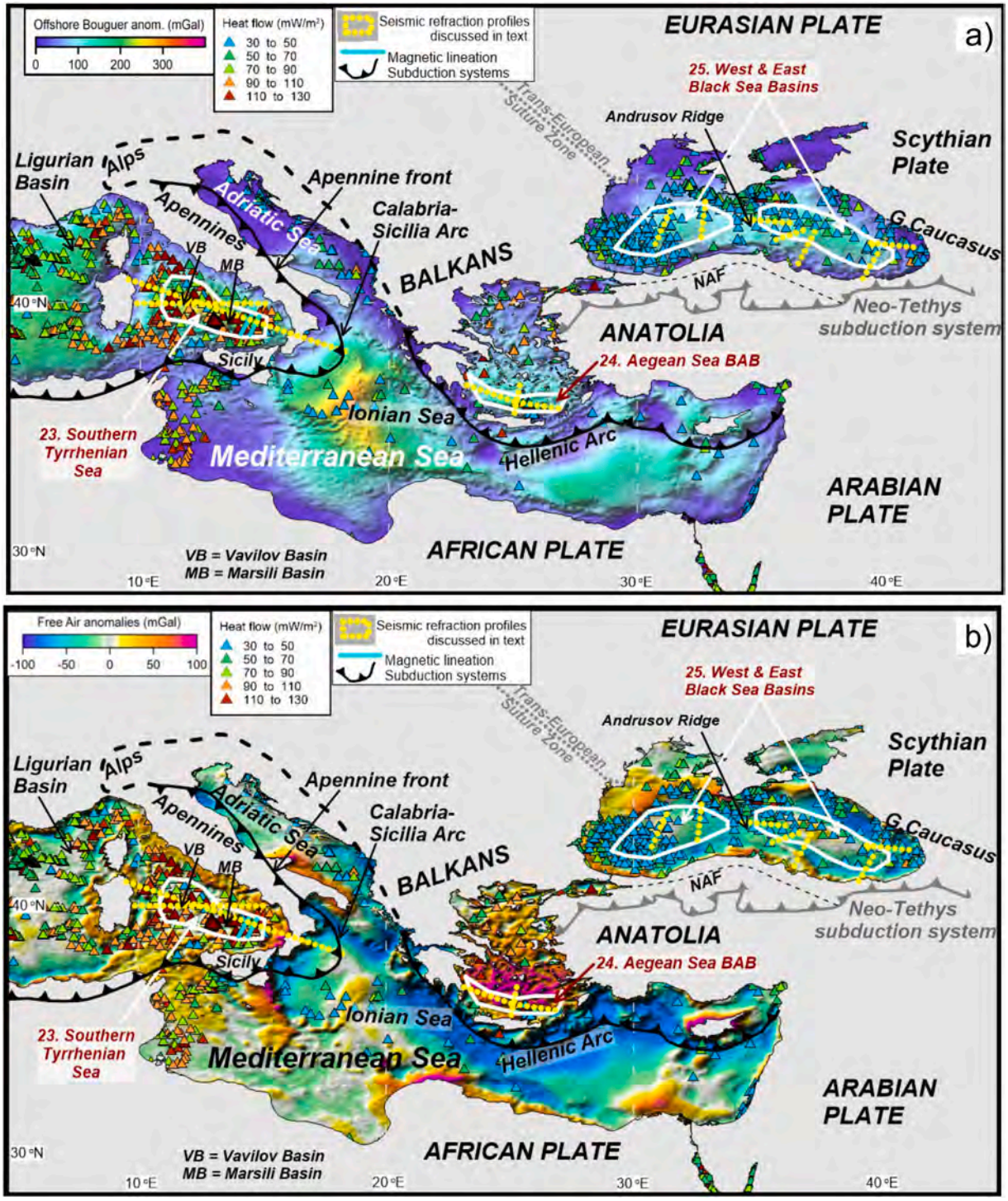

Fig. 8. Back-arc basins of the Mediterranean Sea - Black Sea region (#23–25 in Fig. 1); BABs limits are shown by white outline; red text - BABs names and numbers. Background: Bouguer (a) and free-air (b) gravity anomalies over shaded relief. Symbols - heat flow measurements. Color codes are the same in Fig. 3-9. Yellow dotted lines - seismic reflection/refraction profiles discussed in the text; cyan solid lines - inferred major magnetic anomalies in the Southern Tyrrhenian Sea. Black toothed line - active subduction systems of the Eastern Mediterranean Sea (dashed - inferred); grey toothed line - paleo-subduction systems of the Neo-Tethys realm. For references see the text.

thickness of ca. 7 km was proposed by early seismic refraction profiles in the south-eastern part of the basin (Ludwig et al., 1971) and across the Vitus Arch in its central part where magnetic lineations change the direction (Ludwig, 1974) (Fig. 3). Recent seismic refraction profiles with the length of ~450 km across the central part of the basin (the Vitus Arch) image thick sediments (2 to 5 km, on average ca 4 km thick) overlying a 7–9 km thick oceanic crust (Fig. 11) (Christeson and Barth, 2015). Basement velocities increase from ca. 5.5 km/s below the sedimentary cover to ca. 7.0 km/s at a 8 km depth below the seafloor, and reach upper mantle velocities of 8.1–8.2 km/s at ca. 12 km depth below the seafloor. Significant regional variations in the total crustal thickness (6.2 to 9.6 km at the Vitus Arch) are not related to changes in orientation of magnetic lineaments (Fig. 3) (Christeson and Barth, 2015).

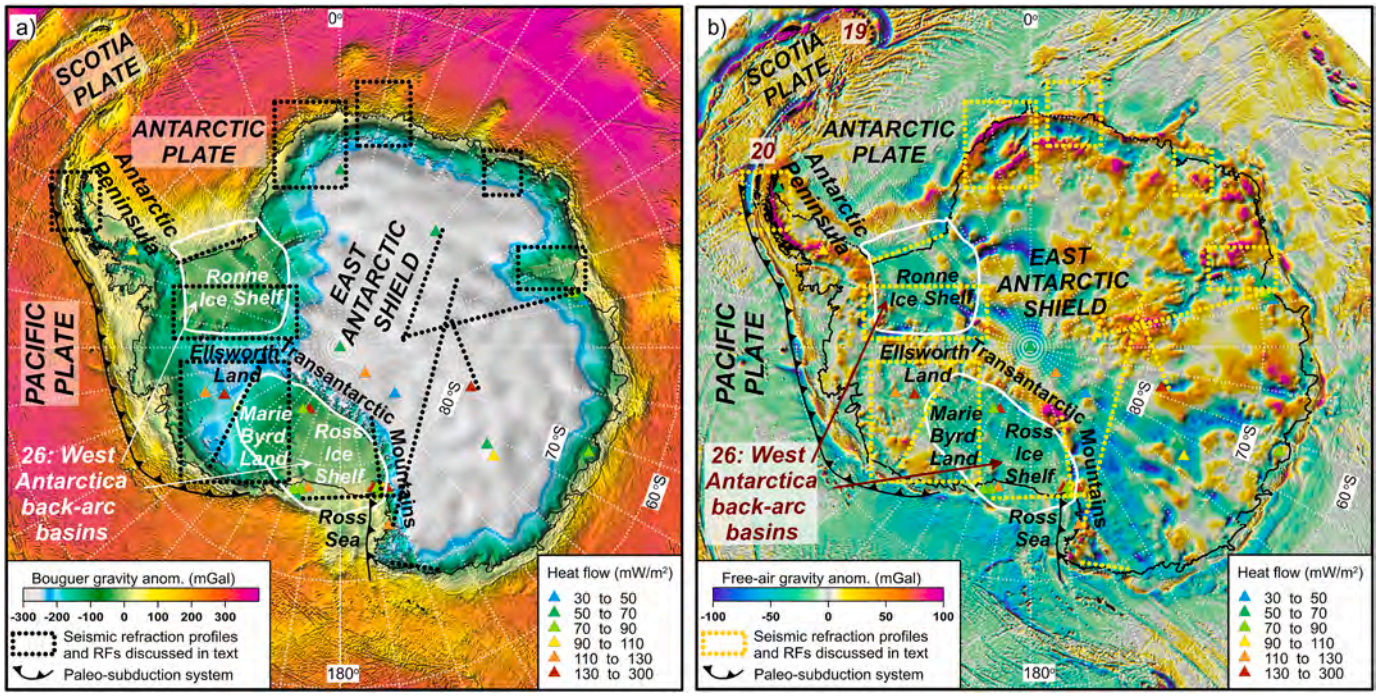

Fig. 9. Back-arc basins of the West Antarctica region (#26 in Fig. 1); BABs limits are shown by white outline. Background: Bouguer (a, note that the color scale is different from Figs. 3-8) and free-air (b) gravity anomalies over shaded relief. Symbols - heat flow measurements color-coded as in Fig. 3-8. Black dotted lines - seismic reflection/refraction profiles and receiver function studies discussed in the text. Black toothed line – extinct subduction system of the Phoenix (paleo-Pacific) Plate. For references see the text. High-resolution free-air gravity for the ice-covered Antarctica is based on Scheinert et al. (2016). Numbers 19 and 20 in (b) mark locations of the corresponding back-arc basins.

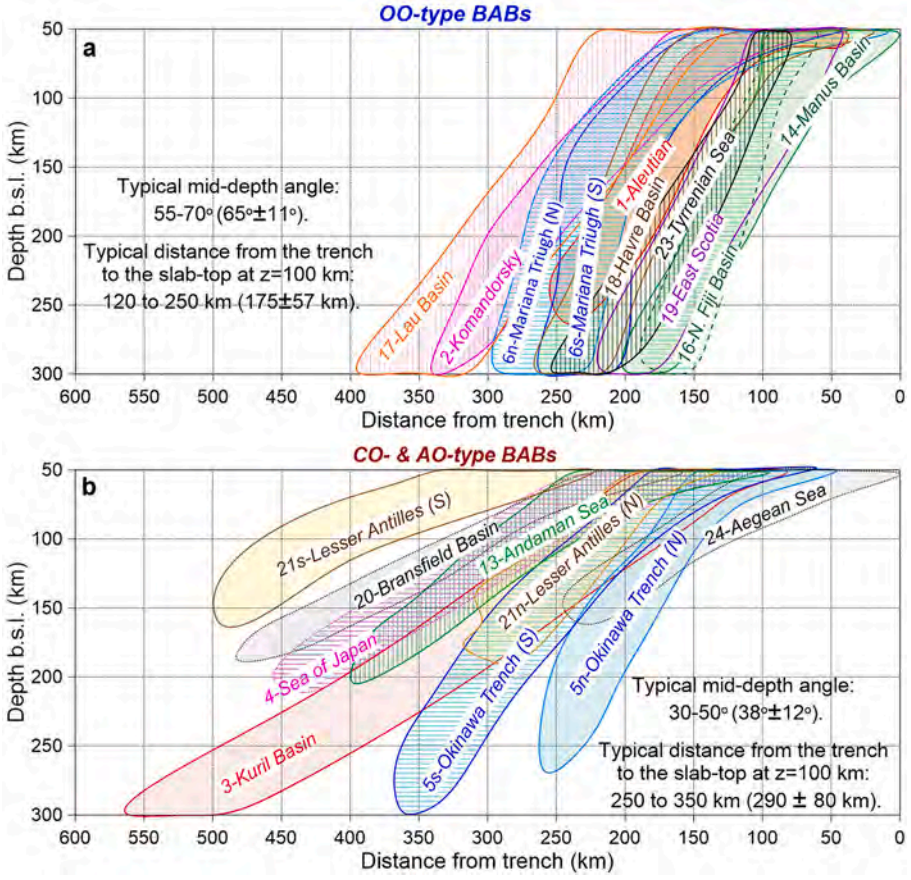

Fig. 10. Outlines of the seismogenic zones associated with ocean-ocean (a), arc-ocean and continent-ocean (b) subduction systems at the back-arc basins. See Table 2 for details.

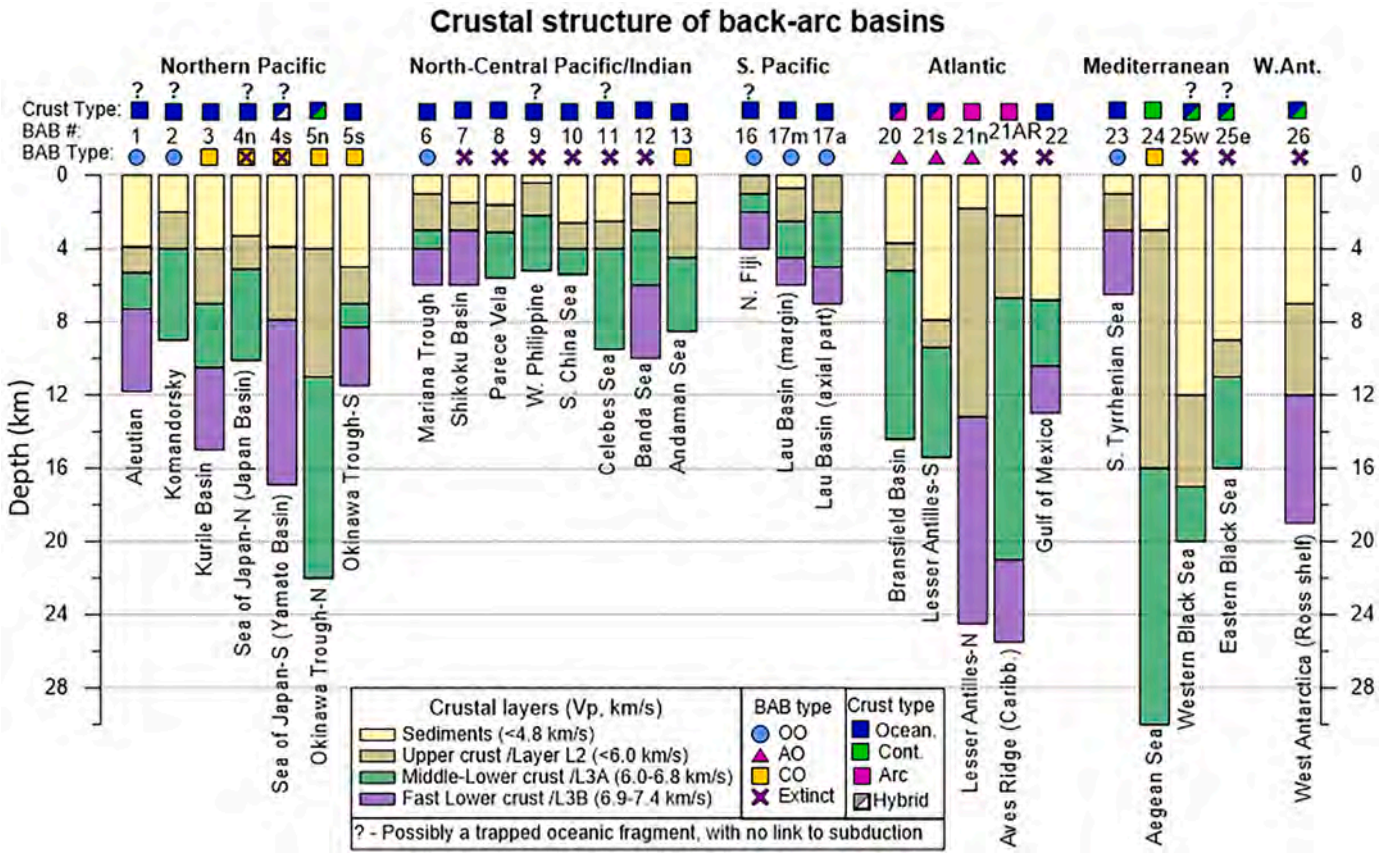

Fig. 11. Crustal cross-sections for the back-arc basins. Interpretations for the top of the lower crust and the top of the fast lower crust (transitions between Layer 2/Layer 3 and Layer 3A/Layer 3B in oceanic-type crust, respectively) are adopted from the original studies. For references to seismic models see the text. For some back-arc basins, interpretations of classical reflection/refraction seismic data are old and with low resolution for the internal crustal structure. For the Eastern Black Sea Basin (#25e) with controversial seismic models, recent results are used. Two crustal columns are shown for back-arc basins (#4, 5, 21, 25) where seismic models show large variations in crustal structure between different parts of BABs. For the Lau Basin, crustal columns show the structure at the extensional axis (#17a) and at the basin margin (#17 m). For the Lesser Antilles, the extinct Aves Ridge is shown for comparison (#21AR). The plot shows an extreme variability of crustal structure in back-arc basins. Symbols atop crustal cross-sections: the upper row – crustal type in BABs, BABs with hybrid (transitional) crust or where different crustal types are inferred are shown by 2 colors; bottom row - BABs grouped by the type of plate collision (OO: ocean-ocean, AO: arc-ocean, CO: continental-ocean); extinct BABs are shown as a separate group.

#2. Komandorsky Basin

The active Komandorsky Basin between Kamchatka and the Shirshov Ridge at the western edge of the Bering Sea formed behind the subducting Pacific Plate (ca. 60 My old along the trench) dipping at ~50–55° at intermediate depth (Jacobsen, 2018). The basin with water depth of 3.5–3.9 km (and much shallower at numerous seamounts) has a complex pattern of NE-SW trending magnetic anomalies and extinct spreading centers (Fig. 3), crossed by orthogonal NW-SE striking fracture zones (Baranov et al., 1991). The estimated age of the back-arc basin formation is 10–20 Ma based on interpretations of magnetic anomalies (Valyashko et al., 1993) and paleo-reconstructions with an estimated total extension of ca. 450 km (Vaes et al., 2019), which yields the total opening rate of 2–4 cm/y.

Similar to the Aleutian and Bowers Basins, the Komandorsky Basin has free-air anomalies of −20 to +20 mGal and Bouguer anomalies of about +250 mGal, and plots next to the Aleutian Basin in Fig. 10. Few heat flow measurements in the basin proper constrain a high mean value of ca. 110 mW/m^2 reducing to 50–60 mW/m^2 towards the basin margins (Fig. 3).

The age of the oceanic crust below the Bowers Basin bounded by the Bowers Ridge and the Aleutian Arc is unknown. The curved shape of the enigmatic intraoceanic arc of the Bowers Ridge suggests that the Bowers Basin was formed as back-arc basin, possibly in Miocene (Vaes et al., 2019), as supported by the presence of Oligo-Miocene arc volcanics on the Bowers Ridge. The only heat flow measurement in the central Bowers Basin (79 mW/m^2) at the SW edge of the Aleutian Basin is similar to the Aleutian Basin after correction for sedimentation.

All three deep basins of the Bering Sea have oceanic crust, but with a thin (<2 km) sedimentary layer in the Komandorsky and Bowers Basins. The seismic profile from the Aleutian Arc in the south to the Koryak margin in the north (Fig. 3) imaged the crustal structure of the Komandorsky and Bowers Basins (Ludwig, 1974). In the Bowers Basin, the crystalline crust has a 2 km thick Layer 2 (Vp ~ 5.6 km/s), underlain by a 5 km thick Layer 3 (Vp ~6.7 km/s). The crustal structure of the Komandorsky Basin is similar (Fig. 11), but it was resolved in less detail (Cooper et al., 1979). Apparently no deep seismic profiling was made in these basins in the later years.

#3. Kuril Basin

The active fan-shaped Kuril Basin located behind the Kuril arc (Figs. 1, 3) is a 3.3 km deep, ca. 250 km wide in its widest SW part, bathymetric depression in the Southern Okhotsk Sea. The basin opening related to subduction of the Pacific oceanic plate (ca. 125 My old at the Kuril Trench and dipping at ca. 45°) possibly started at Miocene/Oligocene (Gnibidenko et al., 1995). Its fan-shaped geometry was interpreted in terms of the clockwise rotation of the continental Okhotsk Plate (Kashubin et al., 2010) that led to a simultaneous opening of the Kuril Basin and the Sea of Japan back-arc basins (Kimura and Tamaki, 1986). Recent geochemical studies constrain spreading rates of ca. 1.5 cm/y (Werner et al., 2020).

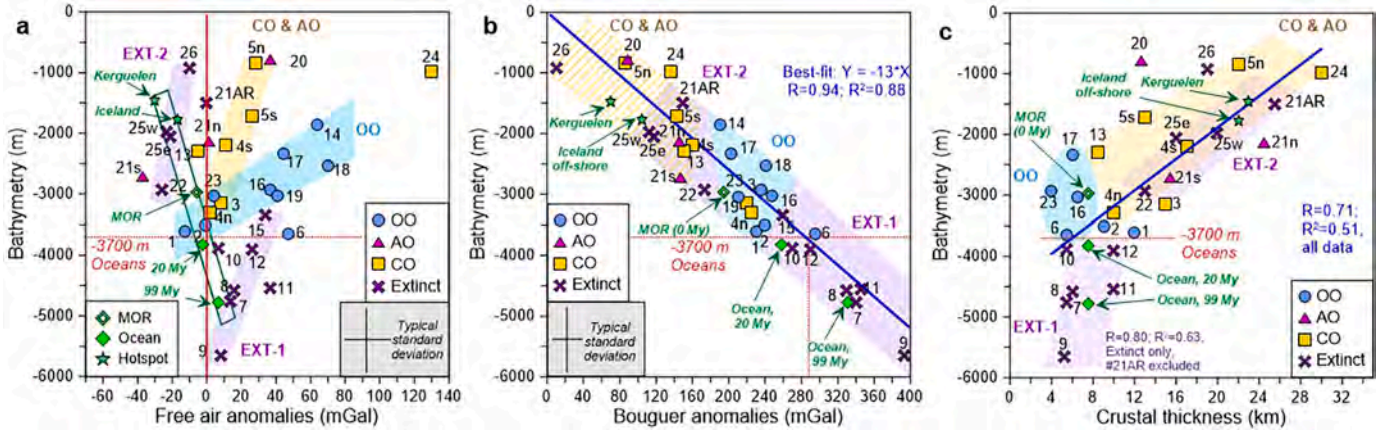

Fig. 12. Correlations between bathymetry, gravity anomalies (a, b) and crustal thickness (c) in back-arc basins of various types. Green symbols – average values calculated for the oceans on a 30′ grid; mid-ocean ridges (MOR) are for ages 0–2 My south of 55 °N latitude; young oceans - for ages 19–21 My, old oceans – for 99–101 My; off-shore hotspot regions include the 40–45 My Kerguelen Plateau (ca 66–71°E, 46–51 °S) (crustal data from Charvis et al., *1995*) and the active Iceland region (ca 12–18 °W, 60–62 °N) (cf. Artemieva and Thybo, 2013). Color shading highlights major recognized trends. In case of the isostatic equilibrium, all slopes are controlled by density contrasts between the crust, seawater, and the mantle. The OO-type BABs (blue shading) close to zero free-air anomaly have bathymetry and gravity characteristics between mid-ocean ridges and young oceans. Extinct back-arc basins (purple shading) split into two subtypes (a, b): the Pacific Ocean extinct BABs, possibly of the OO-type, plot similar to old normal oceans (EXT-1) and the non-Pacific extinct BABs, possibly of the CO- and AO-types, that plot close to the hotspots (EXT-2). Shallow bathymetry in the CO-type basins (yellow shading) may be due to a large portion of extended buoyant continental crust. Horizontal dotted red lines show average oceanic bathymetry; solid blue lines in (b, c) are best-fit lines for all BABs.

The Kuril Basin has no magnetic lineations characteristic of seafloor spreading (Table 2) and, in the absence of direct dredging or drilling sampling, its age is constrained mainly by sediment stratigraphy and bathymetry under assumption that the latter follows oceanic square-root-of-age plate model (Parsons and Sclater, 1977). It will be shown later (section 3.5) that this assumption is incorrect. A 2D thermal modeling along a NW-SE seismic profile from Sakhalin to the Pacific Plate explains the absence of magnetic anomalies in the Kuril Basin by partial demagnetization of lower crustal rocks with Moho temperature of 400–600 °C (Sychev et al., 1983). The basin is covered by a large number of heat flow measurements with common values of 70–80 mW/m^2, which increase to 90–110 mW/m^2 in its three sub-basins (Gnibidenko et al., 1995).

Similar to other back-arc basins, free-air anomalies are slightly positive and close to zero (ca. +10 mGal), suggesting that the basin is close to isostatic equilibrium. However, Bouguer anomalies of +200 + 250 mGal are similar to the back-arc basins formed by an ocean-ocean convergence (the OO-type), and significantly higher than in the back-arc basins formed by continental-oceanic collisions (the CO-type) (Fig. 12).

The Kuril Basin is crossed in its central part by a N-S trending long-range wide-angle seismic profile 2-DV-M (Kashubin et al., 2010) (Fig. 3, only the offshore segment is shown). The profile shows a sharp change in the crustal thickness from ca. 22–25 km in the shelf part of the Southern Okhotsk Sea, where the crust has characteristics of extended continental crust, to a typical oceanic crust in the Kuril Basin with a 7–8 km thick crystalline basement. Seismic studies image a 4–5 km thick tectonically undisturbed sedimentary fill with the oldest sampled sediments at the basin margin of Miocene/Oligocene age (Gnibidenko et al., 1995); thickness of sediments reduces to ca. 3 km at the extensional axis (Kashubin et al., 2010). Layer 2 (4.8–5.2 km/s) varies in thickness from 0.5 to 2 km, and Layer 3 (6.4–7.2 km/s) is 5–7 km thick, yielding 7–8 km for thickness of the crystalline basement (Bikkenina et al., 1987).

The western part of the Kuril Basin was crossed by several deep seismic sounding profiles (Fig. 3). Away from the extensional axis, they also image a 4 km thick sedimentary layer. However, the basement structure is interpreted differently (Piip and Rodnikov, 2004). It includes the upper 5–6 km thick basement layer with velocity between 4.8 and 6.8 km/s and the lower basement layer of a variable thickness (4 to 10 km) with velocity of 7.0–7.6 km/s (Fig. 11). The base of the lower layer is interpreted as the Moho, yielding total crustal thickness of ca. 15 km with the sub-Moho velocity of 7.9 km/s (Piip and Rodnikov, 2004). Alternatively, this fast-velocity layer may have composition of serpentinized peridotite as suggested by large amounts of these mantle rocks dredged and drilled on the Mid-Atlantic Ridge and by ophiolite studies (Minshull et al., 2003). In such a case, the seismic Moho corresponds to a 15 km thick crust in the Kuril Basin, while the petrological Moho corresponds to a 9–10 km thick crust, and marks the transition between lower crustal mafic rocks and mantle ultramafic rocks.

#4. Sea of Japan

The Sea of Japan (Fig. 4) includes a complex system of extinct back-arc basins formed along a continental margin in response to subduction of the Pacific Plate. Two major basins, the 3–3.6 km deep Japan Basin in the north (#4n) and the 2–3 km deep Yamato Basin in the south (#4s), are separated by the topographic high (the Yamato Ridge) with extended (22–26 km thick) continental crust (Sato et al., 2006).

Lineation of magnetic anomalies with NE (60°) trend is recognized in the central part of the Japan Basin, and it is less pronounced, but still recognizable, in the western part of the Japan Basin and in the Yamato Basin, although their presence in the latter was earlier questioned (Fukuma et al., 1998). Due to a complicated pattern of identified magnetic anomalies and lack of coherency in most of the Sea of Japan, their interpretations are non-unique (cf. Van Horne et al., 2017). Based on postulated symmetry of magnetic anomalies with respect to spreading, paleo-spreading centers were identified in both the Japan and Yamato Basins, with the proposed spreading rate of 3 cm/y (cf. Kobayashi, 1985). Other interpretations suggest spreading rate of 6–17 cm/y, assuming that ~500 km of extension was achieved in 3–8 My (Van Horne et al., 2017).

Two principally different models for the opening of Sea of Japan (a rotational 'saloon-door' model, Fig. 2i (Kimura and Tamaki, 1986; Otofuji, 1996) and a pull-apart model, Fig. 2h (Jolivet et al., 1994)) predict a different time for the start of back-arc opening: early Miocene or late Oligocene, respectively. Geophysical interpretations based on poorly delineated magnetic anomalies suggest that extension developed to seafloor spreading at ca. 28 Ma and ceased at ca. 18 Ma (Tamaki, 1995). Other studies based on ocean drilling ages suggest that extension began at ca. 23 Ma and developed to seafloor spreading by 20 Ma, and it is unlikely that the time of the opening differed between the northern

and southern parts (Van Horne et al., 2017). The later evolution of the region was significantly affected by the interplay of several subduction systems around Japan, associated with the subduction of the Philippine Plate in the south (present age along the volcanic arc is ~25 My) and the Pacific Plate in the north (130–140 My old along the arc and dipping at ~30-33^o (Kobayashi, 1985; Jacobsen, 2018)).

The Sea of Japan has one of the densest coverages by heat flow measurements (Fig. 4), which show a huge scatter in values. Typical values in both the Japan and Yamato Basins range between 50 and 90 mW/m^2 and increase to 100–120 mW/m^2 in the north-eastern part of the sea, where the presence of oceanic crust is inferred from seismic data (Tamaki, 1995). The difference between the two basins is also reflected in Bouguer anomalies, which are relatively low positive (+150 + 200 mGal) in the Yamato Basin and ca. 50 mGal higher in the Japan Basin, which plots within the OO-type in the Bouguer gravity-bathymetry plots (Fig. 10b), while free-air anomalies are near zero in both basins.

The Japan and Yamato basins, both with ca. 4 km of sediments, are interpreted to have oceanic crust where seismic profiles exist, but with a strikingly different crustal structure (Fig. 11) (Van Horne et al., 2017). For this reason, the Japan and Yamato basins are analyzed separately as #4n and #4s, respectively. The Japan Basin has a 8–10 km thick oceanic crust (No et al., 2014), while the Yamato Basin has an anomalously thick (15–19 km) oceanic-type crust similar to oceanic plateaux and with a ca. 9–10 km thick basal layer (Vp > 7.0 km/s) (cf. Tamaki, 1995; Sato et al., 2014). Its origin is debated, and while models with extended continental crust were also proposed, low velocities (<6.0 km/s) in the upper crust are used to argue for its oceanic origin (Sato et al., 2014).

#5. Okinawa Trough

The Okinawa Trough is an active ~1000 km long and relatively narrow (60–230 km wide) back-arc basin (Fig. 4) formed along the Ryukyu arc in response to the oblique subduction of the Philippine Sea Plate, the age of which progressively decreases along the trench from ~50 Ma in the northern segment of the basin to ~40 Ma in the south. There are systematic differences in most characteristics between the northern and southern parts of the Okinawa Trough recognized from geological and geophysical observations; therefore the two parts are further analyzed separately (#5n and #5s). The bathymetry is shallow (0.6–1.0 km) in the northern and central segments of the Okinawa Trough and exceeds 1.5 km in the southern segment with the maximum water depth of ~2.3 km reached within a relatively narrow (60–100 km wide) depression. The present convergence rate increases from ~7 cm/y in the north to ~13 cm/y in the south (Argus et al., 2011), while the intermediate-depth subduction dip angle decreases from 61^o in the north to 55^o in the south (Jacobsen, 2018).

Magnetic lineations are widely present in the southern and central parts of the Okinawa Trough but are apparently absent in the northern part which still undergoes rifting (Sibuet et al., 1995). Lithosphere extension started in Miocene (~10–6 Ma). Its second phase, which started ca 1–2 Ma and has continued until present, resulted in rifting (Sibuet et al., 1995). Despite a possible different onset of the rifting in the central-northern and the southern Okinawa Trough (c.f. Sibuet et al., 1995; Liu et al., 2016), the total amount of extension of ~80 km is similar in the northern and southern segments (Sibuet et al., 1995). The average extension rate in the southern segment is estimated 1–2 cm/y, assuming that the rifting started at ca 1 Ma (Park et al., 1998). However, the current extension rates are different in the central-northern and the south Okinawa Trough, 1–2 cm/y and 4–5 cm/y, respectively, although the details are debated (Imanishi et al., 1996; Arai et al., 2017).

The Okinawa Trough has unusually small positive Bouguer anomalies, around +70 + 90 mGal in the northern part (suggesting its lithosphere with a ca. 22 km thick crust essentially preserves the continental structure) and increasing to ca. +140 mGal in the southern part. Positive, typically around +20 + 30 mGal, free are anomalies suggest incomplete isostatic equilibrium, possibly associated with the on-going lithosphere deformation. The two parts of the Okinawa Trough and the two basins of the Sea of Japan define a clear trend of free-air anomalies – bathymetry correlation in the CO-type back-arc basins associated with continent-ocean collisions (Fig. 12a, yellow shading). The anomalously shallow bathymetry in the northern Okinawa Trough (#5n in plots) is likely to be essentially maintained by crustal buoyancy with, possibly, a little contribution from mantle flow.

The Okinawa Trough is covered by a large number of heat flow measurements. Most of them are highly anomalous and imply strong local effects of advection and hydrothermal circulation in thick young sediments. Heat flow is highly heterogeneous even when extremely low and high values are excluded (Fig. 4), and there is an overall trend with a lower heat flow (45–85 mW/m^2) in the northern part and a higher heat flow (typically >90 mW/m^2) in the south-central parts, although the southern tip has low heat flow values (around 45 mW/m^2).

The basin has a dense coverage by seismic profiles along and across the strike (Arai et al., 2017; Nishizawa et al., 2019). They show a progressive thinning of the crust from 18 25 km in the north to 10–16 km in the south, with thinning to 7 km locally (Fig. 11) (Nishizawa et al., 2019). Thus, seismic interpretations suggest that parts of the southern Okinawa Trough may still be in a transitional stage from continental rifting to seafloor spreading (Nishizawa et al., 2019). Thickness of sediments is similar along the strike, ca. 4–5 km, therefore thickness of the crystalline basement is ca. 15–20 km in the north and only 6–10 km in the south. Recent interpretations suggest that the northern Okinawa Trough has rifted continental crust, while new oceanic crust may possibly being formed in the southern part (Table 1).

#6. Mariana Trough

The Mariana Trough (water depth of ca. 3.5–4 km) is a part of the Izu-Bonin-Mariana subduction system which extends over ca. 2800 km along the Pacific margin (Stern et al., 2003) (Fig. 4). Based on the age of the basement rocks, the initial subsidence along the Izu-Bonin-Mariana system started at ca. 43–50 Ma, in response to the abrupt change in the motion of the Pacific Plate from a northward to a westward direction (Richards and Lithgow-Bertelloni, 1996). The oldest segment is the West Philippine Basin (see below, #10), and the ages of extension are getting younger eastwards to the extinct Shikoku - Parece Vela back-arc basins (#7–8) and to the presently active Mariana Trough back-arc basin (#6). Numerical modeling suggests a possible recent (10–5 Ma) development of a double subduction system related to the onset of a new subduction zone along the Ryukyu trench (Faccenna et al., 2018), which should have a control over the recent evolution of the Izu-Bonin-Mariana subduction system.

The Mariana Trough back-arc basin, bounded at the east by the Mariana arc, was initiated by rifting that began <10 Ma (Yan et al., *2022*) and evolved to seafloor spreading at ca. 3–4 Ma (Bibee et al., 1980) with total opening rate of 4.3 cm/y since 6 Ma (Jarrard, 1986). Along the trough, the present mid-depth subduction dip-angle is among the steepest worldwide, around 80^o (Table 2, Fig. 10a), with significant variations along the trench. The age of the Pacific Plate along the trench is ca. 150 Ma. Water depth is around 3.6 km with deepest parts at 4.2 km and the basin has an asymmetric bathymetry since the spreading axis is in the eastern part of the trough.

Bouguer anomalies are around +300 mGal in the central part of the Mariana Trough, and close to those in oceanic plates. Positive (+30 + 70 mGal) free-air anomalies indicating deviation from isostatic equilibrium may possibly be due to lithosphere deformation above a steeply dipping slab. This conclusion is supported by the observation that the Mariana Trough is the only back-arc basin of the ocean-ocean (OO) convergence type that falls outside the OO-type general trend (Fig. 12a, blue shading), therefore suggesting that free-air anomalies are caused not by deep sources but by lithosphere flexure. A highly heterogeneous heat flow ranges from ~30 to ~100 mW/m^2 with typical values around 60 mW/m^2.

Seismic data on the crustal structure of the Mariana Trough is limited (Fig. 4). A seismic refraction profile crossing the Mariana Trough Basin

at ca. 17° N imaged a 5.5 km thick oceanic crust away from the spreading axis, with crustal thickening to 8 km beneath the spreading axis (Takahashi et al., 2007; Grevemeyer et al., 2021). The unusually thin (~5 km) crystalline crust below a ca. 1 km of sediments is composed of two layers (~2 km and ~ 3 km thick) with velocities of 4.5–6.3 and 6.9–7.4 km/s (Fig. 11), respectively, and with significant lateral variations in velocity of the lower crust. At the trough axis, crustal thickness increases by 2 km by an increase in thickness of the lower crustal layer, where velocity decreases to 6.7–7.1 km/s. The velocity structure of the lower crust is in a sharp contrast with the adjacent Parece Vela Basin (#8, see below), which has a 4–5 km thick crust with a low Vp of 6.5–6.8 km/s in the lower layer. The difference between the crust of two back-arc basins can be caused by upper mantle chemical heterogeneity (Shulgin and Artemieva, 2019), a complex pattern of mantle melting (Martinez and Taylor, 2002; Lee and Wada, 2017) and the geometry of mantle wedge convective flow (Billen and Gurnis, 2001; Morishige and Honda, *2011*; Wirth and Korenaga, 2012), which may produce oceanic crust with a variable structure and different from oceanic crust created at mid-ocean ridges (Grevemeyer et al., 2021).

#7. Shikoku Basin

The extinct Shikoku Basin (water depth ca 4.2–5.2 km) is located in the northern part of the present Philippine Plate between the Kyushu-Palau Ridge to the west and the westernmost ridge of the Izu-Bonin arc to the east (Fig. 4). In the south, the basin merges with the extinct Parece Vela back-arc basin, and the two basins have similar evolution (Taylor, 1995).

A north-south trending long-wavelength magnetic lineation immediately east of the volcanic front of the Izu-Bonin arc was interpreted as evidence of back-arc rifting in the Shikoku Basin, where seafloor spreading has started at ca 26 Ma (based on the oldest identified magnetic lineation) and stopped at ca. 15 Ma (Yamazaki and Yuasa, 1998; Yan et al., *2022*). A widespread off-ridge magmatism after termination of spreading formed numerous seamounts (Taylor, 1995).

Free-air anomalies are close to zero in most of the basin, except for seamounts and the margins close to the bounding ridges where they become positive. Bouguer anomalies are very high (around +370 mGal) in the south-western, deep part of the basin and decrease to ca. +320 mGal in the northern part. This pattern associated with the bathymetry variations is, to some extent, repeated in heat flow, which (excluding highly anomalous values) is around 85–95 mW/m^2 in the southern part, ca. 80 mW/m^2 in the north-eastern part and only around 40 mW/m^2 in the north-western part (Fig. 4).

Seismic refraction profiles at the eastern margin of the Shikoku Basin image a ca. 8 km thick (in total) oceanic crust with 1–2 km of sediments (Suyehiro et al., 1996; Takahashi et al., 2009). Layer 2 with Vp ~ 5.6–5.9 km/s is ca. 1.5 km thick, and Layer 3 with Vp ~ 7.0 km/s has ca. 3 km in thickness (Fig. 11). By its geophysical characteristics, the Shikoku Basin is similar to the extinct back-arc basins of the Pacific Oceans, but differs from extinct back-arc basins of other oceans (Figs. 11-12).

#8. Parece Vela Basin

The extinct Parece Vela back-arc basin (typically nearly 5 km deep) south of the Shikoku Basin is located on the Philippine Plate between the extinct Kyushu Palau Ridge to the west and the extinct West Mariana Ridge to the east (Fig. 4). Its Spanish name meaning “sail-like” reflects the geometry of the basin. The geodynamic evolution of the Parece Vela Basin is similar to the Shikoku Basin in the north. A distinct pattern of lineated magnetic anomalies with a N-S axis is interpreted as seafloor spreading which started at Oligocene (29–27 Ma) and ceased in middle Miocene (ca. 15 Ma) (Okino et al., 1998; Yan et al., *2022*).

Similar to the adjacent West Philippine and Shikoku Basins, the basin has weakly positive (ca. +15 mGal) free-air anomalies and its isostatic equilibrium is only marginally disturbed by lithosphere flexure. Bouguer anomalies are high, typically +340 + 350 mGal, similar to oceans basins and have no regional pattern. Surprisingly, the basin has a strong asymmetry in heat flow, which is high to the east from the relict spreading axis (70–100 mW/m^2 with mean value of 85 ± 10 mW/m^2) and is unusually low in the western part (31–46 mW/m^2 with mean value of 40 ± 8 mW/m^2). On the whole, the basin-average value of 74 ± 25 mW/m^2 is similar to several other back-arcs basins of western Pacific.

The number of seismic refraction profiles across the basin is low. A seismic profile at the eastern part of the Parece Vela Basin at ca. 17.5° N (Fig. 4) imaged a ca. 6 km thick oceanic crust (Takahashi et al., 2007; Grevemeyer et al., 2021), with the velocity structure similar to the active Mariana Trough back-arc basin, but with a lower Vp in the lower crustal layer (Fig. 11). A 4–5 km thick crystalline crust is composed of two layers with velocities of 4.5–6.0 km/s and 6.6–6.9 km/s and thicknesses of ca. 1.5 and 2.5 km, respectively, overlain by a 1–2 km thick layer of sediments.

#9. West Philippine Basin

The extinct West Philippine back-arc basin (Fig. 4) is the largest basin on the Philippine Sea Plate and the deepest (typically 5.5 to 6 km) back-arc basin worldwide (Fig. 12, Table 1). It is separated from the Shikoku and Parece Vela basins in the east by the 2600-km-long Kyushu-Palau Ridge, which is an extinct N-S trending arc at the center of the Philippine Sea Plate. From the north-west, the basin is bordered by the Ryukyu Trench and from the south-west - by the Philippine Trench.

A clear pattern of NW-SE trending linear magnetic anomalies identified in most parts of the basin (Fig. 4) suggests that the West Philippine Basin was formed by a symmetric spreading from the Central Basin ridge, a NW-SE bathymetric high in the middle of the basin. Although many details remain controversial, spreading apparently had two distinct phases, with the change in the spreading direction and spreading rate after subduction started along the Kyushu-Palau Ridge at ~45 Ma (Hilde and Lee, 1984). The major phase of spreading at 60–45 Ma had a N*E*-SW direction with a rate of 8.8 cm/y. After 45 Ma, the spreading direction changed to N-S and slowed to 3.6 cm/y. Recent studies based on new magnetic data confirm that the spreading ceased at ca. 35 Ma (Sasaki et al., 2014), whereas the earlier proposed ages for the cessation of spreading varied between 26 and 39 Ma. The NW tip of the Philippine Plate may have an entrapped fragment of Early Cretaceous oceanic crust (Deschamps et al., 2000).

Free-air anomalies in the West Philippine Basin are near zero, suggesting a complete isostatic compensation of the basin. The basin with an anomalously deep bathymetry also clearly stands out by its extremely high Bouguer anomalies, ca. +400 mGal on average (Fig. 10b), and as high as +420 + 440 mGal in the southern part. A combination of an unusually large size of the West Philippine Basin with a pronounced pattern of magnetic lineation in most of the basin and unusually high Bouguer anomalies and deep bathymetry, not observed in other back-arc basins, is typical of oceanic plates (Figs. 4, 10), and suggests that (similar to the Aleutian Basin) the West Philippine Basin is a trapped oceanic fragment, rather than a relict back-arc basin (Table 2).

There is a significant number of good quality heat flow measurements (Fig. 4). Away from the relict spreading axis, heat flow is around 70 mW/m^2 with a pronounced low-heat flow anomaly (ca. 35 mW/m^2) in the east-central part of the basin. Along the paleo-spreading axis, heat flow is highly heterogeneous with an average of ~80 mW/m^2. The mean value for the basin (excluding unreliable data) is 70 ± 25 mW/m^2, reducing to 63 ± 17 mW/m^2 when the axial zone is excluded. Very sparse seismic refraction studies of the West Philippine Basin crust image a typical oceanic crust with total thickness of 5–6 km, a thin (<0.5 km) sediment layer and a thin Layer 2 (Fig. 11) (cf. Louden, 1980).

#10. South China Sea

The extinct South China Sea basin (water depth 3.7–4.5 km), surrounded from three sides by continental lithosphere of the Eurasian Plate and by the Manila Trench in the east, was formed through several extensional phases with ridge jumps. The basin has a pronounced

pattern of magnetic lineations which allows for reconstruction of the basin opening and identification of relict spreading axis (Fig. 4). Magnetic anomalies, discovered in early 1970's (Ben-Avraham and Uyeda, 1973; Rangin et al., 1985) are mostly E-W in the eastern part of the South China Sea and NE-SW in the western part of the basin. The first stage of the basin opening (32–27 Ma) included moderate extension with average full rate of ca. 5 cm/y. Following the ridge jump, the ridge orientation changed from E-W to ENE-WSW, at the second stage (27–16 Ma) extension rate decreased to ~3.5 cm/y, and the extension stopped at ca. 15.5 Ma along the entire ridge (Briais et al., 1993; Barckhausen et al., 2014).

The South China Sea has on average near-zero free-air anomalies, which however have a strongly asymmetric pattern with negative values (down to −20-30 mGal) in the northern part and high positive values (up to +50 + 70 mGal) in the southern part, suggesting deviation from the isostasy with a significant and heterogeneous lithosphere deformation. Strongly positive Bouguer anomalies are similar to most other back-arc basins and exceed +250 mGal in the central part of the basin (Fig. 12c). Heat flow is around 100 mW/m^2 throughout most of the basin with few values <80 mW/m^2 and is at the high end for the extinct back-arc basins (Table 1, Fig. 12d).

Several seismic profiles, mostly in the north-eastern parts of the South China Sea, constrain a thin (5–6 km) oceanic crust, however no details are provided (Zhao et al., 2010, 2018). These results are in accord with gravity modeling across the major bathymetric depression (4.5 to 4.0 km) in the central South China Sea, which predicts a ca. 5 km thick crystalline crust in the central part of the back-arc basin (Gozzard et al., 2018). Hyper-extended, <5 km thick crust, was also imaged seismically at the northern edge of the back-arc basin, close to the continent-ocean transition (Gao et al., 2016). A seismic profile crossing the South China Sea roughly from north to south imaged a sharp transition from a 18–20 km thick crust at the sea margins with shallow bathymetry to a very thin (~5 km) oceanic crust in the central part of the South China Sea (Fig. 11) (Pichot et al., 2014), where magnetic lineations are present. Likewise, a seismic profile across the northeastern margin of the South China Sea imaged a 13 km thick crust with ~2.5 km of sediments (Wang et al., 2006), suggesting an overall crustal thickening towards the continental margin. However, the back-arc basin proper at the end of the seismic line was poorly resolved.

#11. Celebes Sea

The extinct back-arc basins of the Celebes, Sulu and Molucca Seas to the south(east) of the South China Sea were formed in a complex geodynamic environment which presently includes active arc-arc or arc-continent collision zones (Rangin et al., 1990). The Celebes Sea and other small ocean basins between mainland Asia and the Pacific basin are interpreted either as back-arc basins, or entrapped fragments of older ocean basins, or extensional basins formed by rifting of the continental margin (Lewis, 1991; Nichols and Hall, 1999). This overview omits smaller basins and herewith focuses on the Celebes Sea basin.

The Celebes Sea (water depth 4.5–5.5 km) is bordered from the west by the Borneo archipelago, from the south and east - by the North Sulawesi and Cotabato Trenches, respectively, and from the north - by the Sulu island arc (Fig. 4). A complex series of paleo-plate boundaries, ridges and basins separate it from the South China Sea. Geodynamic models for the Celebes Sea formation include an inter-arc subduction-related back-arc basin, a rifted part of the Eurasian Plate, or part of the Philippine Sea basin (cf. Gaina and Mueller, 2007).

The oldest magnetic anomalies mapped in the western part of the Celebes Sea (trending ENE-WSW, 65^o) constrain ages 47 to 42 Ma (Weissel, 1980; Rangin et al., 1990), in agreement with ocean drilling results which reported middle Eocene ages for the basement (Lewis, 1991). The middle Miocene spreading rate is estimated as ca. 4.7 cm/y (Rangin et al., 1990), that is a half of the spreading rate in the West Philippine Sea Basin at the same time.

Most of the back-arc basin has positive free-air anomalies, +25 + 50 mGal, some of the largest among the extinct back-arc basins (Fig. 12a), which drop to −90-100 mGal in the Cotabato and North Sulawesi Trenches. Bouguer anomalies are also among the highest in back-arc basins, ca. +300 + 400 mGal as expected for deep basins (Fig. 12b). At the same time, the basin has one of the lowest heat flow values among the western Pacific back-arc basins. Most reliable measurements, consistent with earlier estimates, constrain the average heat flow of 58 ± 12 mW/m^2 (Lewis, 1991).

Several marine seismic refraction experiments of 1970-ies, compiled by Hayes (1978), imaged a 2–3 km thick sedimentary layer (with P-velocity of 1.7–2.1 km/s), a 1.5–2 km thick layer with velocity between 5.3 and 6.4 km/s, and a 5–6 km thick lower crustal layer (Vp ~ 6.4–6.9 km/s) (Fig. 11). The total crustal thickness is 9.5–11 km, with a 7–8 km thickness of the crystalline basement typical of oceanic crust. More recent seismic studies are still absent.

#12. Banda Basin

The extinct Banda Sea back-arc basin (Fig. 4) is separated from the Celebes Sea in the north by the complex collision between the island of Sulawesi and the Sula Platform (Rangin et al., 1990). The region represents one of rare examples of collision of the island arc (Banda arc) with the continental margin (the North Australian shelf), and the short Banda arc has the greatest curvature of any active arc on the Earth (Bowin et al., 1980). A linear pattern of magnetic anomalies (~70^o), observed only in a part of the Banda Sea, suggests that seafloor spreading may have started ca. 20–25 Ma (Lewis, 1991). Other studies argue that active phase of spreading was very short, between 6 Ma and 3 Ma (cf. Stern and Dickinson, 2010).

The bathymetry of the back-arc basin is highly heterogeneous, with short-wavelength variations from ca. 2.2 km to >5 km, and a typical water depth of 3.5–4 km. Most of the Banda Sea basin has positive free-air gravity anomalies (around +25 mGal). Their shift from the near-zero values may be related to the region's position on the southwest flank of the Earth's largest geoid maximum centered over eastern New Guinea (Bowin et al., 1980). Possibly for the same reason, Bouguer anomalies are also slightly higher (+250 + 350 mGal) than expected from the equivalent bathymetry in ocean basins of such age. Note that both free-air and Bouguer anomalies related to the total crustal thickness are typical of extinct back-arc basins of the western Pacific Ocean (Fig. 12, purple shading). Heat flow is highly heterogeneous (33 to >100 mW/m^2) and reflects a complex geodynamic setting of the Banda Sea. Most reliable heat flow measurements in the South Banda Sea constrain moderate average values of 60–65 mW/m^2 or less (Bowin et al., 1980); later data increased this value to ca. 80 mW/m^2 (Fig. 4).

An old seismic refraction experiment in the central Banda Sea basin (Purdy and Detrick, 1978) reported sediment thicknesses of ca. 1 km atop of oceanic-type crust with 1.5–2.0 km thick Layer 2 (Vp ~ 4.97 km/s, Poisson's ratio ~ 0.33), 2.0–3.5 km thick Layer 3A (Vp ~ 6.47 km/s, Poisson's ratio ~ 0.25–0.28) and an unusually thick (2.5–4.6 km) Layer 3B (Vp ~ 7.18 km/s) underlain by mantle with velocity of 7.97 km/s (Fig. 11). Apparently, no other seismic studies of the Banda Sea crustal structure have been published since then.

2.3. BABs of the Indian Ocean

#13. Andaman Sea

The Andaman Sea is an active back-arc basin in the northwestern part of the Sunda subduction system in the north-eastern part of the Indian Ocean (Figs. 1, 4). Its origin is related to a very oblique subduction of the Indian-Australian Plate (with age along the trench of ca. 70 My in the north and ca. 85 My in the south) beneath the Sunda Plate (Curray, 2005), with the current mid-depth subduction dip angle of ca. 40^o (Fig. 10b). The combination of back-arc extension and the strike-slip motion created a series of extensional basins which opened obliquely starting from ~32 Ma in the Mergui Basin in the south of the Andaman Sea back-arc basin.

Interpretations of magnetic lineations identified in the southwestern part of the back-arc basin (Raju et al., 2004) indicate a ca. 120 km opening in the last ca. 4 My, with the total opening of up to 460 km over the last 11 My (Curray, 2005). These numbers yield opening rate of 3–4 cm/y, close to the estimated total opening rate of 3.7 cm/y since 13 Ma (Jarrard, 1986). The spreading center is marked by a 12 km wide valley with water depth of ca. 3.6 km, while most of the back-arc basin is around 2–3 km deep.

Free-air anomalies, overall close to zero, are weakly positive in the western part and slightly positive along the eastern margin of the back-arc basin with weakly negative values elsewhere. Bouguer anomalies are relatively small, around +150 mGal, with higher values (ca. +230 mGal) along the spreading axis. By the correlations between gravity anomalies, crustal thickness and bathymetry, the Andaman Sea is similar to the back-arc basins formed in ocean-ocean collisional settings (Fig. 12). Heat flow measurements exist only along the western margin, with the values around 90 mW/m^2 (Table 1) and dropping to 30–40 mW/m^2 in the trench.

Numerous reflection profiles show a highly variable thickness of sediments, ranging from ca. 1 km to 5 km and more (Curray, 2005), and possibly affected by the Bengal Fan sedimentation. Two N-S high-resolution seismic reflection profiles across the spreading center of the central Andaman back-arc basin image ~1.5 km thick sedimentary layer which thickness decreases towards the flanks (Jourdain et al., 2016). Assuming P-wave velocities typical for oceanic crust, the interpretation of the crustal structure includes a 3 km thick upper crustal layer and a 3–4.8 km thick lower crust, with total crustal thickness of ~6–7.8 km (Fig. 11). Crustal-scale seismic refraction/wide-angle reflection studies are, apparently, limited to few profiles acquired in 1960–1970's along the northern and eastern margins of the back-arc basin (Curray, 2005). Thus, the details of the back-arc crustal structure remain yet poorly constrained.

2.4. BABs of the south-western Pacific Ocean

#14. Manus Basin (Bismarck Sea)

The Manus Basin in the west-equatorial Pacific Ocean is part of the Bismarck Sea basin. Bounded by New Guinea in the west, the Manus Trench in the north and east, and the New Britain Trench in the south-east, it is an active back-arc basin with respect to the New Britain arc-trench system (NBT in Fig. 5). The ENE-WSW trending magnetic lineations, identified only in the eastern part of the basin, are interpreted as evidence for asymmetric seafloor spreading (spreading direction 60^o) during the past 3.5 My with the total opening rate of 13.2 cm/y (Taylor, 1979). The mid-depth subduction angle is ca. 63^o and similar to most other active back-arc basins (Fig. 10a, Table 2).

Free-air anomalies in the Manus Basin are unusually high, ca. +65 mGal, suggesting on-going lithosphere deformation. Together with the Havre Basin (#18, see below), the Manus Basin is the end-member of the OO-type back arc basins on the free-air gravity versus bathymetry plot (Fig. 12a, blue shading) which indicates a likely contribution of the vertical component of mantle flow (e.g. caused by temperature-induced lateral density variations) in maintaining its unusually shallow bathymetry (ca. 1.9 km) (Molnar et al., 2015). This conclusion is in agreement with Bouguer anomalies which are significantly lower than typical for back-arcs, between +140 and + 220 mGal, suggesting low-density mantle (e.g. due to high mantle temperatures) below this active back-arc basin. Two heat flow measurements have very different values of 38 mW/m^2 in the center and 107 mW/m^2 at the margin. The lower value measured at the end of the spreading axis (as interpreted from magnetic anomalies) may be more representative of regional heat flow. There is, apparently, no seismic data on the crustal structure of the Manus Basin.

#15. Woodlark Basin

Despite its very small size, the extinct Woodlark back-arc basin provides important details on the transition from intra-continental rifting to seafloor spreading (Taylor et al., 1995). The basin located on the Australian Plate between the Papuan Peninsula of New Guinea and the Solomon Islands (Fig. 5) formed by the collision between the Ontong-Java Plateau of the Pacific Plate and the New Guinea continental extension of the Australian Plate (Taylor and Karner, 1983), although other studies propose the rifting of continental and arc lithosphere that has initiated seafloor spreading after ca 2 Ma (Martínez et al., 1999). This created a complex deformation style within the basin, which has later started subducting eastwards beneath the Solomon arc.

Detailed geophysical surveys identified three segments of seafloor spreading separated by ~50 km-long and ~ 30 km-long transform faults. The basin has a symmetric, roughly E-W trending, pattern of magnetic anomalies, with two jumps at the transform faults. The total opening rate of the back-arc basin is between 5.6 and 7.2 cm/y. Seafloor spreading initiated in the eastern part of the basin at ca. 6 Ma (Martínez et al., 1999), and propagated westwards with an estimated rate of 14 cm/y (Taylor and Huchon, 2002) so that in the western part of the basin seafloor spreading began <2 Ma.

East-west variations in water depth and gravity anomalies reflect the evolution of lithosphere extension in the Woodlark Basin with westward propagation of stretching. Water depth shallows from ca. 3.5 km in the eastern part to ca. 2.5–2.9 km in the western part. Free-air anomalies, slightly positive in the entire basin, reach ca. +50 mGal in its eastern part, which undergoes deformation. The basin follows the free-air gravity versus bathymetry trend of the extinct Pacific back-arc basins (Fig. 12a, purple shading) where it plots at the shallow end, with an additional topographic support possibly coming from elastic stress due to lithosphere flexure. Similar to free-air anomalies and reflecting the bathymetry change, Bouguer anomalies increase from +220 mGal in the west to ca. +270 mGal in the east. Gravity modeling indicates that the older, eastern basin has a < 7 km thick oceanic crust and the difference between water depth and Bouguer anomalies between the eastern and western parts can be explained by a 2 km thicker crust or a thinner lithosphere in the western basin (Martínez et al., 1999).

There are, apparently, no seismic refraction studies of the Woodlark Basin to test the gravity model, and all regional seismic models focus on the very western part of the basin. A seismic tomography model at the basin's youngest westernmost tip (ca. 151.5°E, 9.5 ^{o}S, Fig. 5) imaged an oceanic-type crust with a relatively low Vp (<6.0 km/s) in a large fraction of the crust. Due to limitations in ray coverage, crustal thickness of 15–20 km was inferred from seismicity recorded at the ocean bottom array (Zelt et al., 2001). Further westwards, between the western Woodlark Basin and the Papuan peninsula, receiver function analysis indicates the Moho depth of 22–32 km (i.e. crustal thickness of 20–30 km) (Abers et al., 2014), although in the same region a Rayleigh-wave tomography study imaged the upper mantle with a shear-velocity structure similar to mid-ocean ridges (Jin et al., 2015). Four heat flow measurements in the back-arc basin range between 37 and 74 mW/m^2 (excluding values of 100–115 mW/m^2 at the basin flanks). Low values are all measured at the younger, westernmost end of the basin.

#16. North Fiji Basin

The active North Fiji Basin (Fig. 5) was created by back-arc spreading behind the active eastwards-dipping New Hebrides (Vanuatu) subduction zone produced by convergence of the Pacific and Indo-Australian Plates. The basin is limited by the Vanuatu island arc in the west and south-west, the Vitiaz paleo-trench in the north, the Fiji Islands in the east, and the Hunter Fracture Zone in the south-east. The extension history of the basin is reviewed in detail by Auzende et al. (1988, 1995). Most models agree that the basin formed ca. 10 Ma ago as a result of the clockwise rotation of the Vanuatu arc and the counterclockwise rotation of the Fiji Islands, that is apparently similar to the Sea of Japan and with no certain link between the basin opening and the subduction (e.g. Fig. 2i). A N-S trending seafloor spreading zone was initiated ca. 4 Ma ago in the central part of the basin and it is still active at present. An

average total spreading rate over the past 2 Ma is estimated as 6.2–8.2 cm/y (Auzende et al., 1988) and the present convergence rate is 9–12 cm/y around most of the Vanuatu arc, except for its central segment (Baillard et al., 2015). The geometry of the seismogenic zone indicates a steep subduction at 90–150 km depth with dip angle of ~70° (Baillard et al., 2015) with an overall geometry similar to the Tyrrhenian Sea and the East Scotia arcs (Fig. 10a); the age of the downgoing plate is ~57 Ma (Collot et al., 1985).

Magnetic lineations typical of oceanic crust have several segments. The central part of the basin (between 21 and 17 °S) has N-S trending anomalies, which correspond to the recent and still active basin opening (Auzende et al., 1995). The magnetic pattern becomes complicated in the NE part of the basin, where it splits into several segments with a NW-SE trend which results from the superposition of the past rotational and the present plate motions.

The eastern and western parts of the basin are slightly different in bathymetry and gravity. The basin is shallow with water depth of about 3 km, slightly deeper in the western part (~3.2 km) and ~ 2.7 km in the NE part. Strongly positive free-air anomalies range from ca. +30 mGal in the east to ca. +50 mGal in the west. Likewise, Bouguer anomalies range from +220 mGal in the NE basin to +270 mGal in the western basin. The pattern is similar to the Woodlark Basin (#15) and possibly reflects progression of lithosphere extension in the North Fiji Basin.

Early studies from the 1970's reported high average heat flow in the North Fiji Basin (116 mW/m^2) with significant regional variations. The IHFC database (Fuchs et al., 2021) shows that high heat flow (109–168 mW/m^2) is typical mostly of the central-western basin, while low values (30–60 mW/m^2) dominate away from the spreading center. Average basin heat flow based on reliable 26 heat flow values in the IHFC database is 80 ± 32 mW/m^2 (excluding 3 anomalous values between 160 and 168 mW/m^2).

Few low-resolution seismic refraction studies (Larue et al., 1982; Kisimoto et al., 1994) reveal a very thin (ca. 0 km) sedimentary cover and a thin oceanic-type crust in the central basin around the spreading axis. Away from the axial zone, the total crustal thickness in the central basin is ca 4 km only, and the lower 2 km have a high Vp ~ 7.0 km/s (Fig. 11). The pattern may reflect a strong recent stretching of oceanic crust, possibly essentially compensated by magmatic additions. A similar crustal structure was identified in old refraction experiments in the NE and SW parts of the basin, with the total crustal thickness of ca. 5.7 km and 6.5 km, respectively, low average crustal velocities (<6.5 km/s) and 1–2 km of sediments (Shor et al., 1971).

#17. Lau Basin

The active and shallow V-shaped Lau Basin (water depth ca. 2.3 km) is one of the best studied classical examples of back-arc basins. The basin is located behind the Tonga Arc which was formed by the subduction of the Pacific Plate below the Indo-Australian Plate (Fig. 5). Along the trench, an intermediate dip angle of the west dipping Pacific slab (age ~ 110 Ma) is ca. 55° (Jacobsen, 2018). While the dip angle is similar to other back-arc basins formed by ocean-ocean collision, the seismogenic zone below the Lau Basin is most displaced from the trench (Fig. 10a), so that the slab is at ca. 250 km depth below the Lau Basin spreading axis (Table 2). The southern extent of the basin is marked by the subduction of the Louisville Ridge (hotspot track) below the Tonga-Kermadec arc system. The western side of the back-arc basin is delimited by the remnant Lau Ridge volcanic arc (active at ca. 14–2 Ma (Hawkins, 1995)) at the eastern edge of the Indo-Australian Plate. The Lau Ridge was partially dismembered by crustal extension in the Lau Basin.

Ocean drilling data indicate that the present seafloor spreading started at ca. 5.5–5 Ma in the north, from where it propagated southwards, as suggested by the V-shape of the basin (Hawkins, 1995). The pattern of magnetic anomalies is complicated and their interpretations are controversial. Geodetic measurements in the Tonga-Lau region revealed the fastest observed crustal movements, which constrain the present opening rate of the northern Lau Basin of ca 16 cm/y caused by seaward rollback of the trench axis (Bevis et al., 1995). Presently, the Lau Basin is opening along three spreading segments.

The Lau Basin has extremely consistent positive free-air anomalies of ca. +45 mGal commonly attributed to an efficient mantle wedge flow (Martinez and Taylor, 2002). Bouguer anomalies are weakly positive +170 + 220 mGal, with higher values along the spreading axis. By gravity anomalies and bathymetry, the Lau Basin is a typical example of active back-arc basins formed by an ocean-ocean collision (Fig. 12). Except for three high values (97–124 mW/m^2) near the spreading axis, heat flow is unusually low for an active basin with an average of 45 ± 12 mW/m^2 based on about 20 heat flow measurements (Fig. 5).

A recent seismic refraction profile across the Tonga Ridge and the Lau Basin at 18.5° S imaged the crustal structure of the northern Lau Basin (Crawford et al., 2003) (Fig. 4). At the Central Lau Spreading Center, the crust is 7 km thick, and includes a 2 km thick Layer 2 (Vp < 6.0 km/s, interpreted as sheeted-dike section), a 3 km thick intermediate-velocity Layer 3A (Vp ~ 6.0–7.0 km/s) and a 2 km thick fast-Vp (7.0–7.4 km/s) Layer 3B (Fig. 11). The crust thins by ca. 1 km away from the spreading center, despite a 0.5–1 km thick layer of sediments is present there. Away from the spreading center, Layer 2 preserves the same thickness as in the axial zone, but Layers 3A and 3B reduce to 2 km and 1.5 km, respectively, yielding the total crustal thickness of ca 6 km. A seismic experiment at the south-eastern Lau Basin imaged a much thicker crust (8.7 km) with ca. 2.5–3 km of sediments and with a thick lower crustal layer (2.5–3.2 km) (Turner et al., 1999).

#18. Havre Basin

The Havre Basin (Fig. 5) shares its geodynamic evolution with the Lau Basin located northwards, so that most publications consider the Lau-Havre Basin system together (Karig, 1970). Indeed, some characteristics are similar in both basins (Table 1). The basin is bordered to the west by the remnant Colville Ridge (volcanic arc) and to the east by the Kermadec Ridge, related to the Pacific Plate subduction (intermediate depth dip angle ~64°) underneath the Indo-Australian Plate. Importantly, the Lau and Havre basins have significant differences in the displacement of the seismogenic zone from the trench (Fig. 10a), suggesting significant differences in the Pacific Plate rollback dynamics. Indeed, recent seafloor spreading at the Havre Basin started ca. 5.5–5.0 My ago in response to the rollback of the subducting Pacific Plate and terminated abruptly ca. 3.0–2.5 My ago (Tontini et al., 2019). However, the pattern of magnetic anomalies is controversial, and an obvious spreading ridge is absent. These data, interpreted as the lack of evidence for the present-day seafloor spreading, led to interpretations that the Havre Trough may still be in a rifting phase (Wright, 1993; Parson and Wright, 1996; Tontini et al., 2019), while the Lau Basin has seafloor spreading.

Free-air gravity anomalies in the Havre Basin are among the largest in all back-arc basins and increase from ca. +40 mGal in the west to ca. +90 mGal in the east along the Kermadec Trench. Their average value is the end-member on the bathymetry – free-air gravity plot for the OO-type basins (Fig. 10a), and suggests that mantle dynamic component (possibly associated with the Louisville hotspot) may contribute to isostatic disequilibrium. Bouguer anomalies, mostly between +210 + 250 mGal are typical of the OO-type basins with seafloor spreading (Fig. 12c).

There are, apparently, no seismic data on the crustal structure, except that MCS (multi-channel seismic) data show the presence of 0.5–1.5 km of sediments (Tontini et al., 2019). Heat flow measurements are also absent. In further analysis, I consider the Havre Basin as the OO-type, formed in response to the collision of two oceanic plates, and the basin formed on the overriding oceanic plate should clearly have oceanic crust.

2.5. BABs of the Atlantic Ocean

#19. East Scotia Sea

The East Scotia Sea, an active back-arc basin in the southern Atlantic Ocean, has been described as "a complication of the SAM (South America) - ANT (Antarctica) plate boundary" (Barker, 1995). The slow relative west-east motion of the South America and Antarctica Plates is accommodated at the northern and southern boundaries of the Scotia Plate (Fig. 6), which in turn was also formed by extinct back-arc spreading (32 to 7 Ma) (cf. Livermore, 2006).

The East Scotia Sea was formed by spreading at the East Scotia Ridge spreading center, behind the east-migrating South Sandwich Trench, where oceanic lithosphere of the South American Plate is being subducted at the eastern boundary of the Sandwich Plate. Relative motion of the South America and the Sandwich Plates is 70–79 mm/y (Thomas et al., 2003). Along the trench, the age of the subducting plate varies from 27 Ma in the south to ca. 80 Ma in the north, and the dip angle changes from 45° to 55° above 180 km depth (Barker, 1995) to ~63° and more at a greater depth (Fig. 10).

The N-S trending East Scotia Ridge in the central part of the basin is one of the longest-lived back-arc spreading centers with the seafloor spreading age of 15–17 Ma based on magnetic lineations on the western side of the ridge. However, the age of extension at the southernmost tip of the East Scotia spreading center is ~1 Ma only. Spreading rates were accelerating towards the present values of 6.2 cm/y in the north and 7.0 cm/y in the south. The total opening of the East Scotia Sea is ca. 650 km and the present-day rate of rollback of the subduction hinge is estimated as 3.5–5.0 cm/y (cf. Livermore, 2006).

Free-air anomalies of +30 + 45 mGal indicate deviation from regional isostasy. Bouguer anomalies are very uniform, around +250 mGal, and similar to many back-arcs basins (Fig. 12). Typical water depth is ca. 3.0 km and slightly deeper in the western part of the basin. Heat flow measurements exist only in the eastern part of the East Scotia Basin. All values are above 90 mW/m^2 with a mean heat flow of 115 ± 21 mW/m^2, which is among the highest heat flow in the back-arc basins. Crustal-scale seismic studies are absent for the East Scotia Sea back-arc basin.

#20. Bransfield Basin

The Bransfield Strait between the tip of the Antarctic Peninsula and the South Shetland Islands (Fig. 6) is an active back-arc basin formed by rifting within a continental volcanic arc of the Antarctic Peninsula. The associated South Shetland Arc is a remnant of paleo-subduction of the former Phoenix Plate below the entire Pacific margin of the Antarctic Peninsula. At ca. 4 Ma, the lithosphere extension between the Phoenix and Antarctica Plates stopped, and the Phoenix Plate became a part of the Antarctica Plate (Lawver et al., 1995). Along the South Shetland Trench, the age of the SE-subducting Phoenix Plate increases from 14 Ma in SW to 23 Ma in NE. Its dip angle of 25° is the smallest among the back-arc basins worldwide (Fig. 10b, Table 2). The extension in the Bransfield Strait is 4–5 My old and possibly as young as 1.5 My (Lawver et al., 1995), although alternative estimates are possible (Solari et al., 2008). GPS studies indicate the present NW-SE extension rate of ~10 mm/y (Dietrich et al., 2001).

The basin is an unusually shallow with a typical water depth of ca. 0.8 km. However, the bathymetry is highly variable and ranges from ca. 0.5 km in SW to ca. 2 km in the central part and to 2.2–2.5 km close to the NE end. Free-air anomalies are also very heterogeneous, typically around +30 + 40 mGal. Bouguer anomalies between +50 and + 120 mGal are among the smallest of all back-arcs basins worldwide and reflect its shallow bathymetry (Fig. 12). Numerous heat flow measurements are mostly along the spreading axis with nearly all values >100 mW/m^2 yielding a very high mean heat flow of ca. 120–125 mW/m^2 and around 100 mW/m^2 when the extreme values are excluded (Table 1). This combination of shallow bathymetry, high free-air and low Bouguer anomalies, and very high heat flow clearly indicates the presence of a shallow temperature anomaly associated with mantle flow.

Seismic information of crustal structure and Moho depth remains controversial. Crustal-scale seismic refraction study across the Bransfield Strait, from the South Shetland Trench to the Antarctic Peninsula, imaged a 30 km thick continental crust in the central part of the basin. The reported structure, dominated by a ca. 25 km thick high-velocity (Vp > 7.0 km/s) lower layer below 2 km of sediments and 2–3 km thick upper crust, is very unusual (Grad et al., 1997) and suggests misinterpretation of the lower crustal layer and the Moho depth. In contrast, old refraction models (Ashcroft, 1972) and more recent interpretations along eight high-resolution seismic refraction profiles across and along the strike of the back-arc basin (Barker et al., 2003) show crustal thickness of ~10 km (including 3–4 km of sediments) below the extensional axis, and crustal thickness increases to 14–16 km towards the flanks (Fig. 11). A subtle increase in crustal thickness from NE to SW was interpreted to reflect a NE-SW propagation of extension. Despite a thin crust, the seismic structure is interpreted as rifted arc crust of the Antarctic Peninsula, with the conclusion that the back-arc basin does not yet have oceanic crust (Barker et al., 2003).

#21. Eastern Caribbean Sea

The eastern Caribbean Sea (Fig. 7) hosts three separate subduction systems that have been active at different times (Bonini et al., 1984). Two of them (the Great Arc of the Caribbean in the west and the Lesser Antilles Arc in the east) created back-arc basins, which are analyzed as three individual areas. (i) The oldest Cretaceous-Paleocene Great Arc of the Caribbean was active possibly since 88 Ma and became extinct at ca. 59 Ma (Neill et al., 2011). The Aves Ridge (#21AR) is a part of the remnant arc. Clear N-S trending magnetic lineations are interpreted to result from E-W seafloor spreading. (ii) The early Paleocene to Eocene subduction is evidenced by ~40 Ma arc-type magmatism along the NE Caribbean plate boundary. This subduction system apparently did not produce any back-arc spreading and its geodynamic interpretations remain controversial (Bird et al., 1999; Allen et al., 2019).

(iii) The youngest (<25 Ma) subduction system, associated with westward subduction of the Atlantic oceanic lithosphere below the Caribbean Plate (intermediate-depth dip angle of ca. 29-43°), created the active Lesser Antilles Arc and the Grenada Basin (#21n,s) behind the arc (Fig. 7). The geodynamic origin of the Grenada Basin is debated (cf. Boschman et al., 2014). Magnetic anomalies in the northern Grenada Basin (#21n) have no regular pattern, while in the southern Grenada Basin (#21s) and the Tobago Basin on the opposite sides of the Lesser Antilles Arc they have reverse polarities. This magnetic pattern was interpreted as an indicator that roll-back of the Proto-Caribbean slab caused a westward migration of the volcanic arc in Miocene from the Aves Ridge to the Lesser Antilles Arc, which has split the former forearc of the Aves Ridge into the Grenada and Tobago Basins (Allen et al., 2019). Alternative models for the evolution of the Grenada Basin include both an east-west-striking (Pindell and Kennan, 2009) and north-south-striking (Bird et al., 1999) spreading center; however all models consider the Grenada Basin as a back-arc basin. Seismic models suggest that seafloor spreading may exist only in its southern part (south of ca. 13 °N), where the slab dip angle of <30° is one of the smallest among the back-arc basins worldwide, Fig. 10b)

The bathymetry of the active Lesser Antilles back-arc basin of the Grenada Basin deepens from around 2.1 km in the north (#21n) to ca. 2.7 km in the south (#21s). Free-air anomalies decrease southwards from close to zero in the northern part to ca. -40 mGal in the south (the lowest free-air anomaly values among all back-arc basins, Fig. 12a), where back-arc spreading is active and oceanic crust was interpreted from seismic data (Speed and Walker, 1991; Christeson et al., 2008). Bouguer anomalies are positive and uniform, ca. +130 to +180 mGal, in both parts of the basin. Heat flow with a mean value of 69 ± 12 mW/m^2 does not differ between north and south.

The region is well covered by crustal-scale wide-angle seismic reflection/refraction profiles. In the southern Grenada Basin the crust

has a total thickness of ca. 15 km with a structurally homogeneous 6–7-km thick crystalline basement (Fig. 11). The basement has a 1.5 km thick upper crust and ca. 5.0 km thick lower crust with a typical oceanic velocity structure, overlain by a very thick (7 to 11 km) cover of sediments (Allen et al., 2019; Christeson et al., 2008). The crustal structure of the southern Grenada Basin was interpreted as an evidence for an active back-arc spreading, while back-arc spreading in the northern Grenada Basin is ruled out by seismic models. In the northern Grenada basin (ca. 16–17 ^{o}N), the crust is 20–27 km thick and includes a > 10 km thick fast-Vp (6.8–7.2 km/s) lower crust (Fig. 11), similar to the crust of the central Lesser Antilles island arc (Kopp et al., 2011), suggesting that the northern part of the Lesser Antilles back-arc basin preserves the arc crust.

The remnant back-arc basin of the Aves Ridge (#21AR) has water depth of ca 1.5 km, near-zero free-air anomalies and moderately positive Bouguer anomalies between +100 and + 200 mGal, similar to the younger Lesser Antilles back-arc basin. Heat flow between 46 and 88 mW/m^2 (with one high value at the ridge axis) is also similar to the Grenada Basin and yields an average of 64 ± 13 mW/m^2. The crust of the southernmost Aves Ridge has a similar seismic velocity structure and crustal thickness of ca. 25–30 km as the Lesser Antilles Arc (Christeson et al., 2008). Tomographic inversion shows that the ridge has little or no sediments, and the lower 5–6 km of the crust have Vp > 7.3 km/s (Fig. 11). Earlier models with sparse seismic data reported crustal thickness of 30–40 km in a seismic profile along the strike of the Aves Ridge (Boynton et al., 1979).

#22. Gulf of Mexico

The extinct Gulf of Mexico back-arc basin in the southern part of the North American Plate has opened between ca. 165 and 142 Ma behind an arc, possibly associated with an eastward subduction of the Pacific Plate (cf. Stern and Dickinson, 2010; Lin et al., 2019). However, in the absence of clear magnetic anomalies within the Gulf of Mexico, the exact age of seafloor spreading and its duration remain not well constrained and the evolution of this large ocean basin buried under a thick sedimentary cover is not yet well known. The system of paleo-spreading ridges, fracture zones and transform faults (Fig. 7) beneath 6–8 km of sediments has been recognized from satellite gravity data (Sandwell et al., 2014) and high-resolution magnetic data (Imbert and Philippe, 2005). The total extension rate, estimated from a combined gravity and seismic interpretation of the ocean floor area and the location of extinct spreading center, is ca. 2.2 cm/y, assuming that normal seafloor spreading started at ~155–152 Ma and ended at ~142–138 Ma (Christeson et al., 2014).

Water depth within the Gulf of Mexico back-arc basin varies from ca. 3.5–3.7 km to 1.8–2.0 km towards the North America continent and in the NE part of the basin; typical values around the paleo-spreading center are around 3.2–3.4 km and the basin average is ca. 2.9 km. Free-air anomalies are typically negative and increase from ca. -50 mGal in SW to ca. +20 mGal in NE, and overall the basin deviates from the isostatic equilibrium. Bouguer anomalies are between +140 and + 220 mGal with higher values south of the paleo-spreading (Fig. 7). Abundant heat flow measurements constrain a rather uniform low heat flow with mean value of 46 ± 16 mW/m^2, indicating that the basin's lithosphere equilibrated to a platform-type thermal regime since the extension has terminated.

Seismic refraction experiments of the Gulf of Mexico Opening (GUMBO) project (Christeson et al., 2014; Eddy et al., 2014) imaged a typical oceanic crust with ca. 6–7 km of sediments above a 6–7 km thick crystalline basement. In the eastern part of the back-arc basin, the upper layer with an unusually high Vp ~ 6.0–6.7 km/s imaged over a distance of ca. 100 km was interpreted as part of oceanic Layer 3; the lower, 2–3 km thick, crust has Vp > 7.0 km/s (Fig. 11). In other parts of the Gulf of Mexico basin, upper crustal velocities in oceanic crust are 4.5–4.7 km/s. As result, within the back-arc basin average crustal velocities decrease from 6.95 km/s in SW to 6.55 km/s in NE, matching a decrease in water depth towards NE (Christeson et al., 2014). The GUMBO results are consistent with seismic reflection experiments (correlated with deep industrial wells) in the north-central parts of the Gulf of Mexico, which identified a 7–8 km thick sequence of sediments atop an oceanic 8 km thick crust with the total crustal thickness of 14–16 km (Lin et al., 2019).

2.6. BABs of the Mediterranean Region

#23. Southern Tyrrhenian Sea

The active back-arc basin of the Southern Tyrrhenian Sea in the central-eastern Mediterranean is located between the Apennines peninsula to the east, the island of Sicily to the south, and Corsica and Sardinia islands to the west (Fig. 8). The back-arc basin has developed as result of ESE migration of the Calabria-Sicilia arc system in response to subduction of an old, largely oceanic Eastern Mediterranean (Ionian-Levantine) lithosphere (Ritsema, 1979). The age of the subducted Ionian oceanic crust is debated, and late Mesozoic is commonly proposed (cf. Sartori, 2003). The seismicity pattern indicates that presently the slab plunges NW beneath the Southern Tyrrhenian Sea at ca. 50-58^{o} (Rehault et al., 1987; Jacobsen, 2018) and may reach a 300–450 km depth beneath the most extended parts of the basin (Sartori, 2003). The curvature of the arc is among the largest presently active (Fig. 8).

In contrast, subduction of the continental Adriatic slab and its retreat are proposed as mechanism of extension in the Northern Tyrrhenian Sea, where the back-arc basin of the Apennines-Calabria subduction system formed during the last 15 Ma (Jolivet et al., 1999). This small back-arc basin is excluded from the present analysis.

The evolution of the Southern Tyrrhenian back-arc basin, conventionally ascribed to slab roll-back and possibly promoted by the upper mantle flow (e.g. Doglioni, 1991; Panza et al., 2007; Carminati et al., 2012; Balázs et al., 2022) (Fig. 2c), was complicated by the collision of the African and the Eurasian Plates (Doglioni et al., 1997, 2009). The opening of several Mediterranean back-arc basins (Tyrrhenian, Ligurian, Aegean) has been attributed to an interplay of three main processes: (i) N-S shortening due to the convergence of Africa and Europe (Tapponnier, 1977), (ii) slab pull by subduction retreat (i.e. roll-back of the subducting slab) (Malinverno and Ryan, 1986; Doglioni, 1991), (iii) gravitational collapse of the thickened Apenninic lithosphere (Channell and Mareschal, 1989). A combination of these three mechanisms best explains the tectonics of the Tyrrhenian-Apennine system (Faccenna et al., 1996; Doglioni et al., 1997; Jolivet and Faccenna, 2000; Carminati et al., 2012).

Fast extension in the Tyrrhenian Basin started in Lower Miocene (ca. 20 Ma), while the main phase initiated at ca. 9 Ma and led to seafloor spreading in Early Pliocene (5–4 Ma) with the NNE-SSW trending spreading axis and magnetic anomalies recognized in the eastern part of the basin (Kastens and Mascle, 1990). Thus formed oceanic crust is restricted to two small sub-basins (Vavilov and Marsili) in the axial zone of the south-central Tyrrhenian Sea (Rehault et al., 1987; Sartori, 2003). Ocean drilling data suggests that the opening rate in the Marsili Basin during the past 2–1.5 Ma was 3.1–4.5 cm/y (Kastens and Mascle, 1990). These results were challenged by a recent analysis of the NNE-SSW trending magnetic lineations, which suggest that between ca. 2.1 and 1.6 Ma the Marsili Basin (Fig. 8) opened at the highest ever documented full spreading rate of ca. 19 cm/y, and that the back-arc opening was episodic with rapid extensional pulses separated by slow spreading phases (Nicolosi et al., 2006). Averaging this exceptionally high extension rate over 2 Ma (from the start of the rapid extension until present) yields the value of ca. 5 cm/y, which is adopted here for further analysis.

The Southern Tyrrhenian Basin has bathymetry and gravity anomalies typical of the OO-type back-arc basins worldwide (Fig. 12). The bathymetry in the deepest parts of the basin with oceanic crust is 3–3.6 km and is complicated by numerous seamounts. Water depth reduces to ca. 2.4 km in the basin parts with continental crust. Free-air anomalies are close to zero in most of the basin (−10 + 20 mGal), and overall both the bathymetry and free-air anomalies are close to the oceans worldwide

(Fig. 12a). Bouguer anomalies are considerably smaller than in many other back-arc basins, ranging from +150 mGal in parts with continental crust to +250 mGal in the oceanic sub-basins, and the bathymetry-Bouguer anomalies combination is similar to an average mid-ocean ridge (Fig. 12b). Numerous measurements report a highly heterogeneous heat flow (from 34 to >150 mW/m^2) without any systematic trends. The mean heat flow value for the entire back-arc basin constrained by high-quality data is 95 ± 36 mW/m^2 (Table 1), and is significantly lower than suggested by old studies (Della Vedova et al., 1984).

Early seismic studies imaged an oceanic-type crust in the central part of the Southern Tyrrhenian Sea with 2–3 km of sediments, 3 km thick Layer 2 (Vp ~ 5.0–5.2 km/s) and 2 km thick Layer 3 (Vp ~ 6.5–6.8 km/s) (cf. Rehault et al., 1987). These results were confirmed by a NW-SE seismic reflection profile across the central part of the Tyrrhenian back-arc basin (Pepe et al., 2000) and a regional Rayleigh group- and phase-velocity tomography study which imaged a ca. 10 km thick crust beneath the Vavilov and Marsili sub-basins with crustal thickening to ca. 16 km in the northern Tyrrhenian Sea (Manu-Marfo et al., 2019).

A high-resolution E-W striking seismic refraction and wide-angle reflection profile MEDOC along 40 °N revealed in detail crustal structure of the Central Tyrrhenian basin (Prada et al., 2014). From margins seawards, the crustal thickness changes from ~20 km to 13 km and this peripheral zone is interpreted as thinned continental crust. The central domain (between ~10.5°E and ~ 13.8°E) is interpreted as oceanic crust, but with different structure closer to the margins (the Cornaglia Terrace in the west and its conjugate Campania Terrace in the east) and in the axial part (the Vavilov and Marsili sub-basins between ~11.5°E and ~ 13.1°E).

The Cornaglia and Campania Terraces have a two-layer crust ranging in thickness between 7 and 9 km with seismic structure similar to oceanic crust. The upper layer (below a 1 km thick layer of sediments) is ca. 2 km thick, and the lower crust with Vp ~ 6.5–7.1 km/s is ca. 5–7 km thick and thins towards the basin center. In the Vavilov and Marsili sub-basins, the oceanic crust is ca. 6–6.5 km thick due to thinning of the lower crust which has fast Vp > 7.0 km/s (Fig. 11). Lack of Moho reflections beneath the Vavilov and Marsili sub-basins was interpreted as evidence that the entire basement may be composed of chiefly serpentinized mantle peridotites with 20–30% of serpentinization in the upper crustal layer and 80% of serpentinization in the lower crustal layer (Prada et al., 2014). However, such interpretation is in conflict with common petrological definitions of the crust as the layer that is compositionally distinct (felsic-to-mafic) from the dominantly ultramafic mantle (O'Reilly and Griffin, 2013).

#24. Aegean Sea

The Aegean Sea has long been recognized as a typical active extensional back-arc basin (McKenzie, 1978; Le Pichon and Angelier, 1979; Pe-Piper and Piper, 1989), while its origin as a typical back-arc basin has been questioned (Doglioni, 1991; Gautier and Brun, 1994; Doglioni et al., 2002; Agostini et al., 2010) with arguments for its formation in response to the westward escape of the Anatolia Plate associated with the Africa-Eurasia collision (e.g. McClusky et al., 2000) or by a gravitational collapse (e.g. Jolivet, 2001). Without entering the debate on tectonic origin of the Aegean Sea, the region is analyzed together with other back-arc basins, since the mechanisms of lithosphere extension in back-arc basins are not a part of the back-arc definition (see Introduction), and in many BABs subduction may have played a subordinate (or no) role of in back-arc extension (Table 2, Fig. 2).

The back-arc basin, located north of Crete between the Balkanian and Anatolian microplates (Fig. 8), was formed behind the South Aegean Arc in response to subduction of an old oceanic Ionian-Levantine lithosphere (Robertson, 1998; Sartori, 2003), although some studies relate it to subduction of the continental African Plate lithosphere (Snopek et al., 2007). A roughly E-W trend of the Aegean Trench and the Hellenic Arc reflects the N-S convergence between the African and Eurasian Plates and indicates an importance of trench retreat in the Aegean basin extension (Brun and Sokoutis, 2010). Additionally, transtension associated with the right-lateral motion on the North Anatolian Fault (NAF) system and coaxial westward escape of Anatolia played an important role in regional geodynamics (Dewey and Sengör, 1979; Le Pichon and Angelier, 1979; McClusky et al., 2000). An inherited, reactivated lithosphere-scale mechanical discontinuity (the Vardar Suture Zone in the Balkans) has been offered to explain back-arc extension by the combination of trench retreat, rotation of the Aegean microplate (located between the Balkanian and Anatolian microplates) and strike-slip motion on the North Anatolian Fault system (Philippon et al., 2014). A complex pattern of seismic anisotropy in the lower crust and upper mantle (Endrun et al., 2011) suggests an important role of lower crustal and mantle flow in the basin extension and magmatism (Agostini et al., 2010).

In contrast to most other back-arc basins, the Aegean basin has no oceanic spreading center, and the extension rate cannot be assessed from magnetic data. Geological evidence suggests that the first phase of slow extension took place from 45 to 13 Ma (Agostini et al., 2010). At the second stage (from 13 Ma to 4 Ma, with a peak at 8–9 Ma) the extension rate was up to 3 cm/y (Philippon et al., 2014), and the total extension is estimated as 580 km (Brun and Faccenna, 2008).

The Aegean basin is extremely shallow, with typical water depth between 0.6 km and 1.4 km. Such shallow bathymetry is similar to bathymetry in the Okinawa Trough, also formed by ocean-continent collision, and to water depth in the Bransfield Basin formed by arc-ocean collision, but it is neither observed in back-arc basins formed by collision of oceanic plates (Table 1), nor in the extinct back-arc basins of the western Pacific Ocean, which mostly belong to the OO-type (Fig. 12a). Extremely high free-air anomalies, on average + 130 mGal, which indicate a very strong deviation from regional isostasy, are generated by elastic stresses produced by flexure of the elastic portion of the lithosphere and supporting topographic loads (Cochran and Talwani, 1977; Molnar et al., 2015). A truly anomalous pattern of the Aegean Sea on the bathymetry-free-air gravity plot (Fig. 12a) suggests that the departure from isostasy should also be essentially associated with convection flow-induced normal stresses at the lithosphere base, as supported by small values of Bouguer anomalies (typically ca. 250–300 mGal less than in the oceans). The seismogenic zone also indicates that the plunging slab is one of the most shallow among the back-arc subduction systems in the world (Fig. 10b). Heat flow measurements, which exist only in the central part of the back-arc basin, show highly variable values that range from 33 to 95 mW/m^2 with mean value of 62 ± 18 mW/m^2.

Several deep seismic sounding profiles were acquired in the Aegean Sea in 1970's. The most interesting for the present study are two "METEOR 1974" profiles which crossed the entire back-arc basin roughly W-E and its central part N-S (Makris, 1978). These low-resolution profiles imaged a ca. 30 km thick crust with ca. 3 km of sediments; lower crustal velocities are between 6.2 and 6.8 km/s (Fig. 11). Seismic receiver function results for one station (Santorin) at the edge of the Aegean Sea back-arc basin report crustal thickness of ca. 33 km (Zhu et al., 2006). Thus there is no evidence neither for seafloor spreading, nor for the presence of an oceanic-type crust in the Aegean Sea back-arc basin.

#25. Black Sea

The Black Sea between the Eurasian Plate in the north, the Anatolian and Balkanian microplates in the south and west, and the Caucasus orogen in the east includes two deep basins of the West and East Black Sea, separated by the NW-SE oriented Mid Black-Sea basement high (the Andrusov Ridge); the latter is possibly composed of a thinned continental crust (Starostenko et al., 2004). The hypothesis of a back-arc origin of the Black Sea deep basins (Zonenshain and Le Pichon, 1986) replaced the earlier ideas of their origin either as trapped oceanic fragments (Sorokhtin, 1979) or as basins subsided due to crustal

eclogitization (Yanshin et al., 1980). Although no magnetic lineations were identified (possibly due to a very thick, >10 km, sedimentary cover (Nikishin et al., 2015)), the Black Sea is commonly considered to have two back-arc basins (analyzed separately as #25w and #25e) either related to the southwards-dipping subduction of a Paleo-Tethys Ocean (Liu et al., 2018) or to the northwards-dipping subduction of a Neo-Tethys oceanic plate (Fig. 8) with a 1500–2000 km long *E*-W-trending trench (Okay and Tuysuz, 1999; Stephenson and Schellart, 2010; Nikishin et al., 2003; Stephenson and Stovba, 2021). The main rift with the NW-SE orientation is recognized in the Eastern Black Sea basin. However, the direction of extension in the Western Black Sea basin is not constrained.

The time of formation of the Black Sea deep basins is unknown since the basins lack magnetic lineations. A targeted study, based on the assumption that heat flow is related to the age of cooling oceanic lithosphere (and therefore based on the assumption that the Black Sea basins have "normal" oceanic lithosphere) estimated the age of the Western Black Sea deep basin as 130 to 95 Ma, and of the Eastern Black Sea deep basin as ca. 110 Ma (Golmshtok et al., 1992*)*. Recent interpretations based on ages of the sedimentary fill as inferred from seismic reflection surveys suggest that the Eastern Black Sea basin may possibly be much younger, of Paleogene age (about 60–50 Ma) (cf. Nikishin et al., 2003). It is commonly assumed that the Western Black Sea basin was formed in Cretaceous (Stephenson and Schellart, 2010; Stephenson and Stovba, 2021). The lack of seismogenic zones does not allow to constrain the subduction dip angle.

Bathymetry and gravity anomalies of the Black Sea basins plot with the extinct back-arc basins of, possibly, the CO-type (Fig. 12). Both deep basins of the Black Sea are 1.9 to 2.2 km deep, without any significant difference between the western and eastern basins (Table 1). In the western basin, slightly negative free-air anomalies reach the minimum value of ca. -50 mGal in its deepest part around the proposed (roughly W-E-trending) spreading axis. In the eastern basin, free-air anomalies decrease from +20 mGal along the proposed NW-SE-trending spreading axis to ca. -40 mGal close to the basin margins, while Bouguer anomalies decrease from ca. +150 mGal along the proposed spreading zone to ca. +100 mGal towards the margins. There is no significant difference in heat flow between the western and eastern Black Sea basins (Fig. 8). Abundant heat flow measurements constrain a very uniform thermal state across both deep basins of the Black Sea with values ranging from 31 to 56 mW/m^2 and mean heat flow of 40 ± 7 mW/m^2, which is one of the lowest in the back-arc basins globally.

The nature of the crust in the Black Sea is debated (Nikishin et al., 2003; Starostenko et al., 2004; Minshull et al., 2005; Yegorova and Gobarenko, 2010; Nikishin et al., 2015; Stephenson and Stovba, 2021; Petrescu et al., 2022) and the contrasting models infer that its deep basins may have formed on an extended cratonic lithosphere or that they may preserve trapped fragments of the Tethyan oceanic lithosphere. Geodynamic interpretations of recent high-resolution seismic reflection surveys in the entire Black Sea basin, which constrained the structure of the sedimentary cover and the Moho interface, propose that both the Western and Eastern Black Sea deep basins have oceanic crust in their central parts, surrounded by thinned rifted continental crust towards the coasts (Nikishin et al., 2015). Thickness of sediments is ca. 10 km in marginal parts of both back-arc basins and in the central Eastern Black Sea basin and it reaches ca. 15 km in the deep depression of the Western Black Sea basin (Golmshtok et al., 1992; Nikishin et al., 2015).

Seismic refraction surveys in the Black Sea deep basins are chiefly from marine experiments conducted and interpreted in 1960–1970's and summarized in later reviews (Neprochnov et al., 1970; Volvovsky and Volvovsky, 1975; Tugolessov et al., 1985; Beloussov et al., 1988). These old interpretations suggest that the deep basin of the Western Black Sea has a ca. 20 km thick crust, which includes ca. 12 km of sediments and three crustal layers typical for continental crust with thicknesses of 2.5–3.0 km each. A fast velocity (>7.0 km/s) lower crustal layer is absent in this model (see Fig. 11), which is consistent with later gravity-based models calibrated by a large number of controlled-source seismic surveys (Starostenko et al., 2004; Yegorova and Gobarenko, 2010). These models imply that the crystalline crust in the Western Black Sea basin is <8 km thick, and possibly 5 km or thinner if the sedimentary sequence is ca 15 km thick (Nikishin et al., 2015).

Old interpretations infer that, in contrast, the deep basin of the Eastern Black Sea has a ca. 27 km thick crust which includes ca. 10 km of sediments and a ca. 17–18 km thick lower crustal layer (Vp ~6.8–7.2 km/s), while the "granitic" layer is absent (Tugolessov et al., 1985). This unusual crustal structure was interpreted as an oceanic-type crust formed by seafloor spreading (Golmshtok et al., 1992). Recent wide-angle seismic profiles in the Eastern Black Sea (Minshull et al., 2005) questioned the old interpretations. They imaged a ca. 8–9 km thick sequence of sediments, with the deepest layers interpreted to be Upper Jurassic to Lower Cretaceous platform carbonates based on outcrops at the basin margins (Robinson et al., 1996). Thickness of the crystalline basement is significantly smaller than in old seismic models, ca. 7–8 km only, and the fast lower crustal layer is absent (Fig. 11). Therefore, recent seismic interpretations suggest the presence of an oceanic-type crust in the Eastern Black Sea basin, but with crustal velocities lower than in normal oceanic crust (ca. 6.0–6.2 km/s) (Minshull et al., 2005). These values also imply extreme values of crustal thinning (corresponding to β-factor of ca. 4, Table 1), which cannot be explained by a one-phase stretching of an extended continental crust and require a complex paleo-extensional history (Stephenson and Stovba, 2021).

A recent ambient noise tomography of the Black Sea suggests that the Moho depth is ca. 25 km both in the western and eastern basins with a ca. 40 km thick crust below the Mid Black-Sea Ridge (Petrescu et al., 2022). This study imaged a contrasting lithospheric structure below the two basins with seismic velocities slower below the Western Black Sea. These authors suggest that the two basins may have formed on different lithospheric plates, although both of continental affinity, and the eastern basin may have formed on a Precambrian lithosphere. Indeed, the Mid Black-Sea Ridge may possibly be related to the Trans-European Suture Zone (*Ye. Sheremet, personal communication, 2022*), that marks the western edge of the East European Craton. In such a case, the Western Black Sea basin may have formed on a Phanerozoic Tethyan crust, while the Eastern Black Sea basin may have formed on a hyper-extended cratonic crust of the East European Craton or the Scythian Plate.

2.7. *BABs of the West Antarctica*

#26. West Antarctica system of back-arc basins

The West Antarctica system of back-arc basins, that stretches from the Antarctic Peninsula to the Marie Byrd Land and the Ross Sea Ice Shelf (Fig. 9), was formed behind the system of the Antarctic Peninsular - Marie Byrd - Ross Sea arcs by differential slab roll-back during the Mesozoic subduction of the Phoenix (paleo-Pacific) Plate under the West Antarctica continental margin (Artemieva and Thybo, 2020). Earlier studies, which interpreted West Antarctica as a rift system similar to the Basin and Range Province of the western USA (Behrendt et al., 1991), cannot explain the size of the region which is one of the world's largest extensional areas (Cande et al., 2000), neither its topography which is much deeper than any depression on continental crust, including the shelves, nor the patterns of gravity anomalies and seismicity which are typical for subduction systems but not for rifts (Artemieva and Thybo, 2020). Geological data and high-resolution geophysical mapping suggest that West Antarctica represents a broad zone of episodic crustal extension which has possibly started at 68 Ma and continued until recent (Lawver and Gahagan, 1994; Salvini et al., 1997; Studinger et al., 2002). At the Ross Sea segment, the first phase of ~150 km extension between 68 Ma and 46 Ma (Cande and Stock, 2004) and the second phase of ~180 km extension between 43 Ma and 26 Ma (Cande et al., 2000) yield the total opening rates between 6.8 and 10.5 cm/y. Extension slowed down since then, and GPS measurements do not resolve any present-day extension in West Antarctica (Wilson et al., 2015).

The water depth has large variations from near-zero values to 1.9 km with mean values around 0.9–1.0 km, and equivalent bathymetry (compensated for ice load) is ca. – 0.6 km on average (Artemieva and Thybo, 2020). Free-air anomalies between −40 and + 20 mGal are similar to most of back-arc basins globally, while Bouguer anomalies (typically between −30 and + 50 mGal, Fig. 9) are the smallest among off-shore back-arc basins (Table 1). Conventional borehole heat flow measurements, available only along the margins of the Ross Sea segment, constrain a highly variable heat flow between 60 and 142 mW/m^2 (cf. Morin et al., 2010), while studies based on temperature-logs and radar measurements in ice-drill holes report a huge range between 69 mW/m^2 (Engelhardt, 2004) and 285 mW/m^2 (Fisher et al., 2015). Geophysical models based on different approaches predict regionally averaged heat flow in West Antarctica in the range from 52 to 58 mW/m^2 (Artemieva, 2006; An et al., 2015a; Shen et al., 2020) to 70–75 mW/m^2 (Shapiro and Ritzwoller, 2004; Fox Maule et al., 2005), with recently determined regional variations between 80 and 120 mW/m^2 in the West Antarctica back-arc basin system (Artemieva, 2022).

Crustal thickness in West Antarctica is typically between 20 and 30 km with an average value of ca. 20 km in the Ross Sea and ca. 25 km in the Marie Byrd Land (cf. Artemieva and Thybo, 2020). Seismic reflection/refraction studies are largely restricted to the Ross Sea margin, where a 19 km thick crust has ca. 6.5 km of sediments, ca. 5 km thick upper crust and ca. 7.5 km thick lower crust with Vp > 6.8 km/s (Trey et al., 1999) (Fig. 11). Locally, thickness of sediments in the Ross Sea segment may reach 14 km, implying that the crystalline crust may be thinned to ca. 8 km (Behrendt et al., 1991). In the Marie Byrd Land, seismic receiver function studies reported a thin extended continental crust with the total thickness of 20–25 km (Winberry and Anandakrishnan, 2004; Chaput et al., 2014), consistent with a regional surface wave tomography model which constrains crustal thickness of ca. 25 km in the Marie Byrd Land and ca. 10–15 km in the Ross Sea segment (An et al., 2015b).

3. Analysis

3.1. Summary by BAB tectonic types

The analysis aims to recognize similarities and differences between the back-arc basins of different tectonic origin and to identify global trends in their formation and evolution. The section is, in general, arranged from the top (the crust) to the bottom (mantle wedge), although in many cases crust-mantle processes are strongly intermixed. The following discussion builds on the adopted grouping of the back-arc basins as specified and summarized below.

3.1.1. Ocean-ocean (OO) subduction

The OO-group includes 9 presently-active back-arc basins (numbers in brackets refer to Figs. 1, 3-9, Tables 1-2 and are used as labels in the figures to follow) with a good data coverage so that statistical values for this group are well representative:

- the Aleutian basin behind the Aleutians arc (#1) which possibly represents a trapped oceanic crust rather than a back-arc basin proper; since the pattern of magnetic anomalies is irrelevant to the subduction system, the age and dynamics of the subducting Pacific Plate may be poorly related to the basin characteristics and the basin lacks data on the total opening rate;
- the Komandorsky basin behind the Aleutians arc (#2) which may also represent a fragment of trapped oceanic crust and its crustal structure is based on old seismic interpretations;
- the Mariana Trough behind the Marianas arc (#6) with unusually high free-air anomalies indicative of a strong lithosphere deformation in the back-arc basin associated with a near-vertical subduction system;
- the Manus BAB behind the New Britain arc (#14) with unusually high free-air anomalies caused by lithospheric flexure and low Bouguer anomalies suggestive of a low-density mantle; this BAB lacks data on crustal structure and has only two contrasting heat flow values;
- the North Fiji BAB behind the New Hebrides arc (#16) which may possibly be unrelated to the subduction dynamics so that its lithosphere extension may be associated with processes that do not require subduction; an extremely thin crust is constrained by low-resolution vintage refraction profiles;
- the Lau Basin behind the Tonga arc (#17) with a complicated pattern of magnetic anomalies, extremely low heat flow and different crustal structure at the spreading axis and the margins;
- the Havre BAB behind the Kermadec arc (#18) with no regular pattern of magnetic anomalies and the absence of a clear spreading axis; unusually high free-air anomalies may possibly indicate a strong lithosphere deformation during the rifting stage, which remains uncertain since the basin lacks seismic data on the crustal structure;
- the East Scotia BAB behind the short South Sandwich arc (#19) in the southern Atlantics which also lacks seismic data on the crustal structure;
- the Southern Tyrrhenian Sea behind the Calabrian arc of the Mediterranean Sea (#23) with a debated age of the subducted slab which forms a rare semi-circular patter with one of the largest trench curvatures; the basin has seafloor spreading with a localized presence of oceanic crust imaged by high-resolution seismic profiles.

The OO-basins (Fig. 1) usually have a representative coverage by seismic refraction profiles (except for the Manus Basin) and heat flow measurements (except for the Havre Basin). Major characteristics of all OO-type basins are the presence of seafloor spreading, oceanic crust which often represents a mixture of extended, reworked and newly formed crust, and a clearly identified seismogenic zone which allows to determine the slab dip angle. The presence of magnetic lineations allows to constrain the age of basin opening, the opening rate and the age of the basement for most of the OO-type basins (the Aleutian and Komandorsky basins are notable exceptions, which possibly are not associated with the present subduction systems). Mean geophysical characteristics of the OO-type back-arc basins are shown in Fig. 13 in comparison with the other BAB types and the corresponding parameters are discussed in the sections to follow.

The often unknown age of the downgoing slab is often discussed in relation to dynamics of the OO-type and other marine back-arc basins (Molnar and Atwater, 1978; Grellet and Dubois, 1982; Carlson et al., 1983; England et al., 2004; Heuret and Lallemand, 2005; Gaina and Mueller, 2007; Dunn and Martinez, 2011; Long and Wirth, 2013). The slab's age essentially defines the pre-extensional thermal history of the OO-type basins, as reflected in their bathymetry, gravity anomalies, and heat flow. The pre-extensional history is further complicated by the degree and lateral extent of crustal reworking in back-arc settings, where the oceanic nature of the crust at both the pre-extensional and extensional stages hampers an assessment of the degree of crustal reworking. As result, the OO-type BABs are expected to be highly heterogeneous in various geophysical parameters related to oceanic lithosphere.

3.1.2. Island arc-ocean (AO) subduction

The AO-group with only 3 active back-arc (sub)basins is very small, statistically non-representative and is included in the analysis for a general comparison only. Besides, information related to the arc-ocean BABs opening rate, crustal structure and heat flow is often incomplete. The group includes:

- the Bransfield Basin (#20) behind the Southern Shetlands arc in the southern Atlantics along the Antarctic Peninsula; one of the most

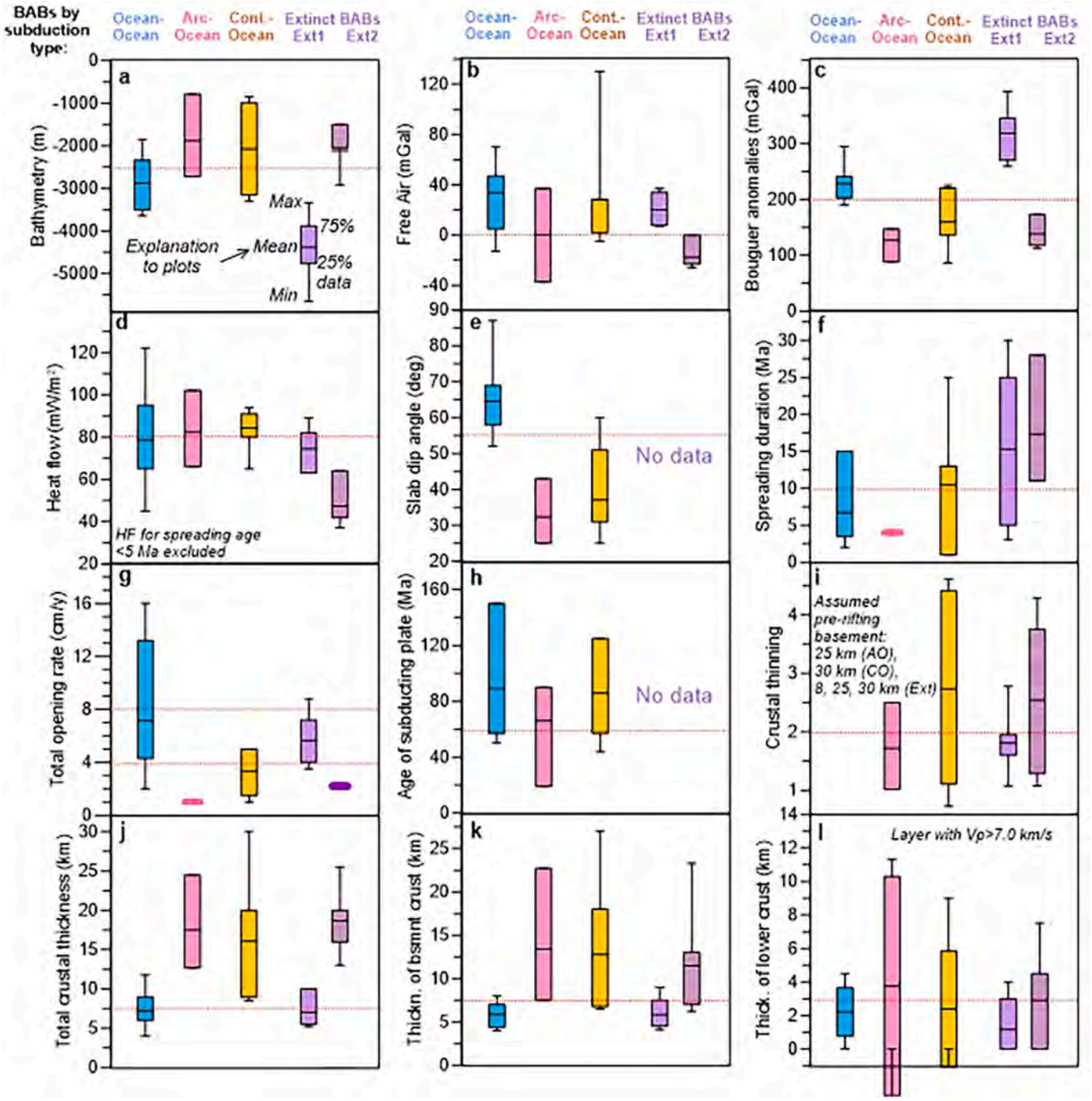

Fig. 13. Whisker plots with statistics for back-arc basins by tectonic settings. The EXT group is split into two subgroups (see Fig. 12). The AO group is statistically non-representative and is shown only for a general overview. Colored bars show the range of values for 25% to 75% of data, black bars - the total span of data, and horizontal lines inside colored bars give the mean value. Horizontal lines are shown to simplify comparison. For references and explanations see the text and Table 3. For details on plot (i) see section 3.3.3.

shallow dipping slabs associated with the back-arc extension apparently has not yet produced seafloor spreading, while a very shallow bathymetry, high free air anomalies with the smallest Bouguer anomalies among all BABs worldwide and high heat flow all require the presence of a hot mantle material at shallow depth;

- the Grenada Basin of the northern (#21n) and southern (#21s) parts of the Lesser Antilles behind the Lesser Antilles arc; the southern and northern parts are different in many geophysical and geodynamic characteristics and therefore are analyzed independently; the southern basin may have a seafloor spreading and has the largest negative free-air anomaly among the back-arc basins worldwide; the northern basin has one of the thickest back-arc basin crust; both parts lack information on the total opening rate and the spreading duration.

On the present Earth, the AO-type basins are rare and are clearly unique, while marine arc-related back-arc basins associated with arc-arc or arc-continent collisions are exotic. Two of such extinct, small-size arc-related basins in the equatorial western Pacific (the Celebes Sea, #11, and the Banda Sea, #12) are discussed below. Both active and extinct

arc-related back-arc basins are very small in size. They apparently all tend to evolve to seafloor spreading and, depending on the stretching stage, may have an arc, hybrid, or newly formed oceanic crust (Table 3). Clearly identified seismogenic zones allow to determine a large scatter in slab dip angles (Fig. 10), while recent seismic refraction profiles indicate a highly variable crustal structure (Fig. 11). Yet the age of extension and the opening rate remain debated.

3.1.3. Continent-ocean (CO) subduction

The CO-group is small but statistically representative and includes 7 back-arc (sub)basins in 4 locations (Table 2):

- the Kurile BAB behind the Kurile arc (#3) with no magnetic anomalies and therefore with the unknown extension rate and the basement age; a highly heterogeneous seismic crustal structure allows for controversial models which may suggest the presence of oceanic or hyper-extended continental crust;
- the Japan Basin (#4n) and the Jamato Basin (#4s) of the Sea of Japan where lithosphere extension may be caused by processes that do not require subduction; the Japan basin with the extinct seafloor spreading has oceanic crust imaged by sparse seismic profiles; the Yamato basin with incoherent magnetic anomalies has a debated extensional history and a disputed crustal origin; while both basins appear extinct, they are analyzed within the CO-group as being closely associated with the active CO-type subduction systems north and south;
- the northern (#5n) and the southern (#5s) parts of the Okinawa Trough located behind the Ryukyu arc; the two parts are different in many characteristics as in the Lesser Antilles and therefore are analyzed independently; crustal stretching progressed from south to north and resulted in an unusually shallow bathymetry with small positive Bouguer anomalies in the north where the crust is possibly still continental, while seafloor spreading is possible in the southern part which has moderate bathymetry and gravity values and, at least in parts, a thin oceanic crust;
- the Andaman Sea behind the Andaman arc (#13) with continuing seafloor spreading caused by an oblique subduction; an oceanic crust may be wide-spread although its details are poorly constrained by old and sparse seismic profiles; thick sediments may be associated with the adjacent Bengal Fan, while nearly zero free-air anomalies suggest insignificant plate deformation;
- the Aegean Sea behind the Hellenic arc (#24) which lacks any signs of seafloor spreading and linear magnetic anomalies; therefore the extension age and the age of the subducting (presumably) oceanic plate are unknown; the dip angle is one of the most shallow and the crust is the thickest among the back-arc basins globally; extremely shallow bathymetry and extremely high free air anomalies require a strong lithosphere deformation, which may be partially caused by the westward escape of Anatolia.

The presently active CO-type back-arc basins (Figs. 1, 13) are some of the most heterogeneous and variable in bathymetry, gravity anomalies, extension rates, subduction dip angle, and crustal structure, which varies from an extended continental type to oceanic crust produced by seafloor spreading. In contrast to the OO-type, the CO-basins are typically elongated with pronounced differences in the extension age and rate along the basins, further reflected in systematic differences in the pattern of magnetic anomalies, bathymetry, gravity anomalies, magmatism, and the crustal structure between the contrasting parts of the basins. Some basins have partially evolved to seafloor spreading, while the other part still undergoes continental rifting. Due to this principal difference, the CO-type back-arc basins may be further split into two sub-types with and without seafloor spreading (Section 4). The along-the-strike differences are non-related to the varying dip angles and the age of subducting oceanic crust along the trenches, where known. However, the commonly absent clear patterns of linear magnetic anomalies preclude conclusions on basement ages and extension rates and the related interpretations. Overall, it appears that nearly all CO-type basins have formed by a complex interplay of several geodynamic factors, where subduction roll-back may have played a subordinate role, if any (Fig. 2c,g,h,i).

3.1.4. Extinct back-arc basins (EXT) of two subtypes

The statistically representative EXT type includes 12 back-arc (sub) basins with a good data coverage (Fig. 1). These basins overall lack seismogenic zones associated with subducting slabs, and slab dip angles are unclear. While geodynamic origin of these basins remains speculative, they clearly fall into two major subtypes with different geophysical characteristics (Fig. 13). One subtype (EXT-1) includes only the extinct basins of the western Pacific Ocean (Table 2):

- the Shikoku Basin behind the Bonin arc (#7) and the adjacent Parece Vela Basin to the south (#8) which both have a thin crust, deep bathymetry, strong positive Bouguer anomalies and share a similar geodynamic evolution with similar trends of magnetic lineations and the paleo-extensional axes;
- the Western Philippine Basin (#9) which is the deepest marginal basin worldwide with the extremely high Bouguer anomalies typical of old oceans; it may possibly represent a trapped oceanic crust;
- the South China Sea (Nan Hai) behind the Manila trench (#10) which has a strong N-S asymmetry in free-air anomalies despite a N-S orientation of the extensional axis; the sea has a poor coverage by conventional seismic profiles and heat flow measurements;
- the Celebes Sea behind the Sangihe arc (#11) which was either formed by arc-arc or arc-continent collision or may include a trapped oceanic fragment; the basin has the largest positive Bouguer anomalies and the lowest heat flow among the extinct BABs consistent with a cold upper mantle typical of entrapped old oceanic fragments; the largest positive free-air anomalies indicate a strong plate deformation in a complex geodynamic setting;
- the small Banda Basin behind the Banda arc (#12) which, at present, is possibly the only BAB that was formed by arc-continent collision; heat flow data are of poor quality and the crustal structure may not be well constrained;
- the Woodlark Basin (#15) which, at present, is possibly the only back-arc basin where the CO-type collision involved a LIP on the oceanic plate (the Ontong-Java Plateau); the basin lacks seismic data on the crustal structure, while its bathymetry and gravity anomaly are similar to the OO-type active back-arc basins (Fig. 12).

The other subtype of the extinct BABs (EXT-2) includes the basins located in the Caribbean Sea, the Black Sea, and the West Antarctica region:

- the Aves Ridge of the Great Arc of the Caribbean (#21AR) which represents a remnant back-arc basin associated with the remnant arc; the basin has one of the thickest crust among all back-arc basins and by other geophysical parameters typically plots with active AO-type and OO-type basins;
- the Gulf of Mexico (#22) which has bathymetry and gravity anomalies closest to the OO-type; however, the spreading duration is not well constrained and the basement age is debated due to the lack of magnetic lineations, while seismic profiles remain restricted;
- the Western (#25w) and the Eastern (#25e) Black Sea Basins which are analyzed independently due to their large sizes and significant differences in many characteristics; similar to the Gulf of Mexico, magnetic lineations are unknown and the spreading duration (which may have pre-dated the Cretaceous) is unconstrained; geodynamic origin of both deep basins of the Black Sea is still uncertain and mechanisms other than back-arc extension cannot be ruled out; the basement high between the two basins may be related to the western

edge of the craton so that the two basins may have formed on the crust of different tectonic origin;
- the subglacial West Antarctica BABs behind the paleo-Pacific Phoenix arc (#26) which are limited by linear belts of magmatism and remnant seismicity along the edge of submerged extended crust; these basins with restricted geophysical and geological data are included only for comparison where possible.

The extinct back-arc basins include an unclear mixture of basins formed at different times in diverse geodynamic environments, so that their generalization is speculative. However, the extinct basins of the western Pacific Ocean (subtype EXP-1) are deep (mean bathymetry of −4381 m) and all have a relatively young (<60 Ma) relict seafloor spreading which ranges in age from Paleocene to Pliocene. These basins often show geophysical characteristics typical of old normal oceans (e.g. Fig. 12). Combined with their relict seafloor spreading, it suggests that they presently have oceanic crust (most likely reworked OO-type) which has sufficiently cooled towards the normal oceanic trend.

The differences in the characteristics within the subtype EXT-1 may be essentially attributed to the age of basin cooling. While direct comparisons with oceans are hampered by the debated cooling history of the basins, some constrains can be made. By the style of bathymetry versus Bouguer anomalies, the extinct BABs split into two distinct sets (Fig. 12b). The extinct BABs of the subgroup EXP-1 with developed seafloor spreading and small crustal thickness typical of normal oceanic plates clearly tend towards old oceans (Fig. 12c), and their clustering around ca. 20 My, ca. 100 My, and ca. 150 My old oceans may be caused by the corresponding differences in lithosphere cooling duration after termination of extension: 20–30 My in the South China and Banda Seas, and the Woodlark Basin; ca. 100 My in the Aleutian Basin (i.e. older than earlier proposed (Vaes et al., 2019)), the Shikoku and the Parece Vela Basins (therefore supporting an idea of their linked origin); ca. 150 My in the W Philippine Basin.

In contrast to this subtype, all other extinct basins (subtype EXP-2 with mean bathymetry of −2115 m) either have a relatively old (Jurassic to Cretaceous) relict seafloor spreading, or the age of seafloor spreading (possibly as old as Cretaceous) is speculative (Table 2). Despite a long time since the cessation of extension and basin cooling, these old basins do not plot next to an old (>60–100 My) oceanic crust due to their too shallow bathymetry and very low values of positive Bouguer anomalies (Fig. 12); they also have crustal thickness ca. 10 km larger than normal oceans (Table 3). This striking discrepancy between the subtype EXP-2 basins and old oceans, together with a common absence of magnetic lineations in the EXP-2 basins, suggests that these basins largely formed by subduction processes that involved a continental or an arc plate, and that these basins still preserve, in full or in large proportion, hyper-extended continental or arc crust. The non-Pacific extinct BABs also appear similar to the relatively young hot-spot provinces (the Kerguelen Plateau and the Iceland region) (Fig. 12a), which both have a > 20 km thick crust which may represent continental fragments (Shulgin and Artemieva, 2019; Foulger et al., 2020; Ponthus et al., 2020).

3.2. Mantle wedge and isostasy

3.2.1. Free-air anomalies and isostasy in BABs

Commonly, near-zero free-air anomalies are associated with regional isostatic equilibrium. Isostasy principal that requires equal hydrostatic pressures at equal (compensation) depths is valid only on geologic timescales, but ignores the slow rate of relaxation in a highly viscous cold lithosphere which can preserve a nonhydrostatic hypsometry for a relatively long time (Hager and Richards, 1989). Non-zero free-air gravity anomalies associated with topography anomalies can be effectively compensated by mantle flow, flexure of the elastic portion of lithospheric plate, lithosphere stresses, and their combinations (cf. McKenzie, 1994; Molnar et al., 2015), therefore providing a nearly equilibrium state. Vice versa, zero free-air anomalies may not mean the isostatic equilibrium, but instead may reflect a delayed effect of gravity equilibrium distorted on relatively short timescales, e.g. by dynamic topography associated with mantle flow (Burov and Gerya, 2014). While conventional isostasy neglects mantle dynamics, seismic anisotropy observed in many back-arc settings is traditionally attributed to mantle wedge convection and deformation in the mantle wedge (Billen and Gurnis, 2001; Kneller and van Keken, 2008; Morishige and Honda, *2011*; Long and Wirth, 2013; Lee and Wada, 2017). For example, mantle wedge convection proposed for the Lau Basin may explain high free-air anomalies (Martinez and Taylor, 2002).

Near-zero free-air anomalies are typical of only a quarter of the back-arc basins with average values showing a significant span from ca. -30 mGal to +70 mGal and with the extreme value of +130 mGal in the Aegean Sea (Fig. 12 and Table 1) where elastic stresses may be important in supporting topographic loads associated with complex regional dynamics (Cochran and Talwani, 1977; Brun and Sokoutis, 2010). There seems to be little consensus on the extent of isostatic equilibrium in various marine back-arc basins. A large amplitude of free-air gravity anomalies implies a disturbed isostatic equilibrium in most of the back-arc basins with many geophysical studies advocating an importance of dynamic topography (Martínez et al., 1999; Abers et al., 2002; Conder and Wiens, 2007; Kneller and van Keken, 2008; Long and Wirth, 2013; Magni, 2019; Balázs et al., 2022). Other studies (smaller in number) favour the isostatic equilibrium (Horváth et al., 1981; Tontini et al., 2007; Molnar et al., 2015), and gravity modeling based on the isostatic principle is still often used to infer the BABs crustal thickness (Tirel et al., 2004; Liu et al., 2016).

A simple way to address the problem of isostatic equilibrium is to test observations by a theoretical "rule of thumb" which suggests that in submerged regions normal tractions of mantle flow applied to the lithosphere base produce a dynamic topographic effect with the ratio of *[free-air gravity anomalies] / [mean hypsometric deviation]* > 30 mGal/km (McKenzie, 1994). A comparison of average free-air anomalies (reflecting long-wavelength features) in various back-arc basins with bathymetry deviations from the BAB-type averages shows that the OO-type BABs typically require a non-isostatic vertical convective traction to explain an extra +20 + 50 mGal of free-air anomalies with respect to the "rule of thumb". The same observation stands for several extinct back-arc basins of western Pacific. In particular, the Woodlark (#15) and the Banda Basins (#12), deviating from a 30 mGal/km theoretical limit towards the OO-trend, may have an incomplete post-extensional relaxation and secondary mantle convection (Martínez et al., 1999; Abers et al., 2002; Spakman and Hall, 2010). In contrast, free-air anomalies in the non-Pacific extinct and presently active AO- and CC-type BABs are, overall, below or close to the dynamic topography minimum bound of ca. 30 mGal per 1 km of extra hypsometry and these back-arc basins may be close to the isostatic equilibrium. However, the conclusions remain highly speculative and essentially assumption-driven, while an incomplete information on crustal structure in back-arc basins precludes meaningful estimates of residual gravity anomalies (Simpson et al., 1986).

3.2.2. Crust-mantle density contrast and mantle temperature

The effect of mantle melting on anomalous bathymetry in back-arc basin settings has been extensively analyzed in geochemical studies (Woodhead et al., 1993; Taylor, 1995; Taylor and Martinez, 2003; Kelley et al., 2006; Mibe et al., 2011; Li et al., 2022), geophysical studies (Cross and Pilger, 1982; Sdrolias and Mueller, 2006; Kneller and van Keken, 2008; Long and Wirth, 2013; Balázs et al., 2022), and numerical simulations (Billen and Gurnis, 2001; Gerya and Yuen, 2003; Syracuse et al., 2010; Lee and Wada, 2017; Magni, *2019*). Nonetheless, the density structure of the BABs mantle remains speculative. Trends in Fig. 12 allow for some simplistic speculations since, under classical isostatic assumptions, their slopes depend on in-situ crust-mantle density contrasts (Fig. 14a). A change in crustal thickness ΔM produces a

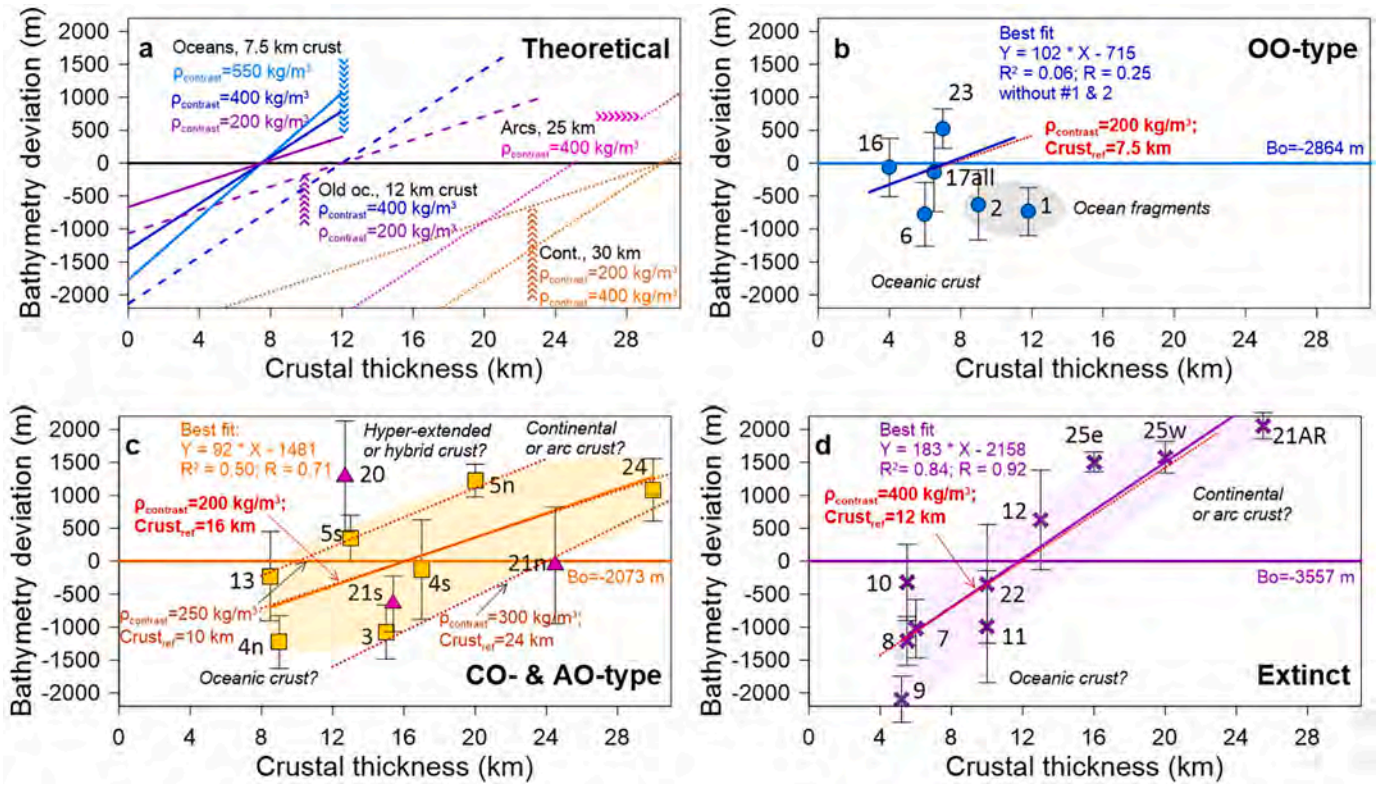

Fig. 14. Correlations between crustal thickness and bathymetry deviation from the mean water depth Bo (labelled at horizontal lines in plots (b-d)) in BABs of various types. (a) Theoretical ratios based on crustal isostasy, mean crustal thickness for various BAB types is shown by black text. The mantle-crust density contrast $\rho_{contrast}$ defines the slope of theoretical lines. (b-d) Data and trends for individual back-arc basins. Plots show observations (colored symbols with BAB numbers) and the best-fits lines (colored lines with text). The overlapped dotted red lines show the best-fitting theoretical isostatic lines (labelled in red with the values of reference crustal thickness and $\rho_{contrast}$). The CO-type in (c) shows a large scatter, which may be fitted by the average, the top and the bottom bounds. The best-fit AO-type line is not shown. The best-fit line in (d) combines both types of extinct BABs, and the best-fit in (b) is one of many options due to data cloud despite it excludes BABs #1 and 2 which are possibly trapped oceanic fragments.

bathymetry change $\Delta B = \Delta M(\rho_m-\rho_c)/(\rho_m-\rho_w)$ with mean in-situ densities of crust ρ_c, mantle ρ_m and seawater $\rho_w = 1050$ kg/m^3. Here ΔB is the deviation from the mean bathymetry determined for each BAB type (Table 3), and for each back-arc basin ΔM is the difference between a real and a typical (reference) crustal thickness (Figs. 11, 13). The best-fit lines for the individual back-arc basins can be fitted by theoretical lines with variable crust-mantle density contracts for various reference crustal thicknesses (Fig. 14b-d). This allows for speculating on, first order, Moho density contrasts in the BABs of different tectonic origin (Fig. 15).

The OO-type BABs have no clear trend, and crust-mantle density contrast of 200 kg/m^3 fits the data, among other options. In the CO-type BABs, an overall trend with a reference crustal thickness of ca. 16 km (hyperextended or hybrid crust typical of this BAB type, Table 3) provides density contrast of 200 kg/m^3, while the upper and lower limits suggest a crustal thickness of 10 or 24 km with the corresponding Moho density contrast of 250 and 300 kg/m^3, respectively (Fig. 14). The AO-type BABs are non-representative due to their small number, but the data from the Lesser Antilles may suggest a Moho density contrast of 150 kg/m^3 which implies a very high-temperature upper mantle. Cessation of extension and crust densification by cooling restore a high original density contrast of ca. 400 kg/m^3 in the extinct BABs (Fig. 16), and a high density contrast at the extinct Aves Ridge agrees with numerical experiments which predict that mantle wedge temperatures should decrease by >200 °C in 300 My after cessation of arc volcanism (Hall, 2012).

A common perception of high temperatures in mantle wedge below back-arc basins (Kincaid and Sacks, 1997; Eberle et al., 2002; Kelemen et al., 2003; Currie et al., 2004; Syracuse et al., *2010*) is usually derived from high seismic attenuation observed below various back-arc basins (Sato, 1992; Stern, 2002; Polatidis et al., 2003; Artemieva et al., 2004; Abers et al., 2014; Wada et al., 2015; Wei and Wiens, 2020). Clearly, the estimated Moho density contrast is insufficient to constrain mantle wedge temperature which depends on a large spectrum of parameters (Fig. 17a). However, the estimated values allow for comparison with independent constraints on mantle temperature in back-arc basins (Fig. 17b). The reported values vary from ca. 1000 °C at a 40 km depth in the mantle wedge of NE Japan (Nakajima and Hasegawa, 2003), 1200 °C in the Kurile Basin and the Alaska wedge (Stachnik et al., 2004), to ca. 1300 °C in the Aegean Sea and to ca. 1450 °C in the Manus Basin, the East Scotia Arc and the Mariana Trough (Syracuse et al., 2010). These values provide a statistically significant correlation with the estimated Moho density contrasts in these back-arc basins (Figs. 15-17b). A broad range of the estimated values implies that patterns of mantle convection and melt extraction, driven by mantle temperature variations, should be essentially different in back-arc basins of various types.

3.3. Seismic crustal structure

3.3.1. Crustal types in BABs

There is no typical crustal thickness in the back-arc basins, since the value is essentially controlled by the BAB tectonic setting, structures of the overriding and downgoing plates and melting regime in subduction system. The latter may depend, among other factors, on age of subducting oceanic plate, its temperature and fluid regime, slab dip, convergence rate, and volume of subducted sediments (Kincaid and Sacks, 1997; Eiler, 2003; Gerya and Yuen, 2003; Karato, 2003; Langmuir et al., 2006; Martinez et al., 2006). The unknown pre-extension crustal structure complicates interpretations in all tectonic settings. A highly

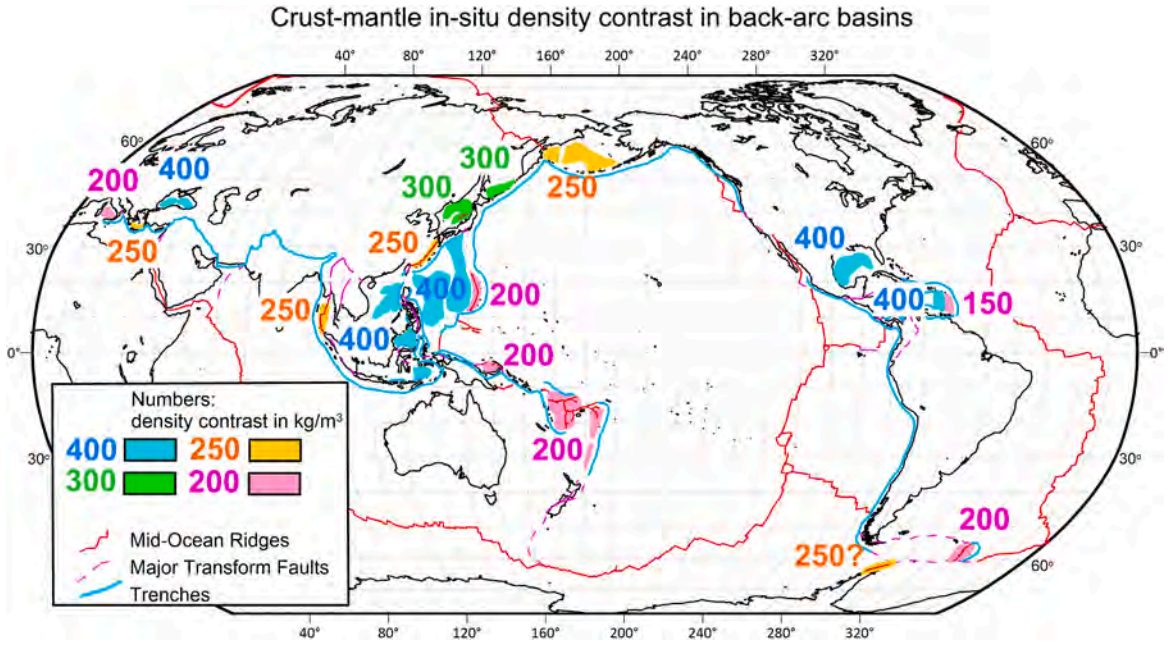

Fig. 15. In situ average crust-mantle density contrast (values in kg/m^3) in back-arc basins. The values are based on Fig. 14.

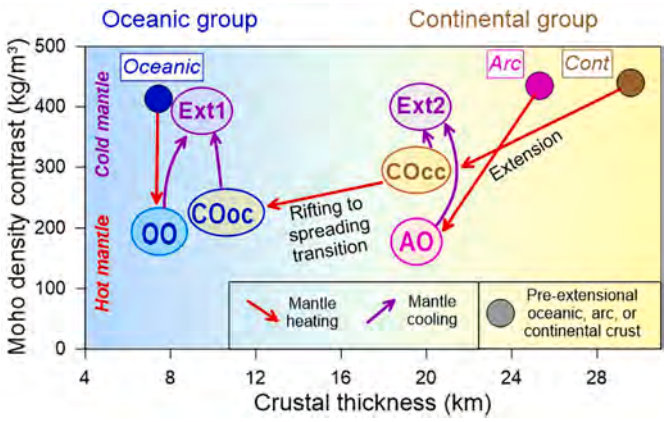

Fig. 16. Links between various BAB types based on correlations between the crust-mantle mean contrast and reference crustal thickness. Small circles correspond to the pre-extensional situation in three types of active BABs with a typical crust-mantle density contrast of 400–450 kg/m^3 and initial crustal thickness typical of normal oceans, arcs, and extended continental crust. Depending on the nature of the overring crust, the oceanic and continental groups of back-arc basins have different evolution, unless extension in the CO-type basins with stretched continental crust (COcc) progresses to seafloor spreading with formation of a significant portion of juvenile oceanic crust (COoc). Termination of BAB extension, associated with mantle cooling, restores a high original density contrast as observed in the extinct BABs.

variable volume of magmatic additions to the crust during extension (Woodhead et al., 1993; Taylor et al., 1995; Charvis et al., 1995; Martinez and Taylor, 2002; Thybo and Artemieva, 2013; Magee et al., 2016; Liu et al., 2018; Buntin et al., 2021; Li et al., *2022*) with possible abrupt short-wavelength changes (Dunn and Martinez, 2011) leads to further complications. Several crustal types may exist in back-arc basins, depending on tectonic setting and extension history, since not all back-arc basins evolve from rifting to seafloor spreading (Tables 1, 2), and many formed on oceanic lithosphere of the overriding oceanic plate. Crustal types in BABs include (Figs. 11, 18):

(i) young oceanic crust in any BAB-type setting if seafloor spreading stage was reached,

(ii) stretched pre-existing oceanic crust of the overriding plate at the OO-type of plate margin, regardless if seafloor opening in a BAB was initiated or not,

(iii) stretched arc crust of the overriding arc plate at the AO-type of plate margin if seafloor opening stage was not reached,

(iv) hyperextended (rifted) continental crust of the overriding plate at the CO-type of plate margin if seafloor opening stage was not reached; crustal structure in this tectonic setting may vary significantly depending on duration of stretching, the total opening rate, pre-extensional crustal structure in the overriding continental plate, and magmatism;

(v) hybrid crust in back-arc basins formed on continental plate and subject to various stages of extension, from rifting to hyperextension to formation of a new oceanic crust.

An oceanic-type crust in cases (i) and (ii) is not expected to be similar to "normal" oceanic crust formed at mid-oceanic ridges because of different spreading conditions (White et al., 1992; White and Klein, 2014; Artemieva and Shulgin, 2019), which in back-arc basins are closely associated with subduction (Wilson, 2007; Dunn and Martinez, 2011). Despite a similar total crustal thickness (Fig. 18), oceanic crust of back-arc basins has a thick fast-velocity lower crustal layer, which statistically makes almost 1/3 of the crust and is typically absent in "normal" oceans. There are, however, exceptions. Juvenile crust of the Mariana Trough formed above one of the steepest, possibly magma-starving subductions is similar to normal oceanic crust produced at mid-ocean ridges, while the pre-extensional crust is strongly anomalous in thickness and includes a ~ 3 km thick lower layer (Vp ~ 6.9–7.4 km/s) (Takahashi et al., 2007; Grevemeyer et al., 2021). A similar pattern is reported for the Lau Basin, where juvenile crust at the spearing axis is thicker than at the margins and in both cases a fast-velocity lower crustal layer is present (Martinez et al., 2006) (Fig. 11).

In the OO-settings, back-arc extension preserves an oceanic crustal structure of the overriding plate, with a typical BAB seismic crustal thickness of 7–8 km and as small as 4–6 km in several back-arc basins of the Pacific ocean (Table 1), including the Mariana Trough, Lau Basin and some extinct (possibly also the OO-type) BABs (Fig. 11). In some basins it is hardly possible to distinguish between pre-extensional and extensional oceanic crust, and it is speculative if a thin crust (Fig. 11) may have formed by an ultra-slow back-arc spreading as at ultra-slow

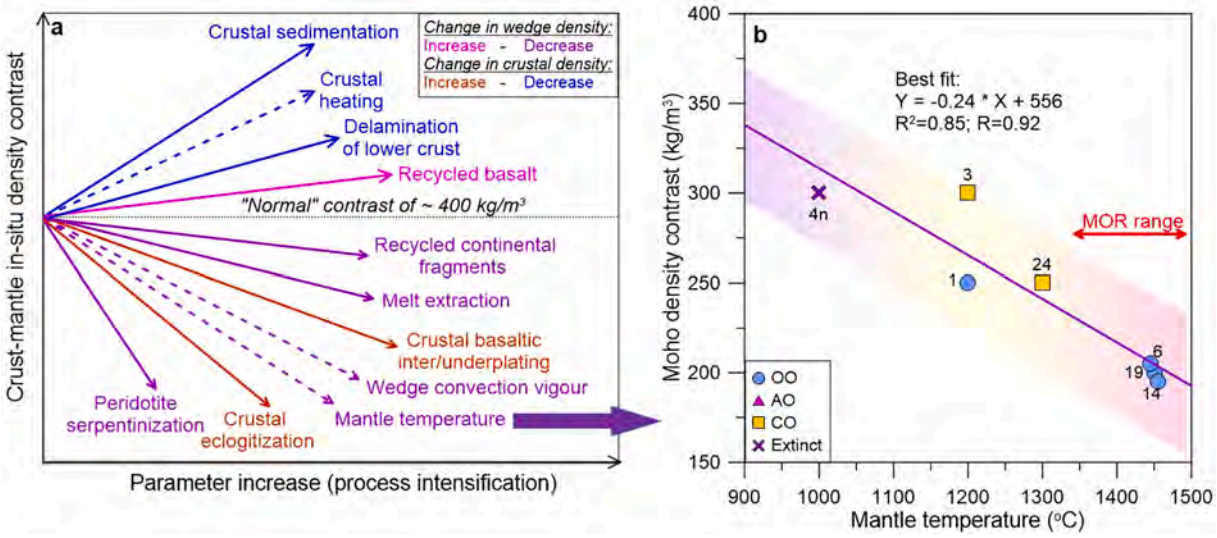

Fig. 17. (a) Sketch illustrating general trends in changes of average crust-mantle density contrast in mantle wedge caused by various thermo-compositional parameters. Relative contributions of various processes may vary in broad regions and their order may change accordingly. (b) The estimated Moho density contrast (Fig. 15) correlates with published estimates on mantle wedge temperatures (Stachnik et al., 2004; Syracuse et al., 2010; Nakajima and Hasegawa, 2003).

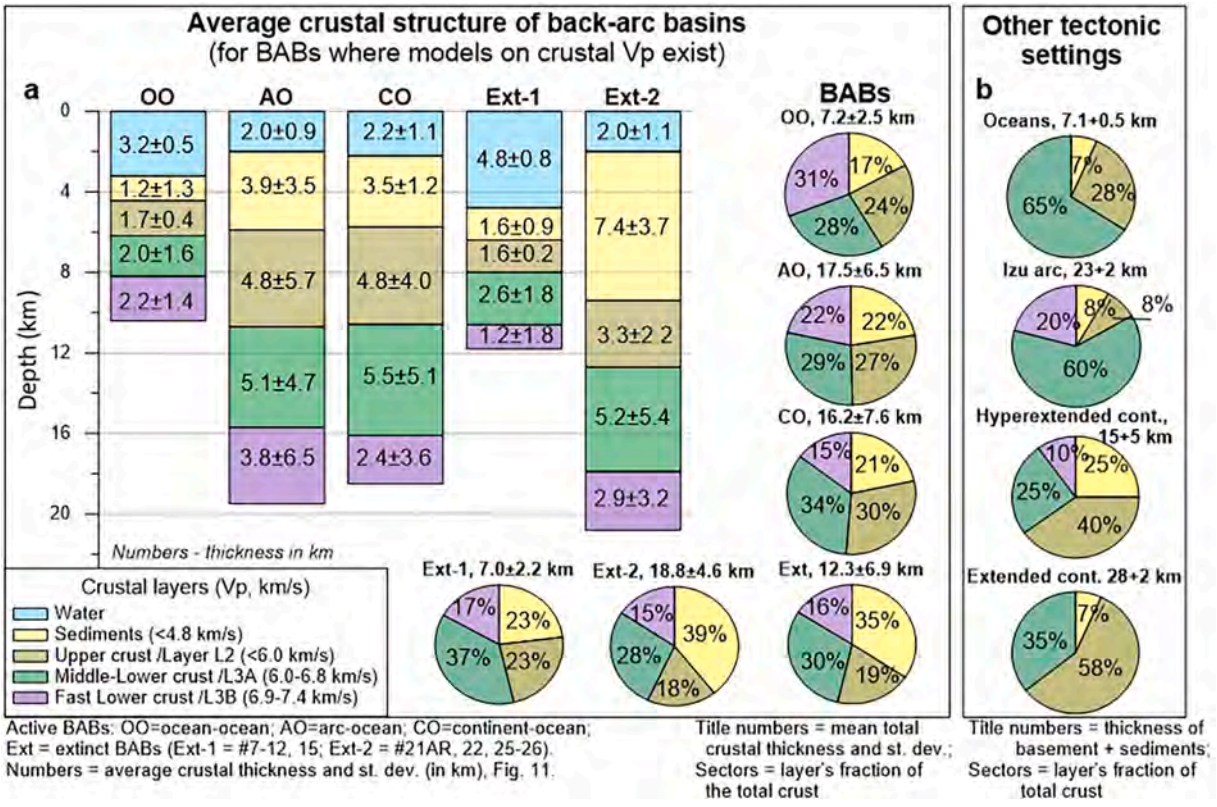

Fig. 18. (a) Average crustal structure in the off-shore back-arc basins by tectonic settings (based on Fig. 11). Right column shows the corresponding pie-sections in percentage of total crustal thickness. Extinct BABs are split into the Pacific (Ext-1) and non-Pacific (Ext-2) types. For references see the text. (b) Typical crustal structure in normal oceans (White et al., 1992), the Izu-Ogasawara island arc system (Takahashi et al., 2009), continental hyperextended crust of the Rockall Trough (Klingelhöfer et al., 2005) and continental extended crust as in the Basin and Range Province of W. USA (Christensen and Mooney, 1995). A characteristic feature of the back-arc basins, especially in the OO-settings, is the presence of a thick (~38% of basement thickness) high-Vp lowermost crustal layer which is absent in "normal" oceans. In the CO- and AO-settings, the crust of the back-arc basins is similar to hyperextended continental and arc crust, respectively (compare the pie-sections).

MORs (Small, 1994; Bown and White, 1994; Weigelt and Jokat, 2001), or resulted from thinning of pre-extensional crust in the overriding oceanic plate, or reflects a combination of both. A thin and ultra-thin oceanic-type crust in the extinct Pacific back-arc basins indicates their possible formation in ocean-ocean plate collisions, while a hybrid or hyper-extensional continental and arc crust in the non-Pacific BABs is similar to the crust of active BABs formed in the CO- and AO-settings (Fig. 18a).

The crust of the AO- and CO-type back-arc basins is, on average, very similar (Fig. 18). Statistically, their crust differs by the thickness of underplated high-Vp (mafic) crustal layer, which is 3.5–4 km thick in arc crust and ca. 2.5 km in extended continental-type BABs (Fig. 18a). This difference may reflect an importance of relamination in generation of lower continental crust in arcs (Kelemen and Behn, 2016). Besides, in the AO-type back-arc basins (case iii listed above) the crust apparently preserves the structure of the pre-extensional island arc crust as exemplified by the Izu-Ogasawara arc system (Takahashi et al., 2009). A hyper-stretched continental crust in the CO-settings (case iv), while preserving the upper felsic layer characteristic of continental crust, may differ significantly from extensional crust, e.g. of continental rift zones. It may, instead, have a crustal structure similar to hyperextended continental crust of the Atlantic passive margins (Skogseid et al., 2000; Klingelhöfer et al., 2005; Shulgin et al., 2020), the Iceland-Faroe Ridge (Shulgin and Artemieva, 2019; Foulger et al., 2020), and possibly the Kerguelen Plateau (Charvis et al., 1995; Ponthus et al., *2020*) (Fig. 18a). Therefore, crustal structure of back-arc basins associated with continental-ocean collisions has little in common with a popular perception of extended continental crust (Fig. 18b).

3.3.2. *High-Vp lower crust*

The presence of a thick high-Vp (>7.0 km/s) lower crustal layer which, statistically, makes 15–30% of the total crustal thickness is a fundamental characteristic of the back-arc basins (Fig. 18a). For the hyperextended BABs, this feature is similar to magma-rich passive margins and, for the OO-type basins, to oceanic hotspots settings where significant crustal thickening is mostly produced by thickening of Layer 3 where it can make up to ca. 50% of the crust as observed in the Alpha Ridge, the Iceland-Faroe Ridge, the Kerguelen-Heard Plateau and the Ontong-Java Plateau (Forsyth et al., 1986; Fyfe, 1992; Charvis et al., 1995; Holbrook et al., 2001; Miura et al., 2004; White et al., 2008; Thybo and Artemieva, 2013). Since pre-extensional crust in the AO and CO back-arc settings may had a high velocity lower crustal layer (Fig. 18b), the volume of magmatically added material associated with back-arc extension is hard to estimate.

The wide-spread presence of a high-velocity crustal layer in the back-arc basins of different types indicates an importance of magmatic underplating in mantle wedge settings and crustal growth by magmatic additions. The added magmatic material may essentially compensate crustal thinning caused by back-arc extension. A correlation between crustal thickness and lower crustal velocity would support an importance of underplating mechanism in crustal growth (Grevemeyer et al., 2021). Indeed, in the back-arc basins considered here, large regional variations in the total thickness of crystalline crust are caused chiefly by variations in thickness of a fast (>7.0 km/s) lowermost crust (Fig. 19b). The correlation apparently exists only for oceanic-type crust <10–12 km in thickness (blue shading in Fig. 19a) and weakens when slower crustal layers (>6.2 km/s) are included (Vp-values are color-coded).

3.3.3. *Crustal thinning by extension*

Estimates of extensional β-factor (the ratio of pre-extensional and present thicknesses of the crystalline basement) are hardly possible for back-arc basins because the present-day crustal thickness reflects a counter-play of crustal extension and magmatic crustal growth above mantle wedge, and pre-extensional crustal structure is unknown. The present-day crustal column without lower crust cannot be adopted as representative of crustal thinning without magma compensation (Thybo and Nielsen, 2009), since pre-extensional lower crust of an unknown thickness may have existed in many back-arc basins. In contrast, a thin oceanic-type crust may be caused not only by crustal stretching, but may reflect magma-starving conditions in making juvenile oceanic crust.

First order estimate of crustal thinning in back-arc basins adopts here typical crustal thickness values for various tectonic settings as pre-extensional thickness of crystalline basement: 25 km in active and paleo-island arcs (#12, 21AR) (Takahashi et al., 2009; Kopp et al., 2011), 30 km in active and paleo-rifted continental crust (#4, 25, 26) (Christensen and Mooney, 1995; Thybo and Nielsen, 2009), and 8 km as in oceanic plate (Bown and White, 1994) in the extinct Pacific BABs (#7–11) and the Gulf of Mexico (#22). The OO-settings are excluded to avoid problems in distinction between juvenile and pre-extensional oceanic crust. While the estimates depend on the assumed thickness of pre-extensional crystalline basement, its variations in normal oceans and island arcs are usually small (White et al., 1992; Calvert, 2011), but the adopted thickness of 30 km for the CO-type BABs is a strong generalization since extended continental crust may be highly variable in basement thickness.

A wide range of estimated crustal thinning factors (Table 1, Fig. 13i) reflects a strong heterogeneity in crustal extension in different back-arc tectonic settings, with mean values ranging from ~1.7 in the AO-type BABs to ~2.8 in the continent-ocean collisional settings and with some extreme values of >4.0 (the southern Okinawa Trough, the Japan Basin, the Andaman Sea, and the Black Sea basins). A reduction in crustal thickness would be equivalent to β-factor if no magmatic material were added to the crust during stretching, which is hardly the case for most of basins (Thybo and Artemieva, 2013). However, extremely high estimated values may also indicate a very minor volume of magmatically-added material.

Yet very high thinning factors (3.75–4.25) in the Black Sea basins (Table 1) cannot be explained by the lack of magmatic additions, which are known from seismic reflection studies (Nikishin et al., 2015). At the same time, the present estimates agree with an analysis of seismically constrained sedimentary sequences, which reported conventional β-factor of 3–4 in the deep NW part of the Western Black Sea Basin and of ca. 5 in the deep SE part of the Eastern Black Sea Basin (Shillington et al., 2008). β-factor values of 4–5 are usually associated with a rupture of continental lithosphere (Keen and Beaumont, 1990), so that the estimated crustal thinning factor should have been high enough to initiate seafloor spreading in the Black Sea basins as interpreted in some studies (Nikishin et al., 2015) but not accepted unanimously. Much smaller values proposed for the Cretaceous (major phase) extension imply that the Black Sea crust may have been significantly stretched by pre-Cretaceous extensional events (Stephenson and Stovba, 2021). This model is not in conflict with the present estimates which are free from constraints on the timing of crustal thinning.

3.4. *Back-arc extension and seafloor spreading*

3.4.1. *Subduction parameters controlling BAB formation*

3.4.1.1. Age of downgoing plate. This section builds on examining possible correlations and trends related to back-arc extension and spreading in order to define the parameter space where back-arc basins may form in relation to the associated subductions and where back-arc extension may progress from rifting to seafloor spreading (Figs. 20, 21). Not all subduction systems form back-arc basins. The reasons why they do or do not form BABs are not yet understood despite numerous studies which addressed magmatic, thermal, mechanical, and kinematic processes associated with various mechanisms proposed for back-arc extension (Karig, 1971; Sleep and Toksöz, 1971; Molnar and Atwater, 1978; Uyeda and Kanamori, 1979; Shemenda, 1993; Faccenna et al., 1996, 2012; Scholz and Campos, 1995; Stern, 2002; Heuret and Lallemand, 2005; Schellart, 2005; Schellart et al., 2007; Doglioni et al., 2009).

With an intuitive notion that old and cold oceanic plates are less buoyant and therefore should subduct easier than young and buoyant plates, a number of studies attempted to find correlations between subduction dynamics and age of subducting plates (Uyeda and Kanamori, 1979; Furlong et al., 1982; Grellet and Dubois, 1982; Carlson et al., 1983; Jarrard, 1986; Sdrolias and Mueller, 2006). The proposed cut-off ages for subducting oceanic plates to form a back-arc basin in any

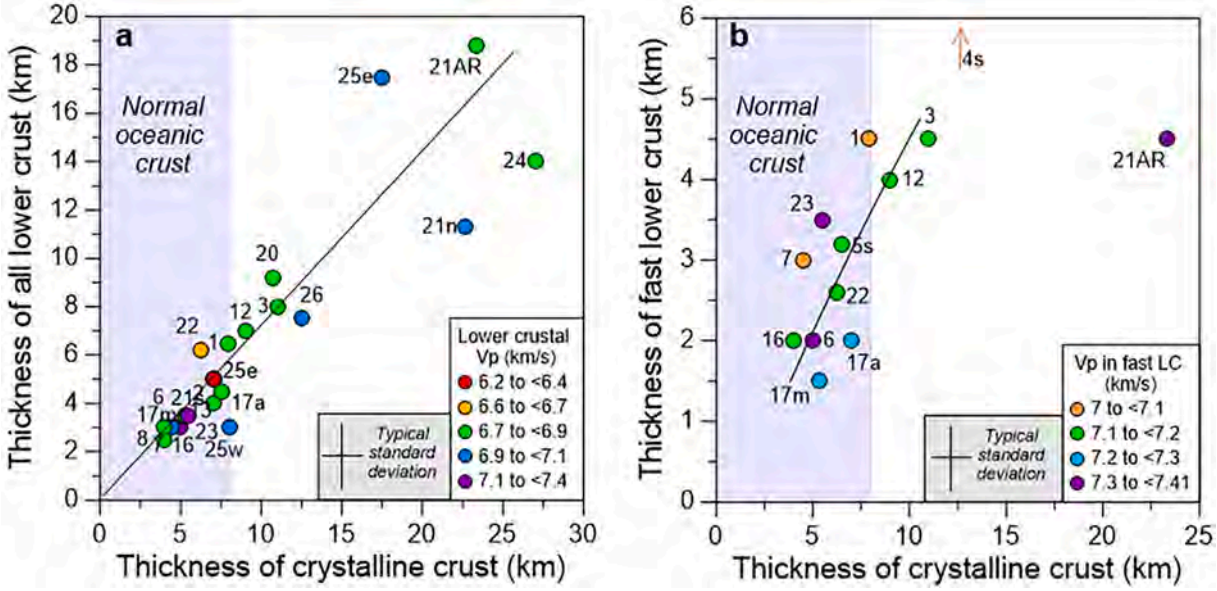

Fig. 19. Thickness of crystalline crust versus thicknesses of lower crust (a) and fast Vp (>7.0 km/s) lowermost crust (b). Color code - average Vp in the lower and lowermost crustal layers, respectively (note different color codes). Interpretations for the top of the lower crust and the top of the fast lowermost crust are adopted from the original seismic studies (see references in the text). For example, the lower part of the crust with Vp ~ 6.3 km/s in the Eastern Black Sea Basin (#25e) was interpreted as Layer 3 (Minshull et al., 2005). Numbers - back-arc basins (see Fig. 1 for locations). The correlation in (b) indicates that growth of oceanic crust in the back-arc basins occurs primarily through magmatic underplating by melts generated in the mantle wedge. The trend includes mostly BABs of the OO-type.

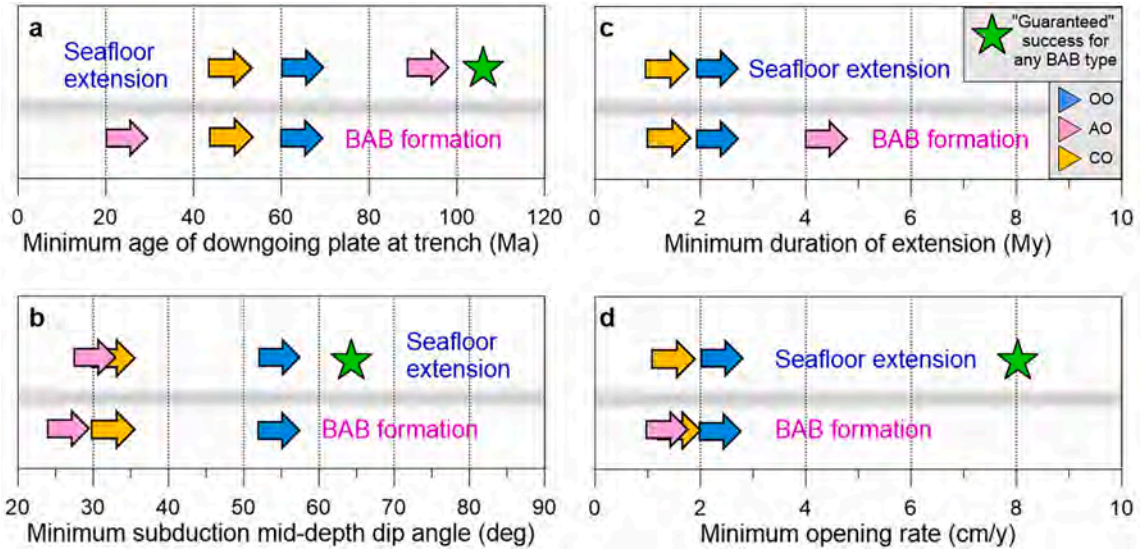

Fig. 20. Sketch summarizing minimum values of subduction process parameters required to initiate formation of back-arc basins and BAB seafloor spreading on the present Earth. The values are based on data for the individual BABs. Arrows – minimal values (color code as in other figures); stars – "guaranteed" successful spreading for any tectonic setting.

tectonic setting range from 55 My (Sdrolias and Mueller, 2006) to 80 My (Furlong et al., 1982).

This study suggests that correlations are obscured when subduction systems of different types are considered together because of significantly different plate cut-off ages in the OO, AO and CO subduction settings where back-arc basins have formed (Fig. 20a). The present analysis shows the following for the present Earth.

- Back-arc basins do not form if downgoing plate is younger than ca. 20 My.
- BABs may evolve to spreading if subducting oceanic plate is at least 45 My old (see below).
- In the OO settings, back-arc basins form only when subducting oceanic plate is old and cold, with mean age of ~87 My and the minimum known age of ~60 My in the East Scotia Basin.
- In the CO settings, back-arc basins form already when subducting oceanic plate is ~45 My old (the southern Okinawa Trough). The AO subduction systems may be less sensitive to the plate age, but the examples are highly limited.
- When oceanic plate subducts below an island arc, it may be as young as ~20 My to form a back-arc basin (e.g. the Bransfield Basin).

3.4.1.2. Subduction dip angle. It has long been noted that all steeply dipping offshore subduction zones are associated with active back-arc extension in marginal seas (Molnar and Atwater, 1978; Cross and

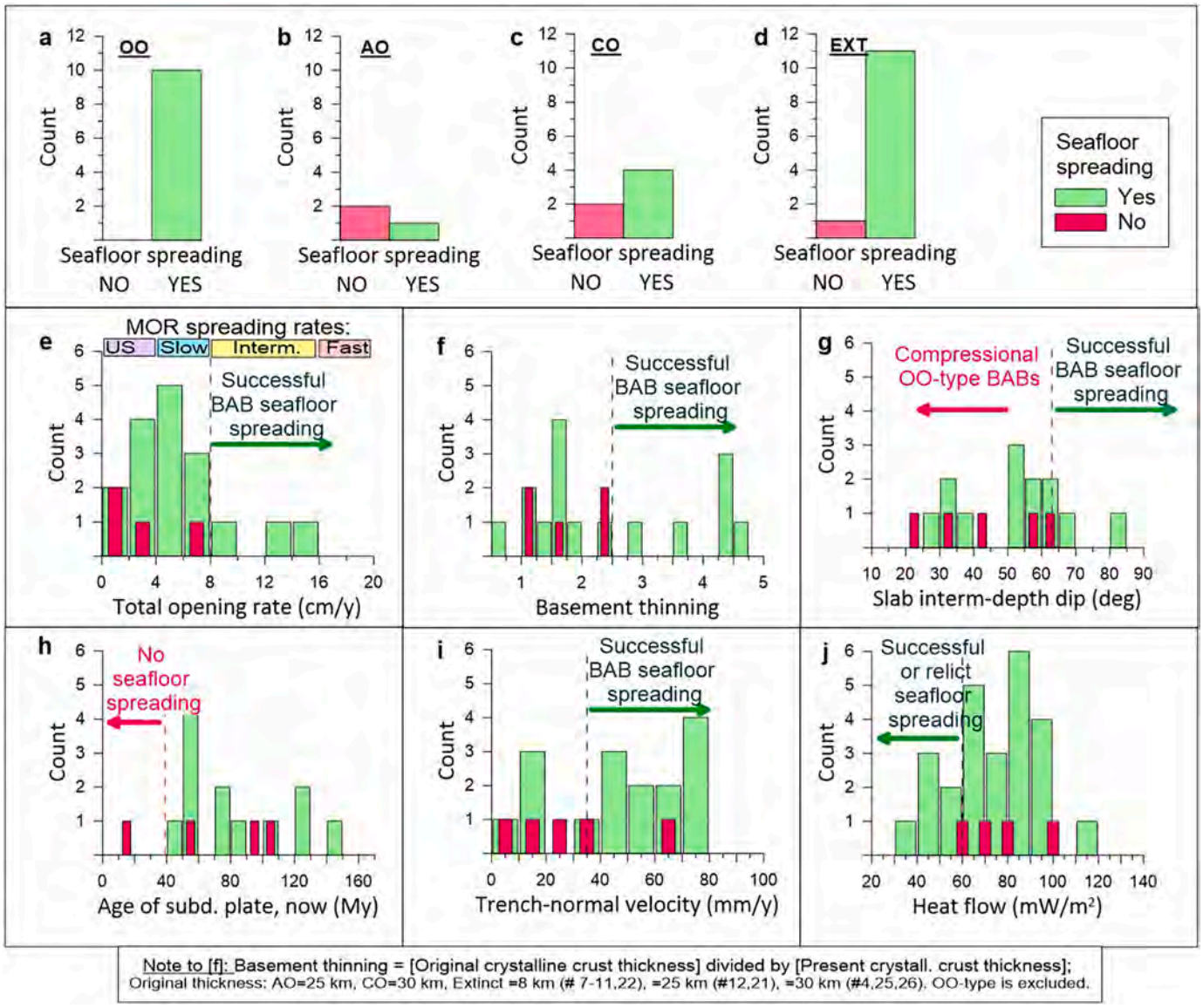

Fig. 21. Global statistics for the presence or the absence of seafloor spreading in the back-arc basins on the present Earth in relation to tectonic settings (a-d, upper row), total opening rate (e), crustal basement thinning during BAB extension (f, the OO-type is excluded, see footnote), subduction parameters (g-i), and average heat flow (j). Red arrows highlight the parameter space with no active seafloor spreading, green arrows highlight the parameter space where seafloor spreading is favored at present.

Pilger, 1982). Therefore, a steep subduction, possibly facilitated by directional preferences (e.g. Doglioni, 1991; Panza et al., 2007), has often been considered as a pre-requisite to form a back-arc basin. Yet recent studies reduce the cut-off intermediate-depth dip angle of subducting slabs to form a back-arc basin from >60° to ~30° (Sdrolias and Mueller, 2006). Note that due to a striking difference in the slab dip angle beneath the OO- and CO-type BAB subduction systems (Fig. 10), a shallow cut-off subduction angle may be expected only for the CO- and AO-type back-arc basins (Fig. 20b). This observation suggests a minor role of a slab dip angle in defining if a back-arc basin develops or not, and it may only be considered here in association with other deciding parameters.

In the present Earth, the minimum observed dip is ~50–55° in the OO-type and 30-35° in the CO-type (Fig. 20b) with mean values of 65° ± 11° and 38° ± 12°, correspondingly. Slab dip-angle controls the trench-slab distance (Fig. 22b) and the lateral location of melting zones, commonly situated at a 100 ± 30 km depth near the upper part of subducting slabs (England et al., *2004*). As result, melting largely occurs 175 ± 57 km away from the trench in the OO-type BABs and 290 ± 80 km away in the CO- and AO-type BABs with a larger distance in the arc-type basins (Table 3, Fig. 22cd). However, neither a trench-slab distance, nor a slab dip angle are correlated with trench-normal slab velocity (Mantovani et al., 2001; Schellart et al., *2011*; Table 2), the effect of which is effectively compensated by other extensional factors in subduction systems.

Arc-ocean subductions can form an extensional back-arc basin at a significantly more shallow (25-45°) slab dip than in other BAB types, as exemplified by the Bransfield and the Lesser Antilles Basins (Fig. 20b). However, back-arc basins formed behind a shallow subduction often do not progress to seafloor spreading (Fig. 21g), and compressional rather than extensional back-arc tectonics is associated with a shallow (<30°) or flat subduction of young buoyant oceanic lithosphere in the eastern

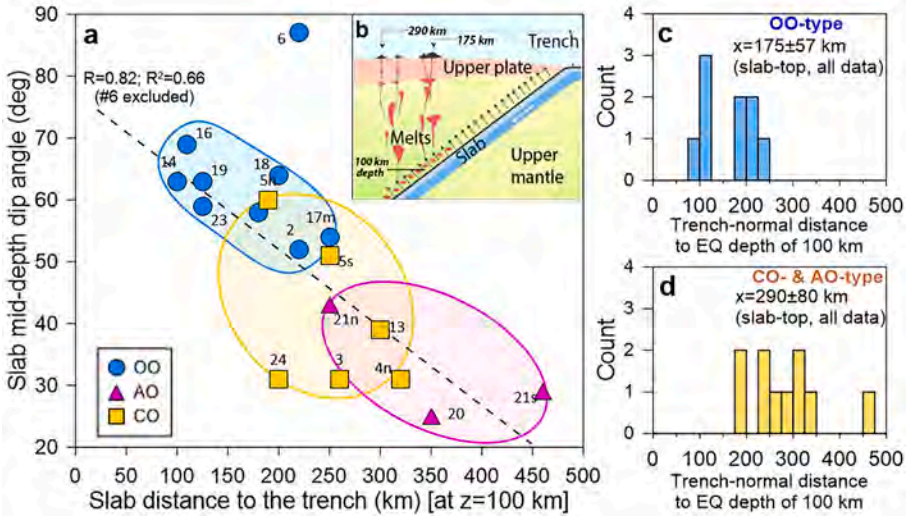

Fig. 22. Relations between subduction parameters in the back-arc basins of various types (numbers - back-arc basins, see Fig. 1 for locations). Dashed line and colored ovals highlight major trends. (a) Dip-angle of a slab is determined from seismicity at ca. 50–200 km depth (Fig. 10). (b-d) The slab's top surface at 100 km depth, where melting largely occurs, is displaced from the trench by 175 ± 57 km in the OO-type BABs and by 290 ± 80 km in the CO- and AO-type BABs. Because of steep subduction in the OO-type basins and shallow subduction in the CO- and AO-type basins (a), melting in the OO-type should occur at distances ca. 100–120 km closer to the trench than in other BAB types (b-d). Trench-normal slab velocity (data of Schellart et al., 2011) does not correlate with trench-slab distance, nor with slab dip angle.

Pacific Ocean (Molnar and Atwater, 1978).

3.4.1.3. Opening rate and duration of extension. Neither total extension rate nor its duration play independent roles in evolution of back-arc basins. Yet opening rate in back-arc basins should be important, if spreading rate affects morphology and crustal structure similar to mid-ocean ridges where juvenile crust formed at the ultra-slow spreading ridges is anomalously thin (Small, 1994; Bown and White, 1994). This expectation is not supported by observations. Crustal thickness in the back-arc basins shows no trend for any of the individual BAB types, and may even become large when slab dip angle is small, if all BABs, regardless of their type, are plotted together. This apparently opposite trend between crustal thickness and opening rate reflects a principal difference between the OO- and CO-type back-arc basins (Figs. 10, 18): the CO-type BABs with a thick crust all have small opening rates, comparable to ultra-slow and slow spreading rates at mid-ocean ridges. In contrast, the OO-type back-arc basins may have opening rate similar to spreading rates at fast-spreading mid-ocean ridges (Fig. 21e).

The duration of extensional phase is, apparently, independent of subduction settings (Fig. 20c) and, therefore, of mechanisms of back-arc extension (Fig. 2). Short spreading duration is typical of the back-arc basins of all types and suggests that BAB formation is essentially controlled by external factors (e.g. subduction dynamics and stress field) rather than by rheology of the overlying plate. Back-arc basins may initiate at very early stages of extension (1–2 My), and extension may typically continue for 5–15 My. An apparently longer duration of extension in the extinct BABs (Fig. 13f) may possibly reflect a large uncertainty in age constraints for paleo-extensional settings.

3.4.2. Parameters controlling BAB seafloor spreading

Lithosphere stretching in back-arc basins may, or may not, progress from rifting to seafloor spreading. A thermo-mechanical subduction modeling suggests that back-arc rifting transfers to back-arc spreading when a nearly vertical slab crosses the mantle transition zone and reaches the 660 km discontinuity with stress transmission up the slab to a low-viscosity mantle wedge where it causes back-arc extension (Ishii and Wallis, 2022). This process, possibly leading to repeated cycles of spreading, has been proposed for the evolution of seafloor spreading in the South Fiji, the Lau Basin, the Parece Vela Basin and the Mariana Trough. Yet it is doubtful that the model requirements for the slab to cut the transition zone are supported by seismic evidence, especially for the extinct Parece Vela Basin and for the Fiji-Lau region with moderate subduction dips (Table 2), while the present seismicity in the Mariana slab apparently terminates within the transition zone (Artemieva et al., 2016).

The present analysis includes 31 back-arc subbasins, most of which have seafloor spreading with magnetic lineations (Tables 2). Despite the analyzed pool is dominated by the active OO-type and the relict Pacific basins (most likely also of the OO-type collisions), seafloor spreading is seemingly a common culmination of a BAB stretching. However, one should make a clear distinction between a *"guaranteed"* successful extension-to-spreading transition (Fig. 21) and *the minimal values* of subduction parameters when seafloor spreading may take place (Fig. 20). The following overall patterns may be recognized in the

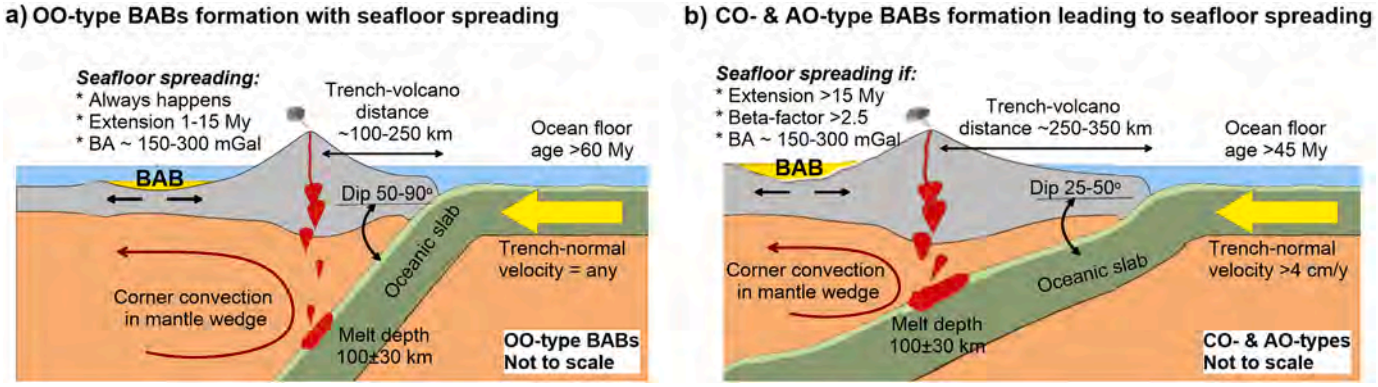

Fig. 23. Sketches illustrating favorable parameter space values for seafloor spearing in the present back-arc basins of various tectonic types. See text for explanations, the values are based on Table 2.

present plate configuration, despite limited data (Figs. 21-23).

- Back-arc extension always evolves to seafloor spreading when the overriding plate is oceanic. A high success rate in the progression of lithosphere stretching to spreading in the extinct back-arc basins indicates that many of them were formed in the OO settings (Fig. 21a,d).
- A "guaranteed" successful transition from crustal extension to seafloor spreading requires the total opening rate > 8 cm/y in back-arc basins, i.e. similar to intermediate and fast spreading rates in normal oceans (Fig. 21e). Under favorable conditions independent of tectonic settings, seafloor spreading may also initiate at much smaller extension rates acting at short times (Fig. 20c,d).
- Strong reduction in crustal thickness ($\beta > 2.5$), possibly compensated by crustal growth through magmatic additions, apparently is required for successful initiation of *seafloor spreading* in the overriding oceanic plate (Fig. 21f) while the amount of extension required to initiate *back-arc basin formation* may be low. In case of the overriding continental lithosphere, the extension factor should reach $\beta \sim 4$–5 to progress to seafloor spreading, in agreement with earlier results (Keen and Beaumont, 1990).
- A successful transition from crustal extension to back-arc seafloor spreading does not take place, when subducting oceanic plate is young (<40–45 My) (Fig. 23), but the age limit increases to >60 My in the OO-type BABs which all dip at steep angles (>50° at intermediate-depth) (Fig. 10a). As a consequence, seafloor spreading in the OO-type BABs always initiates with a slab dip >50°.
- A *guaranteed* success of spreading in any tectonic settings requires even a larger dip angle (Figs. 20b, 21g), although spreading *may initiate* at much smaller dip angles. However, small dip angles typical of the CO-type settings may lead to a compressional back-arc regime as in the Andes (Molnar and Atwater, 1978); the process implies shortening of the overriding plate with a compression of the back-arc region if the plate moves towards the trench. This observation implies a critical role of the mantle wedge geometry in corner-flow dynamics and initiation of back-arc seafloor spreading.

3.4.3. *Eastward global mantle flow and BAB extension*

Eastward mantle flow associated with the westward drift of lithospheric plates with respect to the mantle (Uyeda and Kanamori, 1979; O'Connell and Hager, 1991; Ricard et al., 1991) and supported by seismic shear-wave tomography for the western Mediterranean (Panza et al., 2007) has been proposed to explain the observed asymmetry in the global distribution of subduction systems (Doglioni, 1991), which are usually steep (~65°) in W-ward dipping subductions and shallow (~27°) in E-directed subductions (Ficini et al., 2017; Jacobsen, 2018). The asymmetry in dominant mantle flow direction should assist slab roll-back, eastwards retreat of the slab hinge and lithosphere extension with formation of back-arc basins in W-dipping subductions (Doglioni, 1991) (Fig. 2c). In contrast, shallowing of E-dipping slabs, assisted by

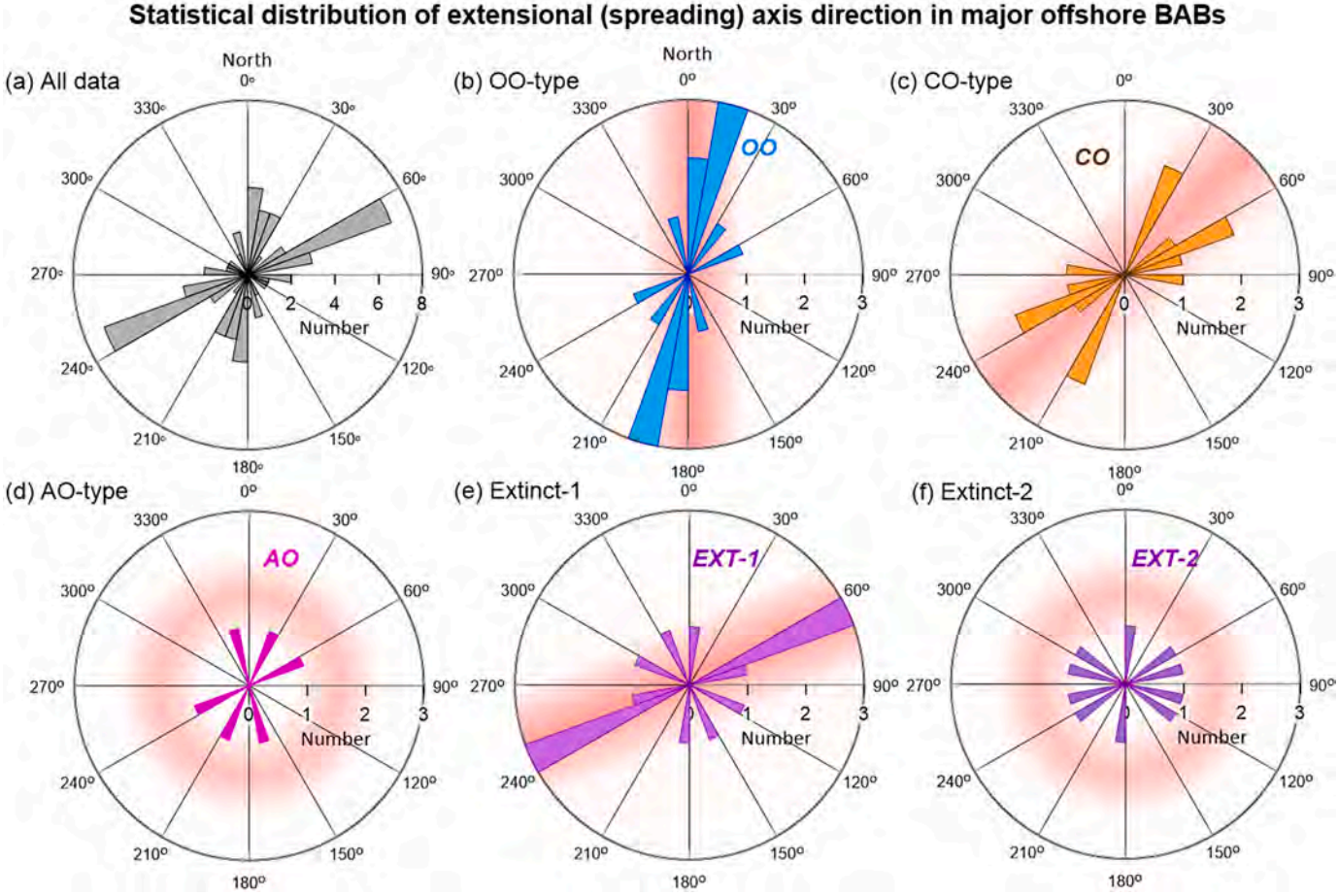

Fig. 24. Statistical distribution of the extensional (spreading) axis direction. Plots are similar to bar histograms. Circular axis – angle in deg. (bin = 10°); radial axis shows number of data points (the same scale is used in (b-f)). For the curved trenches (e.g. #15, 16, 22), an intermediate value (typical of central segments) is used. If eastward mantle "wind" controls subduction direction (Ficini et al., 2017), extensional axes should roughly be N—W oriented as observed in the OO-type (b). The plot illustrates directional preferences for BABs of different types, since orientation of the extensional (spreading) axis does not discriminate between E-ward and W-ward dipping slabs. The CO- and EXT-1 basins tend to have the extensional axes rotated by 50-60° compared to the mantle "wind" predictions, which in case of the Pacific extinct BABs (e) may reflect a paleo-rotation. Both active AO- and EXT-2 basins have randomly oriented extensional axes (d, f).

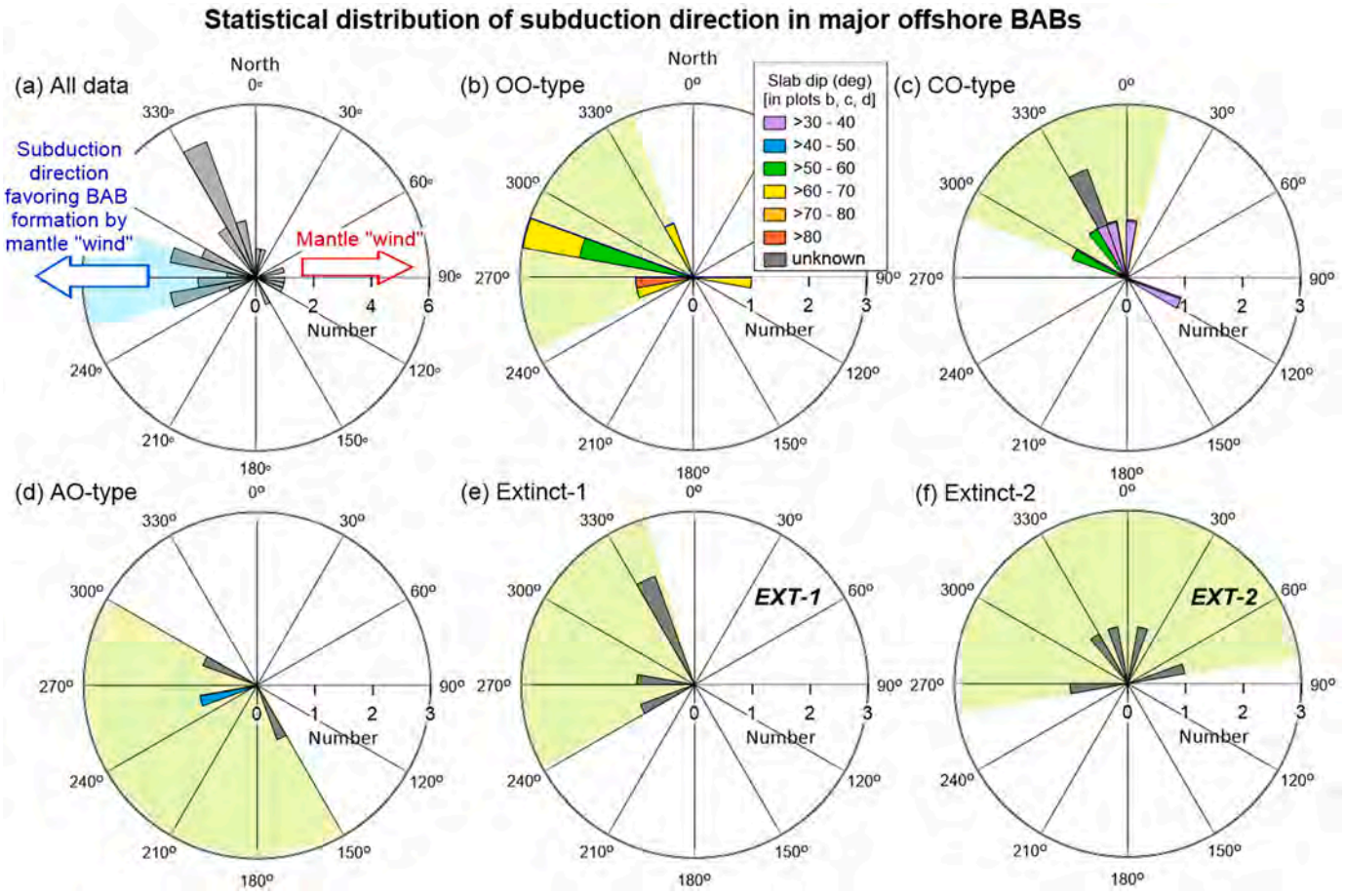

Fig. 25. Testing the role of E-ward mantle flow (Doglioni, 1991; Ficini et al., 2017) in BAB evolution (based on the values in Table 2). Plots are explained in Fig. 24. Relict basins with unknown subduction directions are excluded (#1, 2, 9, 11, 15). Sectors are colored by slab dip angle, where available (b-d). E-ward mantle flow should promote BABs formation in westward dipping subductions (a, blue shading). Green shading highlights dominating slab directions. Most OO-type BABs with steep subductions follow the predicted pattern (b), while BABs of other tectonic types deviate from it.

mantle flowing in the same direction, should hamper formation of back-arc basins in such subduction settings (Doglioni et al., 2009; Ficini et al., 2017).

The present analysis tests this concept by plotting a statistical distribution of directions of the extensional (or spreading, where available) axes based on the values in Table 2 (Fig. 24). Eastward mantle flow should promote a N-S orientation of the extensional axes; however this pattern is observed only in the OO-type back-arc basins, and the roughly N—W oriented spreading axes in the Aleutian and Komandorsky Basins are not related to the present subduction of the Aleutian Arc (Table 2). The CO-type group includes two back-arc basins of the Sea of Japan, with extensional mechanisms that also do not require subduction (Fig. 2 hi). These basins with a 70–75° direction of the spreading axes (Table 2) essentially affect the geographically limited statistics (Fig. 24c). The extinct Pacific BABs tend to have the extensional axes rotated by 50-60° compared to the mantle "wind" predictions, which may possibly reflect a paleo-rotation of these basins. Note that some of them may have also been formed by extensional mechanisms that do not require subductions (Table 2).

The role of eastward mantle flow in BAB evolution and its possible effect on the E-ward and W-ward dipping slabs is further tested in Fig. 25, since the orientation of the extensional axis does not distinguish the opposite directions of subduction polarity. This plot is complementary to Fig. 24, since spreading directions are established for many extinct back-arc basins, while their links to paleo-subductions and paleo-subduction orientation remain controversial. Similar to the previous result, subduction orientation in many OO-type BABs aligns with the pattern predicted by eastward mantle flow (Fig. 25b), while other tectonic types have random orientations of slab directions. Overall, the analysis suggests that the directional preference for back-arc extension and slab direction apparently exists only for the OO-type basins, where eastward mantle flow may play an important role in their evolution ((Doglioni, 1991; Doglioni et al., 2009)).

3.5. *Thermal structure of BABs*

3.5.1. *Heat flow and subduction settings*

Old concepts, dominated by the western Pacific data from marginal seas, considered high heat flow as one of the characteristic features of back-arc basins (Sclater et al., 1972). This conclusion remains controversial (cf. Currie and Hyndman, 2006) and is only partially supported by the present analysis (Table 3). Heat flow in back-arc basins (ignoring transient effects and measurement limitations) is a joint effect of mantle heat flow (including contributions from shear heating, insulating effects of subducting slabs, vigor of mantle wedge secondary convection, and adiabatic upwelling of a hot mantle material in extensional area below any BAB type) and radioactive heat production in the overriding continental plate in the CO (and some extinct) settings. Therefore, lithospheric thermal structure should be extremely complex, heterogeneous at all scales, and essentially affected by mantle convective and advective processes associated with back-arc extension. Indeed, a short-wavelength heterogeneity in the reported heat flow values is a characteristic feature of many back-arc basins (Figs. 3-9).

It is, therefore, somewhat surprising that a uniformity of heat flow

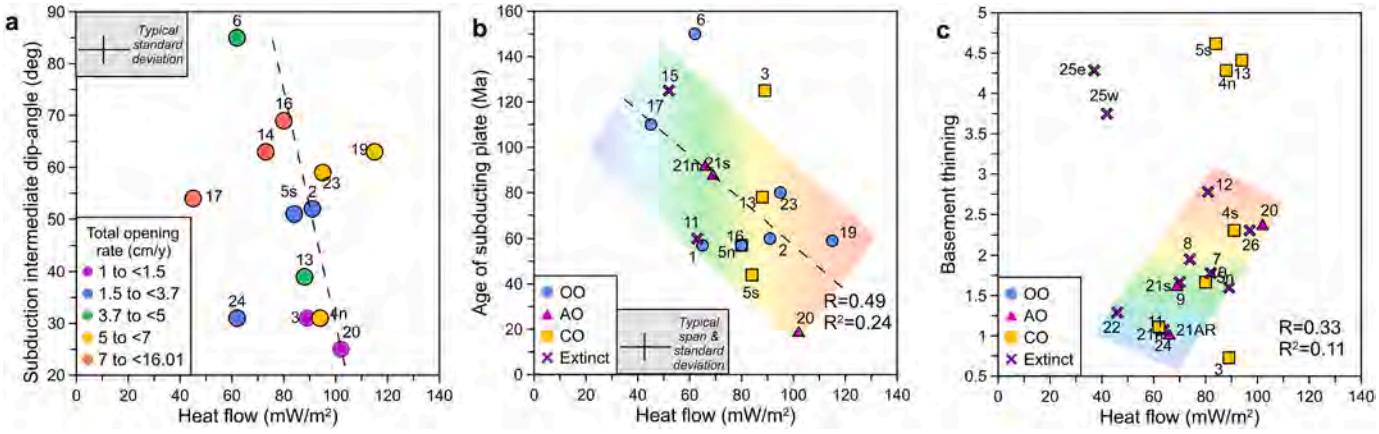

Fig. 26. Correlations between heat flow and subduction parameters in the BABs by tectonic settings. Numbers - back-arc basins (see Fig. 1 for locations). (a) Heat flow does not correlate with mid-depth slab dip-angle, nor with basin opening rate. (b) Heat flow is usually higher above younger slabs, and the overall trend holds for different types of BABs. (c) BABs with a highly stretched crust tend to have higher heat flow, although with a poor correlation between the parameters and with clear outliers.

with high mean values, typically around 70–80 mW/m^2, has earlier been reported for continental and oceanic back-arc basins (Currie and Hyndman, 2006). The present study shows that, statistically, high heat flow (ca. 70–85 mW/m^2) is characteristic only of the active BABs (Fig. 13d, Tables 1, 3). The absence of a clear distinction in heat flow between the active OO- and CO-BABs formed on oceanic and continental overring plates (Table 3) is probably caused by transient effects, e.g. variations in sedimentation composition, age, compaction and water circulation in highly permeable young sediments (Watanabe et al., 1977; Langseth et al., 1980; Sclater et al., 1980; Hutchison, 1985) that mask convectional, advective and radioactive thermal heterogeneities. By analogy with young oceans, where young sediments produce strong heat flow artefacts, heat flow in the active BABs, many of which have juvenile oceanic crust, should be affected by similar processes.

The non-Pacific extinct BABs (possibly formed in the CO- or AO-settings) are unique in having mean heat flow as low as 45–50 mW/m^2 (Table 3), typical of >100 My old oceans and stable continents (cf. Stein and Stein, 1992; Artemieva, 2011). Indeed, heat flow in continent-ocean back-arc basins may be essentially controlled by pre-extensional cold continental geotherms (Kerswell et al., 2021). While low heat flow in the extinct non-Pacific (EXT-2) BABs is probably caused by the absence of subduction-related wedge convection, it is unclear why the extinct Pacific BABs (EXT-1) have mean heat flow similar to the active OO-type BABs (Table 3), unless it is also governed by their pre-extensional thermal structure, complicated by active geodynamic settings in the western Pacific.

Subduction dip angle has a weak (if any) control on heat flow in the BABs (Fig. 26a), despite an efficiency of mantle wedge flow should depend, among other parameters, on the wedge geometry (Billen and Gurnis, 2001; Morishige and Honda, *2011*; Wirth and Korenaga, 2012). Heat flow is usually higher above young and hot slabs (Fig. 26b); however, the correlation is insignificant and heat flow does not correlate with the total opening rate. BABs with a strong crustal thinning in the AO- and CO-settings tend to have a higher heat flow, but many basins of the Black Sea form a clear exception of the general trend (Fig. 26c).

3.5.2. *Age-dependence of heat flow*

The presence of active seafloor spreading in a number of back-arc basins formed basis for an old hypothesis that their geodynamic evolution, including mantle thermal structure, should be similar to oceanic plates (Sclater et al., 1976). In such case, heat flow and bathymetry should follow the oceanic square-root-of-age trends of ocean plate models (Parsons and Sclater, 1977; Stein and Stein, 1992). This hypothesis, popular in the 1980–1990's, was used to infer the age of seafloor spreading from heat flow data in back-arc basins with limited data on the basement age, such as in the Celebes Sea, the Kuril, Japan, and the Black Sea Basins (e.g. Tamaki, 1986; Rangin et al., 1990; Golmshtok et al., 1992). However, several lines of evidence question a potential similarity between "normal" oceans and back-arc basins and, therefore, the applicability of the oceanic square-root-of-age trend to back-arc basins.

The present analysis demonstrates that in most BABs neither heat flow, nor bathymetry follow the age-dependences expected in normal oceans (Parsons and Sclater, 1977; Stein and Stein, 1992) (Fig. 27 ab). While heat flow, in general, shows no correlation with the duration of spreading (i.e. the age of juvenile lithosphere), bathymetry has some correlatations with age, although in different ways depending on geodynamic settings (see below). Indeed, due to transient effects as at mid-ocean ridges with young oceanic crust, e.g. due to water circulation in the vicinity of spreading axes (Watanabe et al., 1977; Hutchison, 1985), heat flow in the OO-type back-arc basins with a short (<6 My) duration of spreading is 30–70 mW/m^2 lower than the oceanic square-root-of-age trends predict (Fig. 27b).

Only the extinct BABs of the Pacific Ocean plot within the heat flow range predicted by the ocean plate cooling models. Two extinct back-arc basins of the Sea of Japan, analyzed here with the adjacent basins #3 and 5, have the same hear flow as other Pacific BABs. A close agreement between the ocean trend and heat flow in all of these basins either suggests that their thermal structure has equilibrated to "normal" oceans since termination of active spreading, or that these extinct BABs represent trapped oceanic fragments with thermal structure irrelevant to back-arc basin extension, such as in the Aleutian and Komandorsky Basins (Table 2). The latter BAB plots on the oceanic trend (#2), while for the former no information on spreading duration is available. Its heat flow of ~70 mW/m^2 may suggest that spreading lasted >30 My (Fig. 27b). The absence of correlation between heat flow and the duration of spreading in all other back-arc basins questions if BAB extension ages can be estimated from heat flow values for oceanic square-root-of-age trends (Tamaki, 1986; Rangin et al., 1990; Golmshtok et al., 1992). Besides, there is no physical reason for the CO-type back-arc basins with a heterogeneous radioactive contribution in a stretched continental lithosphere to follow the oceanic plate cooling trend.

3.5.3. *Age-dependence of bathymetry*

Bathymetry splits into several square-root-of-age trends shifted to shallower values than the oceanic plate model (PS) predictions (Fig. 27a). In the OO-type BABs, bathymetry is ca. 0.7 km shallower than the PS model, but the trend is poorly defined because most BABs of this

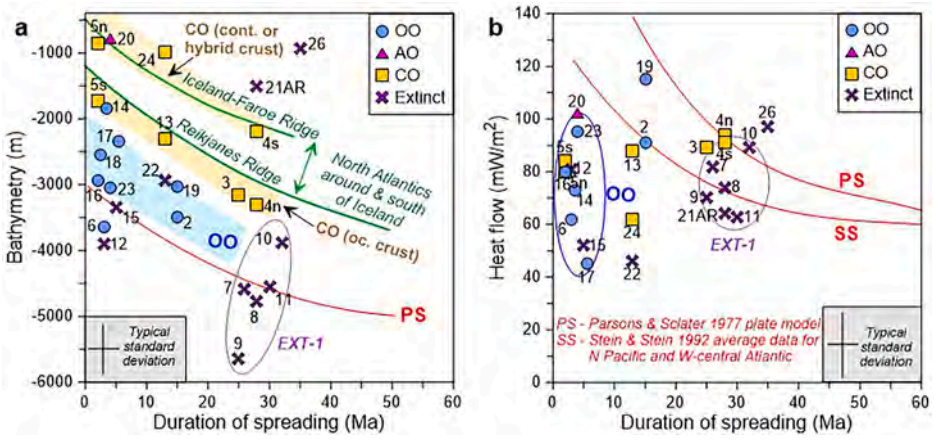

Fig. 27. Relationships between bathymetry and heat flow by tectonic settings in comparison with predictions by the oceanic plate models (red lines labelled PS and SS) (Parsons and Sclater, 1977; Stein and Stein, 1992). Spreading duration in BABs is similar to seafloor age in oceans; duration of extension is used for BABs with no spreading (Table 1). Numbers - back-arc basins (see Fig. 1 for locations).

(a) The OO-type BABs (blue shading) are ca. 0.7 km shallower than the oceanic plate model predicts, and most of them have a very short (<5 My) spreading duration. The CO-type (yellow shading) splits into two trends: the CO BABs with no or little oceanic crust have a very shallow (reduced by ca. 2.5 km) bathymetry trend which closely follows the trend of anomalous bathymetry in the North Atlantics (the Iceland-Faroe Ridge, the upper green line). The CO BABs with seafloor spreading define the deeper trend, which is still ca. 1.5 km shallower than the oceanic plate model predictions and is similar to the trend of anomalous ocean bathymetry south of Iceland (the Reykjanes Ridge, the lower green line) (Shulgin and Artemieva, 2019). Extinct BABs with oceanic crust (EXT-1) may be deeper than normal oceans.

(b) Heat flow in the BABs does not follow the oceanic plate model predictions, except for many extinct BABs that plot close to the oceanic plate models (red lines). Compared to "normal" oceans, the OO-type BABs with <5 Ma spreading are shifted towards both a shallow bathymetry (a) and a lower heat flow than the ocean models predict (b). This shift may be caused by hydrothermal circulation in the absence of sealing sediments as observed in young oceans (Sclater et al., 1980).

type have a very short (<5 My) duration of spreading. A 30 mGal/km rule of thumb for the ratio of [*free-air anomalies]* to [*isostatically unsupported bathymetric anomalies*] (McKenzie, 1994; Molnar et al., 2015) predicts a 20 mGal gravity anomaly for a 0.7 km of anomalous bathymetry, while the mean value of free-air anomalies in the OO settings is ca. 35 mGal (Fig. 13b). Therefore about half of a shallow bathymetry value in the OO-type BABs may be attributed to mantle dynamic effects and flexural deformation.

As noted above, there is no reason why back-arc basins with continental-type crust enriched in radioactive elements should follow the oceanic cooling trend. However, the CO-type basins apparently closely follow the trends of anomalous bathymetry versus ocean floor age in the North Atlantic region around the Iceland hotspot and split into two subtrends (Fig. 27a). In back-arc basins with extended continental or hybrid crust (#4s, 5n, 20, 24, Table 2), bathymetry is ca. 2.5 km more shallow than predicted by the oceanic plate model and the subtrend is remarkably similar to the Iceland-Faroe Ridge (Shulgin and Artemieva, 2019) where hyper-extended continental crust rather than over-thickened oceanic crust may be present (Foulger et al., 2020). Free-air anomalies of about +20 + 30 mGal both in these CO-type BABs and in the Iceland region are too small to explain a 2.5 km bathymetry deviation from the PS model by uncompensated mantle dynamic topography. A similarity with the Iceland-Faroe Ridge suggests that mantle temperature anomaly of a deep origin (i.e. with a long wave-length) and a very small amplitude at the limit of detection by seismic tomography (Shulgin and Artemieva, 2019) may contribute to the anomalous effect with an additional isostatic contribution to shallow bathymetry by a thick continental-type crust.

The other subtrend of the CO-type is ca. 1.5 km more shallow than predictions of the ocean plate mode and it is better defined (Fig. 27a). This group (#3, 4n, 5s, 13) with juvenile oceanic crust shows a remarkable similarity with the bathymetry-age profile across the Reykjanes Ridge south of Iceland. The latter was explained by a strong thermo-chemical mantle heterogeneity with the likely presence of some recycled continental material within otherwise oceanic-type crust (Shulgin and Artemieva, 2019). The same mechanism may explain the subtrend in the CO back-arc basins with a hybrid (mixture of continental, transitional and oceanic) crust, such as in the southern Okinawa Trough, the Kurils, the Japan Basin, and the Andaman Sea (Fig. 11).

3.5.4. *Terminal thermal fate of BABs*

Termination of lithosphere extension and/or seafloor spreading leads to thermal relaxation of the lithosphere (cooling, thermal densification, and gravitational subsidence), which with time achieves its equilibrium state, if no hotspot interaction occurs. The existence of two distinct types of the extinct back-arc basins (Table 3), either with oceanic crust or with continental, hybrid or transitional crust, implies they have a different thermal evolution. In the extinct OO-type back-arc basins (EXT-1, Pacific), thermal relaxation reduces heat flow to the values predicted by the ocean cooling plate models (Fig. 27b), while their average bathymetry and Bouguer anomalies also approach values typical of old oceans (Fig. 28, left). Being indistinguishable from "normal" old oceans, such extinct back-arc basins become parts of an old ocean floor, while preserving the extensional pattern of magnetic lineations and still preserving lithospheric chemical heterogeneity acquired during back-arc extension. This general pattern explains the difficulties in identifying e.g. the W. Philippine Basin and the Celebes Sea as relict back-arc basins or trapped oceanic fragments, whereas the situation becomes straightforward is case of a clear mismatch between the spreading and subduction directions, as in the Aleutian and Komandorsky Basins (Fig. 29).

Extinct back-arc basins formed on overriding continental or arc plates (EXT-2) essentially inherit their distinct pre-extensional characteristics, while they may include small fractions of juvenile oceanic crust embedded within significantly extended and chemically reworked continental or arc lithosphere fragments. Their further evolution may follow various paths depending on the amount of lithosphere reworking; however, the present extinct EXT-2 back-arc basins are unlikely to evolve to "normal" oceans. Yet some active back-arc basins formed on overriding continental or arc plates may experience a significant stretching followed by further seafloor spreading (Fig. 16). Their further evolution may be similar to the extinct BABs of the western Pacific (EXT-1) if spreading produces a large portion of juvenile oceanic crust.

4. Summary: Oceanic-type versus continental-type dynamics of BABs

4.1. *Six major sub-types of marine BABs*

The existence of two principal types of the lithosphere, oceanic and continental, is a principal characteristics of the Earth's evolution.

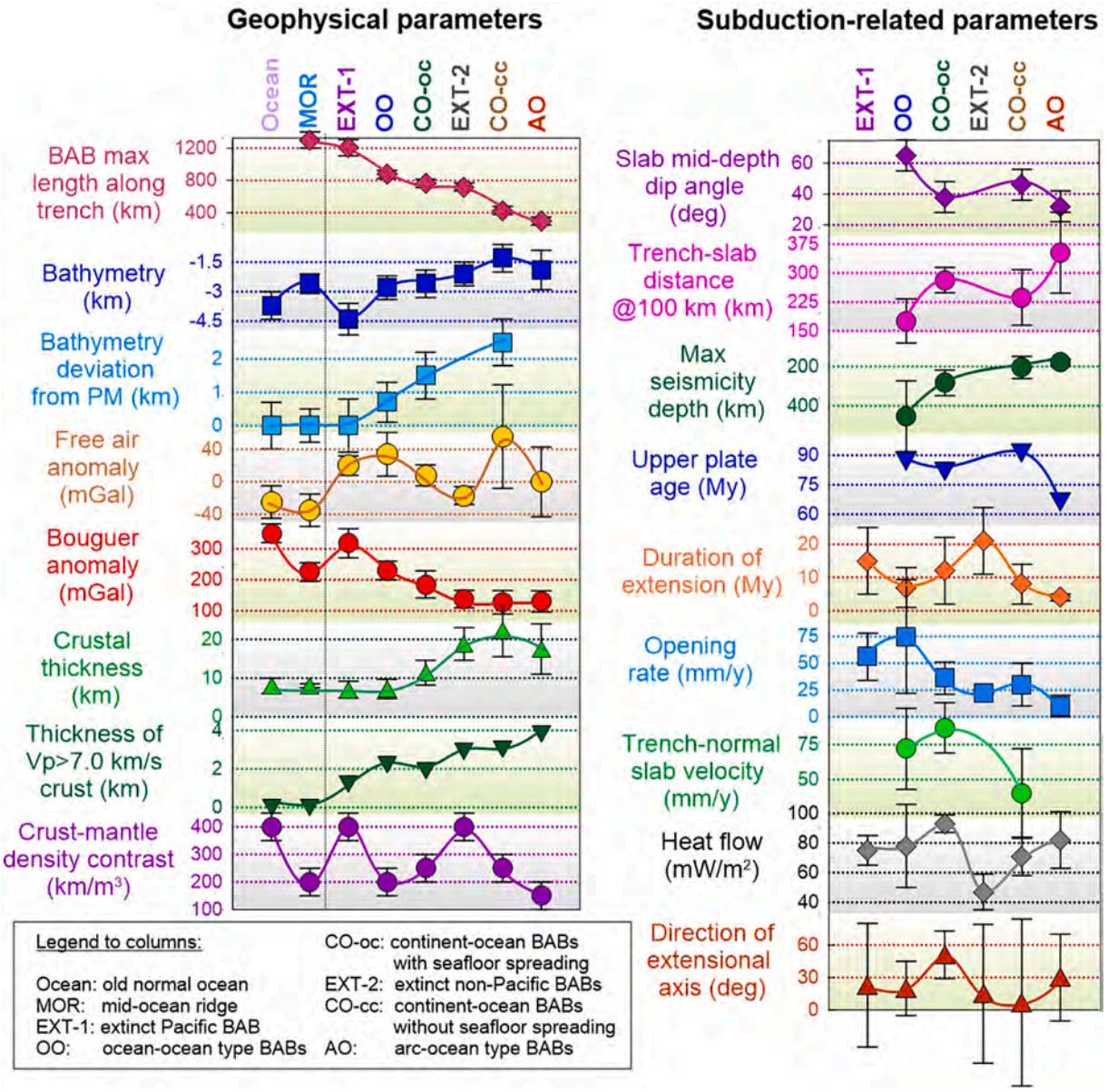

Fig. 28. Major characteristics of six subtypes of marine back-arc basins (see Table 3 for details) sorted by gradual changes in several parameters. Old "normal" oceans and mid-ocean ridges are shown for comparison where available (left column). Vertical bars – standard deviation. PM = oceanic plate model (Parsons and Sclater, 1977).

Unsurprisingly, the presence of oceanic-type and/or continental-type crust has an ultimate importance in geodynamic styles of formation, development and evolution of back-arc basins in the marginal seas. By their geophysical and subduction-related parameters, discussed above, the marginal BABs fall into the six major sub-types that reflect the principal differences between oceanic and continental lithosphere (Figs. 28-29, Table 3). Note that possibly all analyzed back-arc basins have formed above downgoing oceanic plates.

4.1.1. BABs formed on the overriding oceanic plate

4.1.1.1. OO-type. This subtype includes active BABs with pre-existing and juvenile oceanic crust formed on the overriding oceanic plate in the ocean-ocean subductions (#6, 14, 16–19, 23). It also includes "quasi-BABs" with oceanic fragments trapped behind active subductions (#1, 2, Fig. 29). These BABs always evolve to seafloor spreading and typically have a large size along the trench. Active wedge convection leads to positive free-air anomalies, a warm lithosphere with bathymetry ca. 0.7 km more shallow that predicted by the oceanic plate cooling models, but relatively high Bouguer anomalies compared to other BABs (Fig. 28). High mantle wedge temperatures with a potentially intensive melting essentially reduce density contrast across the Moho. The crust with a typical, but variable oceanic (4–7 km) thickness is slightly thicker (8–12 km) in the "quasi-BABs". A distinctive characteristic of the OO sub-type is a steep subduction with a high total opening rate, a high trench-normal velocity and a small distance between the trench and an expected slab melting zone at ca. 100 km depth. It is the only type of back-arc basins which shows a clear alignment with the rotation-related eastward mantle flow (Fig. 25).

4.1.1.2. EXT-1 type. This subtype includes large in size, extinct BABs of the western Pacific Ocean, which all have a relatively recent (<60 Ma) extension (#7–12, 15, Fig. 29). The tectonic settings for their formation are not fully known, but they are likely to have been formed on the overriding oceanic plate in relict OO-type settings, and some BABs (#11–12) may have possibly formed in paleo AC-settings. The EXT-1

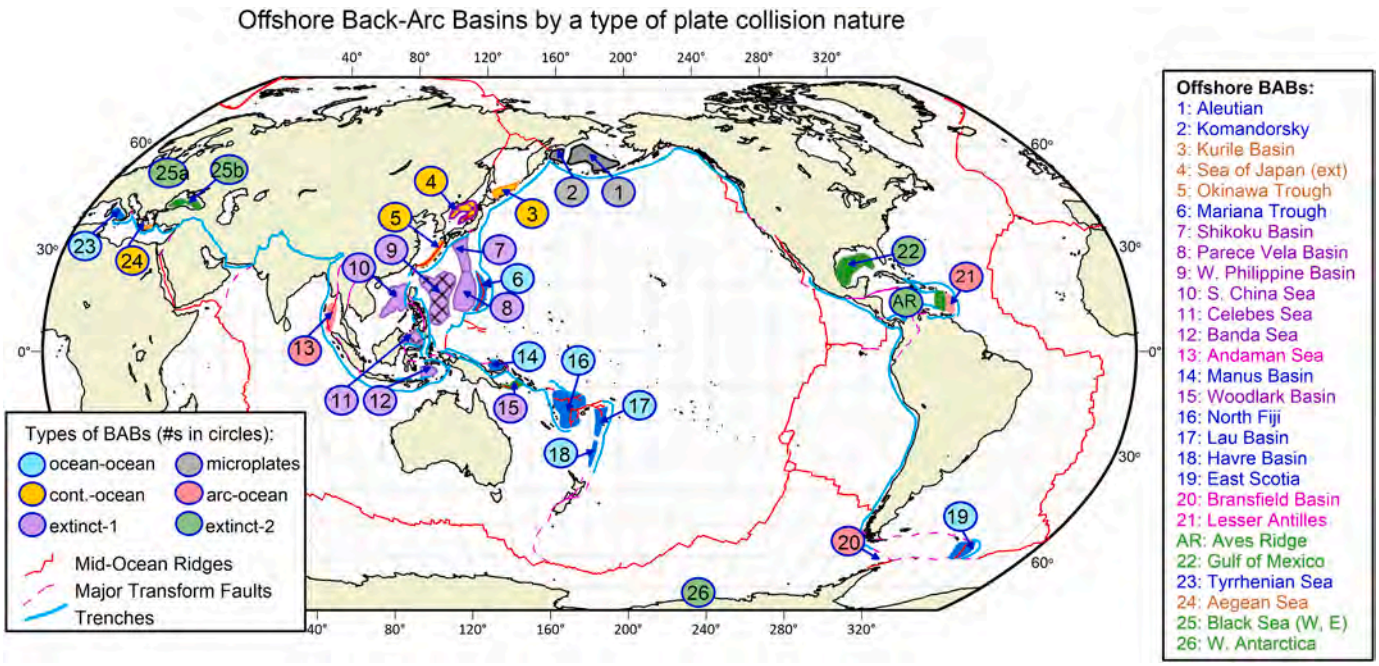

Fig. 29. Six subtypes of marine back-arc basins (BABs) sorted by the nature of the overriding plate. The downgoing plate is always oceanic (maybe except for few possible exceptions in the relict basins). Hatching in #9, 11, 25 marks a possible presence of trapped oceanic fragments (microplates); the extinct #4 was analyzed together with the #3, 5. Extinct-1 basins possibly formed by OO-type collisions, while Extinct-2 basins possibly included CO-, AO-, or AC-collisions.

BABs have a relict spreading, a typical thickness of oceanic crust (6–8 km), often with a high-Vp lower crustal layer, and plot along the oceanic plate cooling model. A large density contrast across the Moho with a very deep bathymetry and large Bouguer anomalies indicates a cold lithosphere which evolves towards old "normal" oceans. The basins of this group are the longest and the largest in size.

4.1.2. BABs formed on the overriding continental or arc-plate

4.1.2.1. CO-oc type. This subtype includes active BABs formed on the overriding continental plate in the CO-type settings (#3, 4n, 5s, 13, Fig. 29). These BABs always have seafloor spreading and include a mixture of juvenile oceanic crust and pre-extensional continental crust which is hyper-extended, at least in parts of basins. A 10–15 km thick crust, atypical of continents, is close in structure to a hybrid or transitional oceanic crust. A small density contrast between the crust and the mantle suggests high temperatures in mantle wedge. Thermal structure of these BABs is similar to the Reykjanes Ridge and hyper-extended passive margins of the North Atlantics with bathymetry ca. 1.5 km shallower that predicted by the oceanic plate cooling models (Fig. 27b, Table 3). Similar to the OO-type, these basins have a high trench-normal velocity but with a relatively moderate total opening rate. Shallow subduction leads to very large melting zone displacements from the trenches (Figs. 22-23).

4.1.2.2. CO-cc type. Similarly, this subtype includes active BABs formed on the overriding continental plate in the CO-type settings (#4s, 5n, 24, and possibly #20 with similar characteristics but formed in the AO-settings, Fig. 29). In sharp contrast to the CO-oc type BABs, these basins have no seafloor spreading, are small in size along the trench, and have an exceptionally thick (15–30 km) crust, similar to hyper-extended or highly stretched continental crust with a thick high-Vp lower crustal layer (Fig. 18). Characteristically, these basins have very high free air anomalies (Fig. 28), suggesting an importance of plate deformation in basin development. A reduced density contrast across the Moho, similar to the CO-oc type basins, suggests high mantle wedge temperatures below a warm lithosphere. High lithosphere buoyancy associated with a continental-type lithosphere structure, with potential contributions of mantle dynamic support and lithosphere deformation, is responsible for an anomalous, exceptionally shallow bathymetry, similar to the Iceland-Faroe Ridge of the North Atlantics Ocean (Fig. 27). The associated subduction systems with a shallow seismicity have a small trench-normal component of the incoming plate velocity (Fig. 28). Small slab dips produce large displacements between the trench and the mantle melting zone (Fig. 23b).

4.1.2.3. AO-type. This subtype includes active BABs formed on the overriding arc plate in the AO-settings (#20, 21n, 21s, Fig. 29). These rare BABs are unlikely to have juvenile oceanic crust (Table 2) and their dynamics is controlled by the presence of a relatively thick (15–25 km) hyper-extended arc-type crust (Fig. 18). A ca. 4 km thick high-Vp lower crustal layer indicates an important role of magmatic crustal growth at the AO-type BABs. These basins have a short duration of lithosphere extension, some of the smallest opening rates, and the smallest size along the trench (Fig. 28). Very high mantle wedge temperatures with a very small density contrast across the Moho contribute to an exceptionally shallow bathymetry (Fig. 28). It is the only type of active BABs with near-zero free air anomalies, despite the expected plate deformation. A very shallow slab dip angle leads to a very large trench-melting zone distance.

4.1.2.4. EXT-2 type. This subtype includes the non-Pacific extinct BABs (#21AR, 22, 25e, 25w, 26, Fig. 29). Similar to the EXT-1 group, the tectonic settings for their formation are not well known, and they are likely to have been formed on overriding continental or arc plates in relict CO-, AO, or maybe AC- or AA-settings. An important characteristic of the EXT-2 type is old (60–160 Ma) extension. Paleo-spreading is possible, but it has been unanimously accepted only for the Gulf of Mexico. A thick (13–25 km) crust, dominated by a mixture of extended pre-existing arc or continental crust, with juvenile oceanic portions or entrapped oceanic fragments and with a thick high-Vp lower crustal layer, contributes to a shallow bathymetry (ca. 2.2 km shallower than in the EXP-1 basins). High Moho density contrast and exceptionally low heat flow values imply low mantle temperatures. These basins do not

Table 3
Average characteristics of back-arc basins of various types and groups.

BAB type	**OO-type**	**AO-type**	**CO-type**			**EXT-type**		
BAB sub-type	**OO-all**	**AO-all**	**CO-all**	**CO-oc**	**CO-cc**	**Extinct-all**	**Ext-1**	**Ext-2**
(number, section4.1.)	**(1)**	**(5)**	**(-)**	**(3)**	**(4)**	**(-)**	**(2)**	**(6)**
BAB examples	**1, 2, 6, 14, 16–19, 23**	**20, 21n, 21s**	**3, 4n, 4s, 5n, 5s, 12, 24**	3, 4n, 5s, 13	4s, 5n, 24	**7–12, 15, 21AR, 22, 22, 25e, 25w**	7–12, 15	21AR, 22, 25e, 25w, 26
Seafloor spreading (number, % of type)	**9 (100%)**	**1 (33%)**	**5 (71%)**	4 (100%)	0 (0%)	**9 (75%)**	7 (100%)	2 (40%)
BAB length, along trench (km)	**874 ± 371**	**297 ± 126**	**620 ± 201**	764 ± 43	428 ± 150	**1029 ± 574**	1205 ± 611	720 ± 392
Bathymetry (m)	**−2864 ± 639**	**−1880 ± 992**	**−2073 ± 955**	−2618 ± 742	−1347 ± 742	**−3557 ± 1335**	−4381 ± 752	−2115 ± 595
Free air (mGal)	**34 ± 27**	**0 ± 43**	**37 ± 49**	8 ± 13	56 ± 64	**7 ± 22**	20 ± 12	−17 ± 11
Bouguer anomaly (mGal)	**230 ± 30**	**130 ± 34**	**149 ± 47**	185 ± 44	127 ± 38	**243 ± 102**	318 ± 47	138 ± 28
Crustal type	**Oceanic only**	**Arc, hybrid, or oceanic**	**Any type**	Oceanic, extended cont. or hybrid	Hyper-extended cont. or transitional	**Mostly oceanic, rarely arc or hybrid**	Mostly oceanic	Mostly hybrid arc, oceanic and transitional
Total crustal thickness (km)	**7.2 ± 2.5**	**17.5 ± 6.5**	**16.2 ± 7.6**	11.4 ± 3.2	22.3 ± 6.8	**12.3 ± 6.9**	7.0 ± 2.2	18.8 ± 4.6
Basement thickness (km)	**5.9 ± 1.5**	**13.4 ± 8.2**	**12.8 ± 7.7**	7.8 ± 2.2	19.3 ± 7.1	**8.1 ± 5.3**	5.4 ± 2.1	11.4 ± 4.3
Fast lower crust (Vp > 7.0 km/s) (km)	**2.2 ± 1.4**	**3.8 ± 6.5**	**2.4 ± 3.6**	1.9 ± 2.3	3.0 ± 5.2	**2.0 ± 2.58**	1.2 ± 1.8	2.9 ± 3.2
Equilibrium crustal thickness (km) (Fig. 14)	**7.5**	**25**	**16 (10 & 24)**	16	16	**12**	12	12
Crust-mantle average density contrast (kg/m^3) (Fig. 14)	**200–250**	**150–200**	**200–300**	200–300	200–300	**400**	400	400
Slab dip-angle, intermediate depth (deg)	**65 ± 11**	**32 ± 10**	**40 ± 11**	38 ± 10	46 ± 20	**NA**	NA	NA
Trench to slab-top distance (km) at z = 100 km	**176 ± 57**	**353 ± 105**	**263 ± 54**	282 ± 33	237 ± 72	**NA**	NA	NA
Max EQ depth (km)	**453 ± 180**	**180 ± 17**	**257 ± 65**	283 ± 56	205 ± 64	**NA**	NA	NA
Maximum BAB length along the trench (km)	**874 ± 50**	**297 ± 50**	**764 ± 50**	764 ± 50	428 ± 50	**764 ± 50**	1205 ± 50	720 ± 50
Spreading (extensional) axis direction (deg)	**20 ± 25**	**30 ± 40**	**35 ± 55**	51 ± 22	7 ± 77	**20 ± 58**	23 ± 57	15 ± 64
Plate age along trench (My)	**87 ± 40**	**66 ± 41**	**76 ± 35**	82 ± 41	91 ± 48	**NA**	NA	NA
Spreading duration (My)	**7 ± 6**	**4 ± 1**	**10 ± 8**	12 ± 10	8 ± 6	**16 ± 9**	15 ± 10	21 ± 10
Total opening rate (mm/y)	**75 ± 53**	**10 ± 10**	**33 ± 15**	36 ± 15	30 ± 20	**50 ± 25**	56 ± 22	22
Trench-normal slab velocity (mm/y)	**72 ± 29**	**NA**	**64 ± 34**	87 ± 18	40 ± 32	**NA**	NA	NA
Heat flow (mW/m^2)	**78 ± 28**	**82 ± 19**	**84 ± 15**	93 ± 6	71 ± 13	**65 ± 17**	75 ± 10	47 ± 12
Bathymetry deviation from ocean plate cooling model (Fig. 27)	**~ 0.7 km shallower**	**NA**	**~ 2 km shallower**	~ 1.5 km shallower	~ 2.5 km shallower	**± 1 km, scatter**	±1 km, scatter	Poor fit

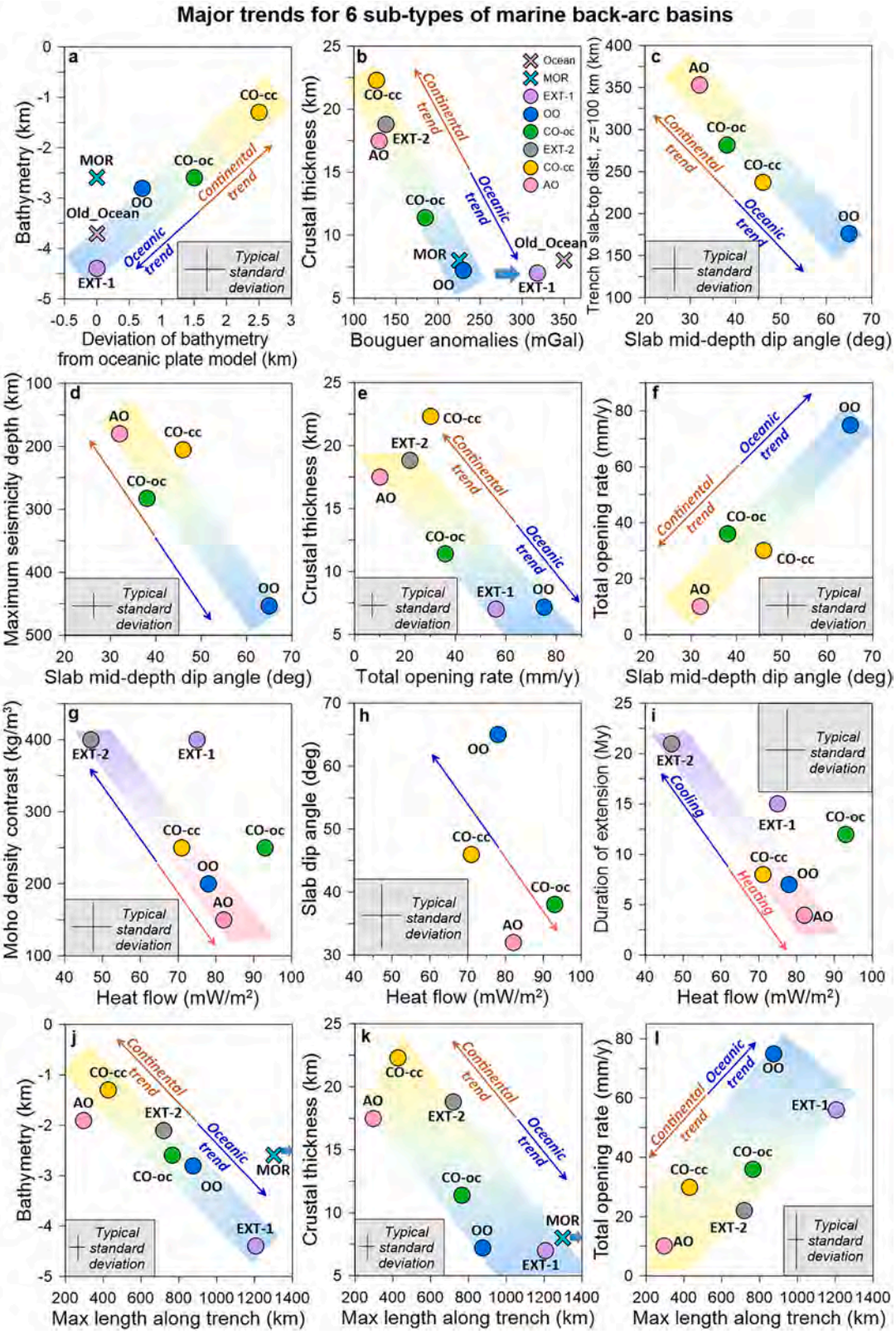

Fig. 30. Correlations between geophysical and subduction-related parameters in marine back-arc basins (see Table 3 for details). See (b) for legend. Color codes for back-arc basins are the same in all plots and refer to the extinct Pacific BABs (EXT-1), the ocean-ocean type BABs (OO), the continent-ocean BABs with seafloor spreading (CO-oc), the extinct non-Pacific BABs (EXT-2), the continent-ocean BABs without seafloor spreading (CO-cc), and the BABs associated with arc-ocean subduction type (AO). Old "normal" oceans and mid-ocean ridges (MORs) are shown by crosses for comparison where available. Possible continental-oceanic trends are highlighted by yellow-blue shading. Grey boxes show typical standard deviations (see Table 3 for details).

evolve to old "normal" oceans.

4.2. Ocean-continent trends

The existence of the continental-type versus oceanic-type groups is an important highlight in the evolution of back-arc basins, largely controlled by the affinities of their lithospheres (Fig. 30). It defines their contrasting types of evolution with a rare switch of the CO-type basins from the continental group (CO-cc) to the oceanic group (CC-oc) (Fig. 16). Clearly, the parameters characterizing the evolution of back-arc basin types are complexly interrelated and the cause-consequence links may include feedback loops. Besides, parameters related to a regional stress regime and plate kinematics are excluded from the analysis.

Bathymetry is a critical factor in understanding back-arc dynamics. A well-defined change in seafloor deepening from shallow back-arc basins with a continental-type lithosphere and a thick crust to oceanic-type back-arc basins and old oceans highlights an important role of inherited thermo-chemical and structural buoyancies of the overriding plate. BABs formed on the overriding continental and arc plates are all small and shallow. A large thickness of the pre-existing crust (and lithosphere) of the overriding continental/arc plate may prevent the development of high extensional stresses in such back-arcs, therefore limiting their total opening rate (Fig. 30e). A small opening rate, possibly resulting in a small size of the continental-type BABs (Fig. 30l), does not promote their evolution to seafloor spreading. In contrast, a collision of two oceanic plates leads to large opening rates with a large length of a stretched area along the trench and favors seafloor spreading with the formation of a thin juvenile oceanic-type crust (Fig. 30k). A small lithosphere buoyancy in such long back-arc basins leads to a deep bathymetry, which increases while they cool, and the largest and the deepest basins are the extinct Pacific basins.

Geometry of subduction zones is equally important in understanding back-arc dynamics. Dip angle of subducting oceanic plate is controlled by a large number of external factors and by structures of the downgoing and the overriding plates (Cruciani et al., 2005; Lallemand et al., 2005; Arcay et al., 2008; Billen, 2008; Jacobsen, 2018; Hayes et al., 2018; Holt and Royden, 2020; Hu and Gurnis, 2020). Back-arc basins formed on continental and arc plates typically overlie slabs with a shallow dip angle, while BABs in ocean-ocean collisions form above steep, up to near-vertical, slabs. Slab dip controls the lateral distance between the trench and slab melting zone leading to a striking difference between oceanic and continental settings in magmatic underplating and slab-related seismicity (Fig. 30 cd). Slab dip also governs opening rate in back-arc basins (Fig. 30f) which creates a feedback loop since a high opening rate is, in turn, directly related to a large length of the back-arc extensional zone along the trench (Fig. 30l): BABs with high opening rates typical of the OO-type settings form behind steeply dipping slabs, possibly due to an intensive slab roll-back.

Previous geodynamic research of back-arc dynamics (e.g. Martínez et al., 1999; Billen and Gurnis, 2001; Abers et al., 2002; Gerya and Yuen, 2003; Spakman and Hall, 2010; Syracuse et al., 2010; Morishige and Honda, *2011*; Wirth and Korenaga, 2012; Ficini et al., 2017; Lee and Wada, 2017; Magni, 2019) has provided an important, largely based on numerical modeling, perspective on a possible evolution of these subduction-related systems. The present study highlights the importance of pre-existing lithospheric structure of colliding plates on the dynamics of back-arc basins and suggests opportunities for further research.

5. Conclusions

An overview and synthesis of geophysical and subduction parameters of 26 back-arc basins (BABs, split into 31 sub-basins) of the marginal seas worldwide (Section 2) made the basis for the analysis aimed to recognize global trends and correlations between their geophysical and subduction-related characteristics (Section 3). Back-arc basins formed on the overriding oceanic and continental/arc plates (the downgoing plate is always oceanic) show a sharp distinction in nearly all characteristics. They are split into active BABs formed by ocean-ocean (OO), island arc-ocean (AO), and continent-ocean convergence (CO), and extinct back-arc basins (EXT). The last two types are further split depending on their known or deduced oceanic versus continental/arc affinity (Section 4) (Fig. 29) into active BABs with (CO-oc) and without seafloor spreading (CO-cc), extinct BABs of the western Pacific Ocean possibly formed on oceanic plates (EXT-1), and other extinct BABs with reworked continental or arc fragments (EXT-2). The analysis, based on the present plate configuration, demonstrates that geodynamic and geophysical characteristics of the back-arc basins and their evolution are pre-defined and governed by the nature of the overring plate (Table 3) (Fig. 30).

1) Back-arc basins formed on the overriding oceanic plate are associated with a steep slab dip (65 ± 11^{o}) due to subduction of old ($> \sim 60$ My) and cold, ca. 100 km thick oceanic plates. Only this oceanic type of the back-arc basins is associated with the directional preference (ca. 290^{o}) of subducting slabs. These basins are numerous, have a high opening rate which possibly reflects an efficiency of slab-roll back with high lithosphere stretching, and always evolve to seafloor spreading. Due to a weak rheology, thin oceanic-type crust, and small lithosphere buoyancy, such extensional systems produce large (long) and deep back-arc basins.

2) Back-arc basins formed on the overriding arc or continental plate show the opposite pattern with a relatively shallow subduction of younger oceanic plates, small opening rates, a thick continental-type or arc-type crust, and a shallow bathymetry. These continental and arc-type basins are small in number and have no directional preferences of subducting plates.

Transition from crustal extension to seafloor spreading requires a high opening rate (>8 cm/y), so that many CO- and AO-type back-arc basins do not evolve to seafloor spreading, and such transition does not happen in back-arc basins formed behind a shallow subduction ($<45^{o}$) of a young (<40 My), hot and buoyant oceanic plate, where slab-roll back and mantle convection are apparently inefficient. Transition from a CO-cc continental-type back-arc basin with hyperextended continental or transitional crust, typical of passive margins, to a CO-oc oceanic-type back-arc basin with a thinner hybrid crust typically requires a long spreading duration with large opening rates and a very high crustal thinning factor (a proxy to β-factor in the absence of magmatic additions) of 2.8 on average, with values up to ~4.0–5.0.

3) Extinct back-arc basins develop by mantle cooling either from the oceanic group (OO and CO-oc) or from the continental group (CO-cc and AO) of back-arc basins and inherit characteristics of the parent active BABs. All extinct oceanic type back-arc basins (EXT-1) have been formed in the western Pacific ocean by a < 60 My extension, they are the longest and the largest in size, very deep, have a paleo-spreading, thin oceanic-type crust, and share many characteristics with "normal" old oceans. Extinct continental and arc-type back-arc basins (EXT-2) are in the Central Atlantics - Mediterranean region, they are old (60–160 My), have thick crust, shallow bathymetry, exceptionally low heat flow, and may not evolve to "normal" oceans.

4) Back-arc basins do not follow the oceanic square-root-of-age plate cooling trends and their spreading (when exist) is different from normal oceanic spreading. All active BABs have a more shallow water depth than the oceanic trend predicts, ca. 0.7 km for the OO-type BABs, ca. 1.5 km for the CO-oc BABs with seafloor spreading and similar to the Reykjanes Ridge, and ca. 2.5 km shallower for the CO-cc BABs with the bathymetry-age trend similar to the Iceland-Faroe Ridge. Extinct BABs have a large scatter around the oceanic plate cooling trends and are often deeper than predictions for "normal" old cooling oceans. These deviations reflect an interplay of thermo-chemical heterogeneity, lithosphere deformation, and mantle flow.

5) Huge variations in crustal structure between the back-arc basins of different types reflect the nature of the pre-extensional crust of the

overriding plate, a complex interplay of crustal thinning by stretching and crustal thickening by magmatic additions. The presence of a high-Vp (>7.0 km/s) lowermost crustal layer, typically 2–4 km thick, is a characteristic feature of most BABs, and indicates an importance of crustal growth by magmatic underplating.

The results substantially simplify the understanding of back-arc basin evolution by identifying six distinct tectonic sub-types with dissimilar geophysical and geodynamic characteristics. The results highlight a critical importance of oceanic, continental, or arc nature of the overriding plate in evolution of back-arc basins: BABs formed on continental/arc plates are likely to preserve their continental/arc affinity even after cessation of extension, while BABs formed on oceanic plates are likely to evolve towards old "normal" oceans. The analysis also demonstrates a principal difference between stretching and spreading in back-arc basins and normal oceans, associated with different processes responsible for lithosphere extension.

Declaration of Competing Interest

The author is unaware of any conflict of interest.

Data availability

Publicly available data published in open press, referred to in the paper

Acknowledgements

The National Science Foundation of China grant No. 92055210 is acknowledged. Comments of the handling editor C. Doglioni, an anonymous reviewer and Li S.-Z. are appreciated. The author is grateful to several colleagues for constructive, detailed and interesting comments to an intermediate version of the manuscript, and to H. Thybo and A. Shulgin for numerous discussions of the initial results.

References

Abers, G.A., Ferris, A., Craig, M., et al., 2002. Mantle compensation of active metamorphic core complexes at Woodlark rift in Papua New Guinea. Nature 418, 862–865.

Abers, G.A., Fischer, K.M., Hirth, G., et al., 2014. Reconciling mantle attenuation-temperature relationships from seismology, petrology, and laboratory measurements. Geochem. Geophys. Geosyst. 15, 3521–3542. https://doi.org/10.1002/2014GC005444.

Agostini, S., Doglioni, C., Innocenti, F., Manetti, P., Tonarini, S., 2010. On the geodynamics of the Aegean rift. Tectonophysics 488, 7–21.

Allen, R.W., Collier, J.S., Stewart, A.G., et al., 2019. The role of arc migration in the development of the Lesser Antilles: a new tectonic model for the Cenozoic evolution of the eastern Caribbean. Geology 47, 891–895.

An, M., Wiens, D.A., Zhao, Y., et al., 2015a. Temperature, lithosphere-asthenosphere boundary, and heat flux beneath the Antarctic Plate inferred from seismic velocities. J. Geophys. Res. 120B, 8720–8742.

An, M., Wiens, D.A., Zhao, Y., et al., 2015b. S-velocity model and inferred Moho topography beneath the Antarctic Plate from Rayleigh waves. J. Geophys. Res. 120, 359–383. https://doi.org/10.1002/2014JB011332.

Arai, R., Kodaira, S., Yuka, K., Takahashi, T., Miura, S., Kaneda, Y., 2017. Crustal structure of the southern Okinawa Trough: symmetrical rifting, submarine volcano, and potential mantle accretion in the continental back-arc basin. J. Geophys. Res. 122, 622–641.

Arcay, D., Lallemand, S., Doin, M.-P., 2008. Back-arc strain in subduction zones: statistical observations versus numerical modeling. Geochem. Geophys. Geosyst. 9, Q05015. https://doi.org/10.1029/2007GC001875.

Argus, D.F., Gordon, R.G., DeMets, C., 2011. Geologically current motion of 56 plates relative to the no-net-rotation reference frame. Geochem. Geophys. Geosyst. 12, Q11001. https://doi.org/10.1029/2011GC003751.

Artemieva, I.M., 2022. Antarctica ice sheet basal melting enhanced by high mantle heat. Earth Sci. Rev. 226, Art. No. 103954 https://doi.org/10.1016/j.earscirev.2022.103954.

Artemieva, I.M., 2011. The Lithosphere: An Interdisciplinary Approach. In: Cambridge University Press, Cambridge, U.K., p. 794

Artemieva, I.M., 2006. Global 1°×1° thermal model TC1 for the continental lithosphere: implications for lithosphere secular evolution. Tectonophys. 416, 245–277.

Artemieva, I.M., Thybo, H., 2013. EUNAseis: a seismic model for Moho and crustal structure in Europe, Greenland, and the North Atlantic region. Tectonophysics 609, 97–153. https://doi.org/10.1016/j.tecto.2013.08.004.

Artemieva, I.M., Thybo, H., 2020. Continent size revisited: geophysical evidence for West Antarctica as a backarc system. Earth Sci. Rev. 202, Art. No. 103106 https://doi.org/10.1016/j.earscirev.2020.103106.

Artemieva, I.M., Shulgin, A., 2019. Making and altering the crust: a global perspective on crustal structure and evolution. Earth Planet. Sci. Lett. 512, 8–16.

Artemieva, I.M., Thybo, H., Shulgin, A., 2016. Geophysical constraints on geodynamic processes at convergent margins: a global perspective. Gondwana Res. 33, 4–23. https://doi.org/10.1016/j.gr.2015.06.010.

Artemieva, I.M., Billien, M., Leveque, J.J., Mooney, W.D., 2004. Shear wave velocity, seismic attenuation, and thermal structure of the continental upper mantle. Geophys. J. Int. 157, 607–628.

Ashcroft, W.A., 1972. Crustal structure of the South Shetland Islands and Bransfield Strait. British Antarctic Survey Scientific Reports, no. 66, 43 pp.

Auzende, J.M., Eissen, J.P., Lafoy, Y., et al., 1988. Seafloor spreading in the North Fiji Basin (Southwest Pacific). Tectonophysics 146, 317–351.

Auzende, J.M., Pelletier, B., Eissen, J.P., 1995. The North Fiji Basin: geology, structure, and geodynamic evolution. In: Taylor, B. (Ed.), Backarc Basins: Tectonics and Magmatism. Plenum Press, New York, pp. 139–176.

Baillard, C., Crawford, W.C., Ballu, V., et al., 2015. Seismicity and shallow slab geometry in the Central Vanuatu subduction zone. J. Geophys. Res. 120, 5606–5623.

Balázs, A., Faccenna, C., Gerya, T., Ueda, K., Funiciello, F., 2022. The dynamics of forearc – back-arc basin subsidence: numerical models and observations from mediterranean subduction zones. Tectonics. https://doi.org/10.1029/2021TC007078.

Baranov, B., Seliverstov, N., Murav'ev, A., Muzurov, E., 1991. The Komandorsky Basin as a product of spreading behind a transform plate boundary. Tectonophysics 199, 237–269.

Barckhausen, U., Engels, M., Franke, D., Ladage, S., Pubellier, M., 2014. Evolution of the South China Sea: revised ages for breakup and seafloor spreading. Mar. Pet. Geol. 58, 599–611.

Barker, D.H.N., Christeson, G.L., Austin, J.A., Dalziel, I.W.D., 2003. Backarc basin evolution and cordilleran orogenesis: Insights from new ocean-bottom seismograph refraction profiling in Bransfield Strait, Antarctica. Geology 31 (2), 107–110.

Barker, P.F., 1995. Tectonic Framework of the East Scotia Sea. In: Taylor, B. (Ed.), Backarc Basins: Tectonics and Magmatism. Plenum Press, New York, pp. 281–314.

Behrendt, J.C., LeMasurier, W.E., Cooper, A.K., et al., 1991. Geophysical studies of the West Antarctica rift system. Tectonics 10, 1257–1273.

Beloussov, V.V., et al., 1988. Structure and evolution of the Earth's crust and upper mantle of the Black Sea. Boll. Geof. Teor. Appl. 30, 109–196.

Ben-Avraham, Z., Uyeda, S., 1973. The evolution of the China Basin and the Mesozoic Paleogeography of Borneo. Earth Planet. Sci. Lett. 18 (2), 365–376.

Bevis, M., Taylor, F.W., Schutz, B.E., et al., 1995. Geodetic observations of very rapid convergence and back-arc extension at the Tonga arc. Nature 374, 249–251.

Bibee, L.D., Shor Jr., G.G., Lu, R.S., 1980. Inter-arc spreading in the Mariana Trough. Mar. Geol. 35, 183–197. https://doi.org/10.1016/0025-3227(80)90030-4.

Bikkenina, S.K., Anosov, O.I., Argentov, V.V., Sergeyev, K.F., 1987. Crustal structure of the Southern Okhotsk Sea based on seismic data. Moscow, Nauka (in Russian)..

Billen, M.I., Gurnis, M., 2001. A low viscosity wedge in subduction zones. Earth PlanetSci. Lett. 193, 227–236.

Billen, M., 2008. Modeling the dynamics of subducting slabs. Annu. Rev. Earth Planet. Sci. 36 (1), 325–356.

Bird, D.E., Hall, S.A., Casey, J.F., Millegan, P.S., 1999. Tectonic evolution of the Grenada Basin. In: Mann, P. (Ed.), Sedimentary Basins of the World, V. 4. Elsevier, pp. 389–416. https://doi.org/10.1016/S1874-5997(99)80049-5.

Bonini, W.E., Hargraves, R.B., Shagam, R. (Eds.), 1984. The Caribbean-South American Plate Boundary and Regional Tectonics: Geol. Soc. America Memoir, 162. https://doi.org/10.1130/MEM162.

Boschman, L.M., van Hinsbergen, D.J.J., Torsvik, T.H., Spakman, W., Pindell, J.L., 2014. Kinematic reconstruction of the Caribbean region since the Early Jurassic. Earth Sci. Rev. 138, 102–136.

Bowin, C., Purdy, G.M., Johnston, C., et al., 1980. Arc-Continent Collision in Banda Sea Region. AAPG Bull. 64, 868–915.

Bown, J.W., White, R.S., 1994. Variation with spreading rate of oceanic crustal thickness and geochemistry. Earth Planet. Sci. Lett. 121, 435–449.

Boynton, C.H., Westbrook, G.K., Bott, M.H.P., Long, R.E., 1979. A seismic refraction investigation of crustal structure beneath the Lesser Antilles island arc. Geophys. J. RAstron. Soc. 58, 371–393.

Briais, A., Patriat, P., Tapponnier, P., 1993. Updated interpretation of magnetic anomalies and seafloor spreading stages in the South China Sea: implications for the Tertiary tectonics of Southeast Asia. J. Geophys. Res. 98, 6299–6328.

Brun, J.P., Sokoutis, D., 2010. 45 Ma of Aegean crust and mantle flow driven by trench retreat. Geology 38, 815–818.

Brun, J.-P., Faccenna, C., 2008. Exhumation of high-pressure rocks driven by slab rollback. Earth Planet. Sci. Lett. 272, 1–7.

Buntin, S., Artemieva, I.M., Malehmir, A., Thybo, H., et al., 2021. Long-lived Paleoproterozoic eclogitic lower crust. Nat. Comm. 12, 6553. https://doi.org/10.1038/s41467-021-26878-5.

Burov, E., Gerya, T., 2014. Asymmetric three-dimensional topography over mantle plumes. Nature 513, 85–89.

Calvert, A.J., 2011. The seismic structure of island arc crust. In: Brown, D., Ryan, P.D. (Eds.), Arc-Continent Collision. Frontiers in Earth Science. Springer, Berlin, pp. 87–119.

Cande, S.C., Stock, J.M., 2004. Cenozoic reconstructions of the Australia-New Zealand-South Pacific sector of Antarctica. In: The Cenozoic Southern Ocean: Tectonics, Sedimentation, and Climate Change between Australia and Antarctica. AGU, Washington, D. C, pp. 5–17.

Cande, S.C., Stock, J.M., Muller, R.D., Ishihara, T., 2000. Cenozoic motion between East and West Antarctica. Nature 404, 145–150.
Carlson, R.L., Mortera-Gutiérrez, C.A., 1990. Subduction hinge migration along the Izu-Bonin-Mariana Arc. Tectonophysics 181, 331–344.
Carlson, R.L., Hilde, T.W.C., Uyeda, S., 1983. The driving mechanism of plate tectonics: relation to age of lithosphere at trenches. Geophys. Res. Lett. 10, 297–300.
Carminati, E., Lustrino, M., Doglioni, C., 2012. Geodynamic evolution of the central and western Mediterranean: tectonics vs. Igneous petrology constraints. Tectonophysics 579, 173–192.
Channell, J.E.T., Mareschal, J.C., 1989. Delamination and asymmetric lithosphere thickening in the development of the Tyrrhenian rift. In: Dietrich, D., Coward, M.P., Park, R.G. (Eds.), Alpine Tectonics. Geol. Soc. Spec. Publ., 45, pp. 285–301.
Chaput, J., Aster, R.C., Huerta, A., et al., 2014. The crustal thickness of West Antarctica. J. Geophys. Res. 119, 378–395. https://doi.org/10.1002/2013JB010642.
Charvis, P., Recq, M., Operto, S., Brefort, D., 1995. Deep structure of the northern Kerguelen Plateau and hotspot-related activity. Geophys. J. Int. 122, 899–924.
Christensen, N.I., Mooney, W.D., 1995. Seismic velocity structure and the composition of the continental crust: a global view. J. Geophys. Res. 100, 9761–9788.
Christeson, G., Van Avendonk, H., Norton, I., et al., 2014. Deep crustal structure in the eastern Gulf of Mexico. J. Geophys. Res. 119 (9), 6782–6801.
Christeson, G.L., Barth, G.A., 2015. Aleutian basin oceanic crust. Earth Planet. Sci. Lett. 426, 167–175.
Christeson, G.L., Mann, P., Escalona, A., Aitken, T.J., 2008. Crustal structure of the Caribbean-northeastern South America arc-continent collision zone. J. Geophys. Res. 113, B08104. https://doi.org/10.1029/2007jb005373.
Christie, D.M., et al., 2006. Back-arc spreading systems: geological, biological, chemical and physical interactions. Geophysical Monograph Series, 166. American Geophysical Union, 303 pp.
Cochran, J.R., Talwani, M., 1977. Free–air gravity anomalies in the world's oceans and their relationship to residual elevation. Geophys. J. Royal Astron. Soc. https://doi.org/10.1111/j.1365-246X.1977.tb01334.x.
Collot, J., Daniel, J., Burne, R., 1985. Recent tectonics associated with the subduction/collision of the d'Entrecasteaux zone in the Central New Hebrides. Tectonophysics 112, 325–356.
Conder, J.A., Wiens, D.A., 2007. Rapid mantle flow beneath the Tonga volcanic arc. Earth Planet. Sci. Lett. 264, 299–307.
Cooper, A.K., Scholl, D.W., Marlow, M.S., et al., 1979. Hydrocarbon potential of Aleutian Basin, Bering Sea. Amer. Ass. Petrol. Geol. Bull. 63, 2070–2087.
Cooper, A.K., Marlow, M.S., Scholl, D.W., Stevenson, A.J., 1992. Evidence for Cenozoic crustal extension in the Bering Sea region. Tectonics 11, 719–731.
Crawford, W.C., Hildebrand, J.A., Dorman, L., et al., 2003. Tonga Ridge and Lau Basin crustal structure from seismic refraction data. J. Geophys. Res. 108, 2195.
Cross, T.A., Pilger Jr., R.H., 1982. Controls of subduction geometry, location of magmatic arcs, and tectonics of arc and back-arc regions. Bull. Geol. Soc. Am. 93, 545–562.
Cruciani, C., Carminati, E., Doglioni, C., 2005. Slab dip vs. Lithosphere age: no direct function. Earth Planet. Sci. Lett. 238 (3–4), 298–310. https://doi.org/10.1016/j.epsl.2005.07.025.
Curray, J.R., 2005. Tectonics and history of the Andaman Sea region. Earth Planet. Sci. Lett. 25, 187–232.
Currie, C., Wang, K., Hyndman, R.D., He, J., 2004. The thermal effects of steady state slab-driven mantle flow above a subducting plate: the Cascadia subduction zone and backarc. Earth Planet. Sci. Lett. 223, 35–48.
Currie, C.A., Hyndman, R.D., 2006. The thermal structure of subduction zone back arcs. J. Geophys. Res. 111, B08404. https://doi.org/10.1029/2005JB004024.
Davies, J.H., Stevenson, D.J., 1992. Physical model of source region of subduction zone volcanics. J. Geophys. Res. 97, 2037–2070.
Della Vedova, B., Pellis, G., Foucher, J.P., Rehault, J.P., 1984. Geothermal structure of the Tyrrhenian Sea. Mar. Geol. 55, 271–289.
Deschamps, A., Monie, P., Lallemand, S.E., Hsu, S.K., Yeh, K.Y., 2000. Evidence for Early Cretaceous oceanic crust trapped in the Philippine Sea Plate. Earth Planet. Sci. Lett. 179, 503–5016.
Dewey, J.F., Sengör, A.M.C., 1979. Aegean and surrounding regions: complex multiplate and continuum tectonics in convergent zone. Geol. Soc. Am. Bull. 90, 84–92.
Dietrich, R., Dach, R., Engelhardt, G., et al., 2001. ITRF coordinates and plate velocities from repeated GPS campaigns in Antarctica - an analysis based on different individual solutions. J. Geod. 74, 756–766.
Doglioni, C., 1991. A proposal for the kinematic modeling of W-dipping subductions – possible applications to the Tyrrhenian-Apennines system. Terra Nova 3, 423–434.
Doglioni, C., Gueguen, E., Sàbat, F., Fernandez, M., 1997. The western Mediterranean extensional basins and the Alpine orogen. Terra Nova 9, 109–112.
Doglioni, C., Agostini, S., Crespi, M., et al., 2002. On the extension in western Anatolia and the Aegean Sea. J. Virtual Explor. 8, 169–184.
Doglioni, C., Tonarini, S., Innocenti, F., 2009. Mantle wedge asymmetries along opposite subduction zones. Lithos 113, 179–189.
Dunn, R., Martinez, F., 2011. Contrasting crustal production and rapid mantle transitions beneath back-arc ridges. Nature 469, 198–202.
Eberle, M.A., Grasset, O., Sotin, C., 2002. A numerical study of the interaction between the mantle wedge, subducting slab, and overriding plate. Phys. Earth Planet. Inter. 134, 191–202.
Eddy, D., Van Avendonk, H., Christeson, G., et al., 2014. Deep crustal structure of the North-Eastern Gulf of Mexico: implications for rift evolution and seafloor spreading. J. Geophys. Res. 119 (9), 6802–6822.
Eiler, J. (Ed.), 2003. Inside the Subduction Factory. American Geophysical Union, Geophysical Monograph Series, 138. https://doi.org/10.1029/GM138.
Endrun, B., Lebedev, S., Meier, T., et al., 2011. Complex layered deformation within the Aegean crust and mantle revealed by seismic anisotropy. Nat. Geosci. 4, 203–209.
Engelhardt, H., 2004. Ice temperature and high geothermal flux at Siple Dome, West Antarctica, from borehole measurements. J. Glaciol. 50, 251–256.
England, P., Engdahl, R., Tatcher, W., 2004. Systematic variation in the depths of slabs beneath volcanoes. Geophys. J. Int. 156, 377–408.
Faccenna, C., Becker, T.W., Lallemand, S., Steinberger, B., 2012. On the role of slab pull in the Cenozoic motion of the Pacific plate. Geophys. Res. Lett. 39, L03305.
Faccenna, C., Holt, A., Becker, T., Lallemand, S., Royden, L., 2018. Dynamics of the Ryukyu/Izu-Bonin-Marianas double subduction system. Tectonophysics 746, 229–238.
Faccenna, C., Davy, P., Brun, J.P., et al., 1996. The dynamics of back-arc extension: an experimental approach to the opening of the Tyrrhenian Sea. Geophys. J. Int. 126, 781–795.
Ficini, E., Dal Zilio, L., Doglioni, C., Gerya, T., 2017. Horizontal mantle flow controls subduction dynamics. Sci. Rep. 7, 7550. https://doi.org/10.1038/s41598-017-06551-y.
Fisher, A.T., Mankoff, K.D., Tulaczyk, S.M., et al., 2015. High geothermal heat flux measured below the West Antarctic Ice Sheet. Science Adv. 1, e1500093.
Forsyth, D.A., Morelalhuissier, P., Asudeh, I., Green, A.G., 1986. Alpha-Ridge and Iceland — products of the same plume. J. Geodyn. 6, 197–214.
Foulger, G.R., Doré, T., Emeleus, C.H., et al., 2020. The Iceland Microcontinent and a continental Greenland-Iceland-Faroe Ridge. Earth Sci. Rev. 206, 102926.
Fournier, M., Jolivet, L., Davy, P., Thomas, J.C., 2004. Backarc extension and collision: an experimental approach to the tectonics of Asia. Geophys. J. Int. 157, 871–889.
Fox Maule, C., Purucker, M.E., Olsen, N., Mosegaard, K., 2005. Heat flux anomalies in Antarctica revealed by satellite magnetic data. Science 309, 464–467.
Fuchs, S., Norden, B., Artemieva, I., 2021. The Global Heat Flow Database: Release 2021. GFZ Data Services. https://doi.org/10.5880/fidgeo.2021.014.
Fukuma, K., Shinjoe, H., Hamano, Y., 1998. Origin of the absence of magnetic lineations in the Yamato Basin of the Japan Sea: magnetic properties of mafic rocks from Ocean Drilling Program Hole 794 D. J. Geophys. Res. 103, 17791–17805. https://doi.org/10.1029/98JB01486.
Furlong, K.P., Chapman, D.S., Alfeld, P.W., 1982. Thermal modeling of the geometry of subduction with implications for the tectonics of the overriding plate. J. Geophys. Res. 87, 1786–1802.
Fyfe, W.S., 1992. Magma underplating of continental-crust. J. Volcanol. Geotherm. Res. 50, 33–40.
Gaina, C., Mueller, D., 2007. Cenozoic tectonic and depth/age evolution of the Indonesian gateway and associated back-arc basins. Earth-Sci. Rev. 83, 177–203.
Gao, J., Wu, S., McIntosh, K., Mi, L., Liu, Z., Spence, G., 2016. Crustal structure and extension mode in the northwestern margin of the South China Sea. Geochemem. Geophys.Geosyst. 17, 2143–2167.
Gautier, P., Brun, J.P., 1994. Crustal-scale geometry and kinematics of late orogenic extension in the Central Aegean (Cyclades and Evia island). Tectonophysics 238, 399–424.
Gerya, T.V., Yuen, D.A., 2003. Rayleigh-Taylor instabilities from hydration and melting propel 'cold plumes' at subduction zones. Earth Planet. Sci. Lett. 212, 47–62.
Gnibidenko, H.S., Hilde, T., Gretskaya, E.V., Andreyev, A.A., 1995. Kuril (South Okhotsk) Backarc Basin. In: Taylor, B. (Ed.), Backarc Basins: Tectonics and Magmatism. Springer, New York, pp. 421–450.
Golmshtok, A.Y., Zonenshain, L.P., Terekhov, A.A., Shainurov, R.V., 1992. Age, thermal evolution, and history of the Black Sea Basin based on heat flow and multichannel reflection data. Tectonophysics 120, 273–293.
Gozzard, S., Kusznir, N., Franke, D., et al., 2018. South China Sea crustal thickness and oceanic lithosphere distribution from satellite gravity inversion. Pet. Geosci. 25 (1) https://doi.org/10.1144/petgeo2016-162.
Grad, M., Shiobara, H., Janik, T., Guterch, A., Shimamura, H., 1997. Crustal model of the Bransfield rift, West Antarctica, from detailed OBS refraction experiment. In: Ricci, C.A. (Ed.), The Antarctic Region: Geological Evolution and Processes: Siena, Terra Antarctica, pp. 675–678.
Grellet, C., Dubois, J., 1982. The depth of trenches as a function of the subduction rate and age of the lithosphere. Tectonophysics 82, 45–56.
Grevemeyer, I., Kodaira, S., Fujie, G., Takahashi, N., 2021. Structure of oceanic crust in back-arc basins modulated by mantle source heterogeneity. Geology 49. https://doi.org/10.1130/G48407.1.
Hager, B.H., Richards, M.A., 1989. Long-wavelength variations in Earth's geoid: physical models and dynamical implications. Phil. Trans. Royal Soc. London. Series A 328, 309–327.
Hall, P.S., 2012. On the thermal evolution of the mantle wedge at subduction zones. Phys. Earth Planet. Inter. 198–199, 9–27.
Hawkins, J.W., 1995. The geology of the Lau Basin. In: Taylor, B. (Ed.), Backarc Basins: Tectonics and Magmatism. Plenum, New York, pp. 63–138.
Hayes, D.E. (Ed.), 1978. A Geophysical Atlas of the East and Southeast Asian Seas. Geol. Soc. Am. Map and Chart Ser., MC-25.
Hayes, G.-P., Moore, G.-L., Portner, D.-E., et al., 2018. Slab2, a comprehensive subduction zone geometry model. Science 362, 58–61.
Heuret, A., Lallemand, S., 2005. Plate motions, slab dynamics and back-arc deformation. <sb:contribution><sb:title>P</sb:title></sb:contribution><journal-title><sb:contribution><sb:title>hys. Earth Planet</sb:title></sb:contribution><sb:host><sb:issue><sb:series><sb:title>Inter.</sb:title></sb:series></sb:issue></sb:host></journal-title> 149, 31–51.
Hilde, T.W.C., Lee, C.-S., 1984. Origin and evolution of the West Philippine Basin: a new interpretation. Tectonophysics 102, 85–104.
Holbrook, W.S., Larsen, H.C., Korenaga, J., et al., 2001. Mantle thermal structure and active upwelling during continental breakup in the North Atlantic. Earth Planet. Sci. Lett. 190, 251–266.

Holt, A.F., Royden, L.H., 2020. Subduction dynamics and mantle pressure: 2. Towards a global understanding of slab dip and upper mantle circulation. Geochem. Geophys. Geosyst. 20 https://doi.org/10.1029/2019GC008771 e2019GC008771.
Horváth, F., Berckhemer, H., Stegena, L., Coulon, C., 1981. Models of Mediterranean Back-Arc Basin Formation. Phil. Trans. Royal Soc. London. Series A 300 (1454), 383–402. http://www.jstor.org/stable/36758.
Hu, J., Gurnis, M., 2020. Subduction duration and slab dip. Geochem. Geophys. Geosyst. 21 https://doi.org/10.1029/2019GC008862 e2019GC008862.
Hutchison, I., 1985. The effects of sedimentation and compaction on oceanic heat flow. Geophys. J. R. Astron. Soc. 82, 439–459.
Imanishi, M., Kimata, F., Inamori, N., Miyajima, R., Okuda, T., Takai, K., 1996. Horizontal displacements by GPS measurements at the Okinawa-Sakishima islands (1994–1995). Zisin J. Seism. Soc. Japan 49 (3), 417–421.
Imbert, P., Philippe, Y., 2005. The Mesozoic opening of the Gulf of Mexico: part 2, Integrating seismic and magnetic data into a general opening model. In: Post, P.J. (Ed.), Trans. 25th ann. GCSSEPM Research Conf.: Petroleum Systems of Divergent Continental Margins. SEPM, Tulsa, pp. 1151–1189.
Ishii, K., Wallis, S.R., 2022. A possible mechanism for spontaneous cyclic back-arc spreading. Prog Earth Planet Sci 9, 27. https://doi.org/10.1186/s40645-022-00486-3.
Jacobsen, B.M., 2018. Variability of subduction systems along and across the strike: Synthesis and analysis. MS Thesis supervised by Artemieva I.M. University of Copenhagen, 120 p.
Jarrard, R.D., 1986. Relations among subduction parameters. Rev. Geophys. 24, 217–284.
Jin, G., Gaherty, J.B., Abers, G.A., Kim, Y., Eilon, Z., Buck, W.R., 2015. Crust and upper mantle structure associated with extension in the Woodlark Rift, Papua New Guinea from Rayleigh wave tomography. Geochem. Geophys. Geosyst. 16, 3808–3824.
Jolivet, L., 2001. A comparison of geodetic and finite strain pattern in the Aegean, geodynamic implications. Earth Planet. Sci. Lett. 187, 95–104.
Jolivet, L., Faccenna, C., 2000. Mediterranean extension and the Africa-Eurasia collision. Tectonics 19, 1095–1106.
Jolivet, L., Faccenna, C., D'Agostino, N., 1999. The kinematics of back-arc basins, examples from the Tyrrhenian, Aegean and Japan Seas. In: Mac Niocaill, C., Ryan, P. D. (Eds.), Continental Tectonics. Geological Society, London, Sp. Publ., 164, pp. 21–53.
Jolivet, L., Tamaki, K., Fournier, M., 1994. Japan Sea, opening history and mechanism: a synthesis. J. Geophys. Res. 99 (B11), 22237–22259.
Jourdain, A., Singh, S.C., Escartin, X., et al., 2016. Crustal accretion at a sedimented spreading center in the Andaman Sea. Geology 44, 351–354.
Karato, S.-I., 2003. Mapping water content in the Upper Mantle. In: Eiler, J. (Ed.), Inside the Subduction Factory. Amer. Geophys. Union, Geophys. Monogr. Ser., 138, pp. 135–152.
Karig, D.E., 1970. Ridges and basins of the Tonga-Kermadec island arc system. J. Geophys. Res. 75, 239–254.
Karig, D.E., 1971. Origin and development of marginal basins in the western Pacific. J. Geophys. Res. 76, 2542–2561.
Karig, D.E., 1974. Evolution of arc systems in the western Pacific. Annu. Rev. Earth Planet. Sci. 2, 51–75.
Kashubin, S.N., Milshtein, E.D., Miasnikov, F.V., 2010. Multi-wave deep seismic studies of the crust and upper mantle: A case study of the South Okhotsk Sea deep trough. Proc. 14th Int. Symp. on Deep Seismic Profiling, Cairns, Australia.
Kastens, K., Mascle, J., 1990. The geological evolution of the Tyrrhenian Sea: an introduction to the scientific results of ODP Leg 107. Proc. Ocean Drill. Program Sci. Results 107, 3–26.
Keen, C.E., Beaumont, C., 1990. Geodynamics of rifted continental margins. In: Keen, M. J., Williams, G.L. (Eds.), Geology of Continental Margins of Eastern Canada. Geol. Surv. Can., Geol. Can., 2, pp. 391–472.
Kelemen, P.B., Rilling, J.L., Parmentier, E.M., Mehl, L., Hacker, B., 2003. Thermal structure due to solid-state flow in the mantle wedge beneath arcs. In: Eiler, J. (Ed.), Inside the Subduction Factory. Geophys. Monogr. Ser., 138, D.C.. AGU, Washington, pp. 293–309.
Kelemen, P.B., Behn, M.D., 2016. Formation of lower continental crust by relamination of buoyant arc lavas and plutons. Nat. Geosci. 9, 197–205.
Kelley, K.A., Plank, T., Grove, T.L., Stolper, E.M., Newman, S., Hauri, E., 2006. Mantle melting as a function of water content beneath back-arc basins. J. Geophys. Res. 111, B09208. https://doi.org/10.1029/2005JB003732.
Kerswell, B.C., Kohn, M.J., Gerya, T.V., 2021. Backarc lithospheric thickness and serpentine stability control slab-mantle coupling depths in subduction zones. Geochem. Geophys. Geosyst. 22 https://doi.org/10.1029/2020GC009304 e2020GC009304.
Kimura, G., Tamaki, K., 1986. Collision, rotation and back arc spreading: the case of the Okhotsk and Japan Seas. Tectonics 5, 389–401.
Kincaid, C., Sacks, I.S., 1997. Thermal and dynamical evolution of the upper mantle in subduction zones. J. Geophys. Res. 102, 12295–12315.
Kisimoto, K., Tanahashi, M., Auzende, J.-M., 1994. Crustal structure variation along the central rift/ridge axis in the North Fiji Basin: implications from seismic reflection and refraction data. In: Auzende, J.-M., Urabe, T. (Eds.), North Fiji Basin: STARMER French Japanese Program. Mar. Geol., 116, pp. 101–111 e2020GL086955.
Klingelhöfer, F., Edwards, R.A., Hobbs, R.W., England, R.W., 2005. Crustal structure of the NE Rockall Trough from wide-angle seismic data modeling. J. Geophysical Res. 110 (B11).
Kneller, E.A., van Keken, P.E., 2008. The effects of three-dimensional slab geometry on deformation in the mantle wedge: implications for shear wave anisotropy. Geochem. Geophys. Geosyst. 9 https://doi.org/10.1029/2007GC001677.
Kobayashi, K., 1985. Sea of Japan and Okinawa Trough. In: Nairn, A.E.M., Stehli, F.G., Uyeda, S. (Eds.), The Ocean Basins and Margins, v. 7A. Plenum Publ, Corp., pp. 419–459
Kohlstedt, D.L., Evans, B., Mackwell, S.J., 1995. Strength of the lithosphere: constraints imposed by laboratory experiments. J. Geophys. Res. 100, 17587–17602.
Kopp, H., et al., 2011. Deep structure of the Central Lesser Antilles island arc: relevance for the formation of continental crust. Earth Planet. Sci. Lett. 304, 121–134.
Lallemand, S., Heuret, A., Boutelier, D., 2005. On the relationships between slab dip, back-arc stress, upper plate absolute motion, and crustal nature in subduction zones. Geochem. Geophys. Geosyst. 6, Q09006. https://doi.org/10.1029/2005GC000917.
Langmuir, C.H., Bezos, A., Escrig, S., Parman, S.W., 2006. In: Fisher, C.R., Lee, S.-M., Givens, S. (Eds.), Back-Arc Spreading Systems: Geological, Biological, Chemical, and Physical Interactions. Geophys. Monogr. AGU, 166, pp. 87–146.
Langseth, M.G., Hobart, M.A., Horai, K.-I., 1980. Heat flow in Bering Sea. J. Geophys. Res., Atmos. 85 (B7), 3740–3750. https://doi.org/10.1029/JB085iB07p03740.
Larue, B.M., Pontoise, B., Malahoff, A., Lapouille, A., Latham, G.V., 1982. In: Bassins marginaux actifs du sud-ouest Pacifique: Plateau Nord-Fidjien, Bassin de Lau. Trav. Dot. ORSTOM, 147, pp. 361–406.
Lawver, L.A., et al., 1995. Bransfield Strait, Antarctic Peninsula. In: Taylor, B. (Ed.), Backarc Basins: Tectonics and Magmatism. Plenum Press, New York, pp. 315–380.
Lawver, L.A., Gahagan, L.M., 1994. Constraints on timing of extension in the Ross Sea Region. Terra Antarct. 1, 545–552.
Le Pichon, X., Angelier, J., 1979. The Hellenic arc and trench system: a key to the evolution of the Eastern Mediterranean. Tectonophysics 60, l-42.
Lee, C., Wada, I., 2017. Clustering of arc volcanoes caused by temperature perturbations in the back-arc mantle. Nat. Commun. 8, 1575. https://doi.org/10.1038/ncomms15753.
Lewis, S., 1991. Geophysical setting of the Sulu and Celebes Seas. In: Rangin, C., Silver, E., von Breymann, M.T. (Eds.), Proceedings of the Ocean Drilling Program, Initial Reports, Texas, 124, pp. 65–73.
Li, H., Lin, J., Zhou, Z., Zhang, F., Guo, L., 2022. Variations in magmatism and the state of tectonic compensation of the Mariana subduction system. Terra Nova 34, 20–27.
Li, S.Z., Suo, Y.H., Li, X.Y., et al., 2018. Microplate Tectonics: new insights from micro-blocks in the global oceans, continental margins and deep mantle. Earth Sci. Rev. 185, 1029–1064.
Lin, P., Bird, D.E., Mann, P., 2019. Crustal structure of an extinct, late Jurassic-to-earliest Cretaceous spreading center and its adjacent oceanic crust in the eastern Gulf of Mexico. Marine Geophys. Res. 40, 395–416.
Liu, B., Li, S.Z., Suo, Y.H., Li, G.X., Dai, L.M., Somerville, I.D., Guo, L.L., Zhao, S.J., Yu, S., 2016. The geological nature and geodynamics of the Okinawa Trough, Western Pacific. Geol. J. 51, 416–428.
Liu, Z., Zhu, D.-C., Wang, Q., Eyuboglu, Y., Zhao, Z.-D., Liu, S.-A., Xu, L.-J., 2018. Transition from low-K to high-K calc-alkaline magmatism at approximately 84 Ma in the eastern Pontides (NE Turkey): magmatic response to slab rollback of the Black Sea. J. Geophys. Res. 123, 7604–7628.
Livermore, R., 2006. The East Scotia Sea: Mantle to Microbe. In: Christie, D.M. (Ed.), Back-Arc Spreading Systems: Geological, Biological, Chemical and Physical Interactions. American Geophysical Union, Geophysical Monograph Series, 166, pp. 243–263.
Long, M.D., Wirth, E.A., 2013. Mantle flow in subduction systems: the mantle wedge flow field and implications for wedge processes. J. Geophys. Res. 118, 583–606.
Louden, K.E., 1980. The crustal and lithospheric thicknesses of the Philippine Sea as compared to the Pacific. Earth Planet. Sci. Lett. 50, 275–288.
Ludwig, W.J., 1974. Structure of the Bering Sea Basins. In: Burk, C.A., Drake, C.L. (Eds.), The Geology of Continental Margins. Springer, New York, pp. 661–668.
Ludwig, W.J., Murauchi, S., Den, N., et al., 1971. Structure of Bowers Ridge, Bering Sea. J. Geophys. Res. 76, 6350–6366.
Magee, C., Muirhead, D., Karvelas, A., et al., 2016. Lateral magma flow in mafic sill-complexes. Geosphere 12 (3). https://doi.org/10.1130/GES01256.1.
Magni, V., 2019. The effects of back-arc spreading on arc magmatism. Earth Planet. Sci. Lett. 519, 141–151. https://doi.org/10.1016/j.epsl.2019.05.009.
Makris, J., 1978. The crust and upper mantle of the Aegean region from deep seismic soundings. Tectonophysics 46, 264–284.
Malinverno, A., Ryan, W.B.F., 1986. Extension in the Tyrrhenian Sea and shortening in the Apennines as result of arc migration driven by sinking of the lithosphere. Tectonics 5, 227–245.
Mantovani, E., Cenni, N., Albarello, D., et al., 2001. Numerical simulation of the observed strain field in the Central-Eastern Mediterranean region. J. Geodynamics 31, 519–556.
Manu-Marfo, D., Aoudia, A., Pachhai, S., et al., 2019. 3D shear wave velocity model of the crust and uppermost mantle beneath the Tyrrhenian basin and margins. Sci. Rep. 9, 3609. https://doi.org/10.1038/s41598-019-40510-z.
Martinez, F., Taylor, B., 2002. Mantle wedge control on back-arc crustal accretion. Nature 416, 417–420.
Martinez, F., Taylor, B., 2006. In: Christie, D.M. (Ed.), Back-arc Spreading Systems: Geological, Biological, Chemical and Physical Interactions. American Geophysical Union, Geophysics Monograph Series 166, pp. 5–30.
Martinez, F., Taylor, B., Baker, et al., 2006. Opposing trends in crustal thickness and spreading rate along the back-arc Eastern Lau Spreading Center: implications for controls on ridge morphology, faulting, and hydrothermal activity. Earth Planet. Sci. Lett. 245, 655–672.
Martínez, F., Taylor, B., Goodliffe, A., 1999. Contrasting styles of seafloor spreading in the Woodlark Basin: indications of rift-induced secondary mantle convection. J. Geophys. Res. 104, 12909–12926.

McClusky, S., Balassanian, S., Barka, A., et al., 2000. Global Positioning System constraints on plate kinematic and dynamics in the eastern Mediterranean and Caucasus. J. Geophys. Res. 105 (B3), 5695–5719.
McKenzie, D., 1994. The relationship between topography and gravity on Earth and Venus. Icarus 112, 55–88.
McKenzie, D.P., 1978. Active tectonics of the Alpine Himalayan belt: the Aegean Sea and surrounding areas. Geophys. J. R. Astron. Soc. 55, 217–254.
Mibe, K., Kawamoto, T., Matsukage, K.N., et al., 2011. Slab melting versus slab dehydration in subduction-zone magmatism. Proc. Nat. Acad. Sci. 108, 8177–8182.
Minshull, T.A., Bruguier, N.J., Brozena, J.M., 2003. Seismic structure of the Mid-Atlantic Ridge, 8–9S. J. Geophys. Res. 108 (B11), 02513. https://doi.org/10.1029/2002JB002360.
Minshull, T.A., White, H.J., Edwards, R.A., et al., 2005. Seismic data reveal Eastern Black Sea Basin structure. EOS Trans. AGU 86 (43), 413–428.
Miura, S., Suyehiro, K., Shinohara, M., et al., 2004. Seismological structure and implications of collision between the Ontong Java Plateau and Solomon Island Arc from ocean bottom seismometer–airgun data. Tectonophysics 389, 191–220.
Molnar, P., Atwater, T., 1978. Interarc spreading and Cordilleran tectonics as alternates related to the age of subducted oceanic lithosphere. Earth Planet. Sci. Lett. 41, 330–340.
Molnar, P., England, P.C., Jones, C.H., 2015. Mantle dynamics, isostasy, and the support of high terrain. J. Geophys.Res.Solid Earth 120, 1932–1957.
Morin, R.H., Williams, T., Henrys, S.A., et al., 2010. Heat flow and hydrologic characteristics at the AND-1B borehole, ANDRILL McMurdo Ice Shelf Project, Antarctica. Geosphere 6, 370–378.
Morishige, M., Honda, S., 2011. Three-dimensional structure of P-wave anisotropy in the presence of small-scale convection in the mantle wedge. Geochem. Geophys. Geosyst. 12, Q12010.
Mueller, R.D., Sdrolias, M., Gaina, C., et al., 2008. Age, spreading rates, and spreading asymmetry of the world's ocean crust. Geochem. Geophys. Geosyst. 9, Q04006.
Nakajima, J., Hasegawa, A., 2003. Estimation of thermal structure in the mantle wedge of northeastern Japan from seismic attenuation data. Geophys. Res. Lett. 30 (14), 1760.
Neill, I., Kerr, A.C., Hastie, A.R., Stanek, K., Millar, I.L., 2011. Origin of the Aves Ridge and Dutch-venezuelan Antilles: interaction of the Cretaceous "Great Arc" and Caribbean-Colombian Oceanic Plateau? J. Geol. Soc. 168, 333–348.
Neprochnov, Y.P., et al., 1970. Structure of the crust and upper mantle of the Black and Caspian seas. Tectonophysics 10, 517–538.
Nichols, G., Hall, R., 1999. History of the Celebes Sea Basin based on its stratigraphic and sedimentological record. J. Asian Earth Sci. 17, 47–59.
Nicolosi, I., Speranza, F., Chiappini, M., 2006. Ultrafast oceanic spreading of the Marsili Basin, southern Tyrrhenian Sea: evidence from magnetic anomaly analysis. Geology 34, 717–720.
Nikishin, A.M., Korotaev, M.V., Ershov, A.V., Brunet, M.-F., 2003. The Black Sea basin: tectonic history and Neogene-Quaternary rapid subsidence modeling. Sediment. Geol. 156, 149–168.
Nikishin, A.M., Okay, A.I., Tuysuz, O., et al., 2015. The Black Sea basins structure and history: new model based on new deep penetration regional seismic data. Part 1: Basins structure and fill. Mar. Pet. Geol. 59, 638–655.
Nishizawa, A., Kaneda, K., Oikawa, M., Horiuchi, D., Fujioka, Y., Okada, C., 2019. Seismic structure of rifting in the Okinawa Trough, an active backarc basin of the Ryukyu (Nansei-Shoto) island arc-trench system. Earth Planet Space 71, 21–47. https://doi.org/10.1186/s40623-019-0998-6.
No, T., Sato, T., Kodaira, S., et al., 2014. The source fault of the 1983 Nihonkai-Chubu earthquake revealed by seismic imaging. Earth Planet. Sci. Lett. 400, 14–25.
O'Connell, R., Hager, B., 1991. Toroidal-poloidal partitioning of lithospheric plate motions. In: Sabadini, R., et al. (Eds.), Glacial Isostasy, Sea-Level and Mantle Rheology. Kluwer, Dordrecht, pp. 535–551.
O'Reilly, S.Y., Griffin, W.L., 2013. Moho vs crust-mantle boundary: evolution of an idea. Tectonophysics 609, 535–546.
Okay, A.I., Tuysuz, O., 1999. Tethyan sutures of northern Turkey. In: Durand, B., Jolivet, L., Horvath, F., Seranne, M. (Eds.), The Mediterranean Basins: Tertiary Extension within the Alpine Orogen. Geological Soc., London, Sp. Publ., 156, pp. 475–515.
Okino, K., Kasuga, S., Ohara, Y., 1998. A new scenario of the Parece Vela basin genesis. Mar. Geophys. Res. 20, 21–40.
Otofuji, Y., 1996. Large tectonic movement of the Japan Arc in late Cenozoic times inferred from paleomagnetism: review and synthesis. Island Arc 5, 229–249.
Panza, G.F., Raykova, R.B., Carminati, E., Doglioni, C., 2007. Upper mantle flow in the western Mediterranean. Earth Planet. Sci. Lett. 257, 200–214.
Park, J.O., Tokuyama, H., Shinohara, M., Suyehiro, K., Taira, A., 1998. Seismic record of tectonic evolution and backarc rifting in the southern Ryukyu island arc system. Tectonophysics 294, 21–42.
Parson, L., Wright, I., 1996. The Lau-Havre-Taupo back-arc-basin: a southward propagating, multi-stage evolution from rifting to spreading. Tectonophysics 263, 1–22.
Parsons, B., Sclater, J.G., 1977. An analysis of the variation of ocean floor bathymetry and heat flow with age. J. Geophys. Res. 82, 803–827.
Pavlis, N.K., Holmes, S.A., Kenyon, S.C., Factor, J.K., 2012. The development and evaluation of the Earth Gravitational Model 2008 (EGM2008). J. Geophys. Res. 117 https://doi.org/10.1029/2011jb008916.
Pepe, F., Bertotti, G., Cella, F., Marsella, E., 2000. Rifted margin formation in the South Tyrrhenian Sea: a high-resolution seismic profile across the North Sicily passive continental margin. Tectonics 19, 241–257.
Pe-Piper, G., Piper, D.J.W., 1989. Spatial and temporal variation in late Cenozoic back-arc volcanic rocks, Aegean Sea region. Tectonophysics 169, 113–134.
Petrescu, L., Borleanu, F., Placinta, A.O., 2022. Seismic structure of a Tethyan back-arc: trans-dimensional ambient noise tomography of the Black Sea lithosphere. Phys. Earth Planet. Inter. 325 (106854).
Philippon, M., Brun, J.P., Gueydan, F., Sokoutis, D., 2014. The interaction between Aegean back-arc extension and Anatolia escape since Middle Miocene. Tectonophysics 631, 176–188. https://doi.org/10.1016/j.tecto.2014.04.039.
Pichot, T., Delescluse, M., et al., 2014. Deep crustal structure of the conjugate margins of the SW South China Sea from wide-angle refraction seismic data. Mar. Pet. Geol. 58, 627–643.
Piip, V.B., Rodnikov, A.G., 2004. The Sea of Okhotsk crust from deep seismic sounding data. Russian J. Earth Sci. 6 (1), 35–48. https://doi.org/10.2205/2003ES000140.
Pindell, J.L., Kennan, L., 2009. Tectonic evolution of the Gulf of Mexico, Caribbean, and northern South America in the mantle reference frame: an update. In: James, K.H., Lorente, M., Pindell, J.L. (Eds.), and Evolution of the Caribbean Plate. Geol. Soc., London, Sp. Publ., 328, pp. 1–55. https://doi.org/10.1144/SP328.1.
Ponthus, P., Blanquat, M.D.S., Guillaume, D., Le Romancer, M., Pearson, N., O'Reilly, S., Grégoire, M., 2020. Plutonic processes in transitional oceanic plateau crust: structure, age and emplacement of the South Rallier du Baty laccolith, Kerguelen Islands. Terra Nova 16. https://doi.org/10.1111/ter.12471.
Polatidis, A., Kiratzi, A., Hatzidimitriou, P., Margaris, B., 2003. Attenuation of shear-waves in the back-arc region of the Hellenic arc for frequencies from 0.6 to 16 Hz. Tectonophysics 367 (1–2), 29–40.
Prada, M., Sallares, V., Ranero, C.R., et al., 2014. Seismic structure of the Central Tyrrhenian basin: geophysical constraints on the nature of the main crustal domains. J. Geophys. Res. 119, 52–70.
Purdy, G.M., Detrick, R.S., 1978. A seismic refraction experiment in the central Banda Sea. J. Geophys. Res. 83, 2247–2257.
Raju, K.A.K., Ramprasad, T., Rao, P.S., Rao, B.R., Varghese, J., 2004. New insights into the tectonic evolution of the Andaman basin, Northeast Indian Ocean. Earth Planet. Sci. Lett. 221, 145–162.
Rangin, C., Stephan, J.R., Müller, C., 1985. Middle Oligocene Ocean crust of South China Sea jammed into Mindoro collision zone (Philippines). Geology 13, 425–428.
Rangin, C., Silver, E., von Breymann, M.T. (Eds.), 1990. Proceedings of the Ocean Drilling Program, Initial Reports, Texas, Vol. 124.
Rehault, J.P., Moussat, E., Fabbri, A., 1987. Structural evolution of the Tyrrhenian back-arc basin. Mar. Geol. 74, 123–150.
Ricard, Y., Doglioni, C., Sabadini, R., 1991. Differential rotation between lithosphere and mantle: a consequence of lateral mantle viscosity variations. J. Geophys. Res. 96, 8407–8415.
Richards, M.A., Lithgow-Bertelloni, C., 1996. Plate motion changes, the Hawaiian-Emperor Bend, and the apparent success and failure of geodynamic models. Earth Planet. Sci. Lett. 137, 19–27. https://doi.org/10.1016/0012-821X(95)00209-U.
Ritsema, A.R., 1979. Active or passive subduction at the Calabrian Arc. In: Van der Linden, W.J.M. (Ed.), Fixism, Mobilism or Relativism: Van Bemmelen's Search for Harmony. Geologie en Mijnbouw, 58, pp. 127–134.
Robinson, A.G., et al., 1996. Petroleum geology of the Black Sea. Mar. Pet. Geol. 13, 195–223.
Robertson, A.H.G., 1998. Mesozoic-Tertiary tectonic evolution of the easternmost Mediterranean area: integration of marine and land evidence. Proc. ODP Sci. Results 160, 723–782.
Salvini, F., Brancolini, G., Busetti, M., et al., 1997. Cenozoic geodynamics of the Ross Sea region, Antarctica: crustal extension, intraplate strike-slip faulting, and tectonic inheritance. J. Geophys. Res. 102, 24669–24696.
Sandwell, D., Müller, R., Smith, W., Garcia, E., Francis, R., 2014. New global marine gravity model from CryoSat-2 and Jason-1 reveals buried tectonic structure. Science 346, 65–67.
Sartori, R., 2003. The Tyrrhenian back-arc basin and subduction of the Ionian lithosphere. Episodes 26, 217–223.
Sasaki, T., Yamazaki, T., Ishizuka, O., 2014. A revised spreading model of the West Philippine Basin. Earth Planet. Space 66 (1), 83. https://doi.org/10.1186/1880-5981-66-83.
Sato, H., 1992. Thermal structure of the mantle wedge beneath northeastern Japan: magmatism in an island arc from the combined data of seismic anelasticity and velocity and heat flow. J. Volcanol. Geotherm. Res. 51, 237–252.
Sato, T., No, T., Kodaira, S., Takahashi, N., Kaneda, Y., 2014. Seismic constraints of the formation process on the back-arc basin in the southeastern Japan Sea. J. Geophys. Res. 119, 1563–1579.
Sato, T., Shinohara, M., Hino, R., Nishino, M., Kanazawa, T., 2006. P-wave velocity structure of the margin of the southeastern Tsushima Basin in the Japan Sea using ocean bottom seismometers and airguns. Tectonophysics 412, 159–171.
Scheinert, M., et al., 2016. New Antarctic gravity anomaly grid for enhanced geodetic and geophysical studies in Antarctica. Geophys. Res. Lett. 43, 600–610.
Schellart, W.P., 2005. Influence of the subducting plate velocity on the geometry of the slab and migration of the subduction hinge. Earth PlanetSci. Lett. 231, 197–219.
Schellart, W.P., 2007. The potential influence of subduction zone polarity on overriding plate deformation, trench migration and slab dip angle. Tectonophysics 445, 363–372.
Schellart, W.P., Freeman, J., Stegman, D.R., Moresi, L., May, D., 2007. Evolution and diversity of subduction zones controlled by slab width. Nature 446, 308–311.
Schellart, W.P., Stegman, D.R., Farrington, R.J., Moresi, L., 2011. Influence of lateral slab edge distance on plate velocity, trench velocity, and subduction partitioning. J. Geophys. Res. 116, B10408. https://doi.org/10.1029/2011JB008535.
Scholl, D.W., 2016. The Argument that the Oceanic Crust of the Backarc Aleutian Basin (Bering Sea) is a Terrane of Pacific Oceanic Crust, possibly the Kula Plate, Accreted to the north American Plate at 50–55 Ma. Am. Geophys. Union FM2016. T23F-03.

Scholl, D.W., Buffington, E.C., Marlow, M.S., 1975. Plate tectonics and the structural evolution of the Aleutian-Bering sea region. In: Forbes, R.B. (Ed.), Contributions to the Geology of the Bering Sea Basin and Adjacent Regions. In: Geol. Soc. Am. Spec. Pap., 151, pp. 1–32.
Scholz, C.H., Campos, J., 1995. On the mechanism of seismic decoupling and back arc spreading at subduction zones. J. Geophys. Res. 100, 22103–22115.
Sclater, J.G., Hawkins, J.W., Mammerickz, J., Chase, C.G., 1972. Crustal extension between the Tonga and Lau ridges: petrologic and geophysical evidence. Bull. Geol. Soc. Am. 83, 505–518.
Sclater, J.G., Karig, D.E., Lawver, L.A., Louden, K., 1976. Heat flow, depth, and crustal thickness of the marginal basins of the south Philippine Sea. J. Geophys. Res. 81, 309–318.
Sclater, J.G., Jaupart, C., Galson, D., 1980. The heat flow through oceanic and continental crust and the heat loss of the Earth. Rev. Geophys. Space Phys. 18, 269–311.
Sdrolias, M., Mueller, R.D., 2006. Controls on back-arc basin formation. Geochem. Geophys. Geosyst. 7, Q04016. https://doi.org/10.1029/2005GC001090.
Sengör, C., Burke, K., 1978. Relative timing of rifting and volcanism on Earth and its tectonic implications. Geophys. Res. Lett. 5, 419–422.
Shapiro, N.M., Ritzwoller, M.H., 2004. Inferring surface heat flux distributions guided by a global seismic model: particular application to Antarctica. Earth Planet. Sci. Lett. 223, 213–224.
Shemenda, A.I., 1993. Subduction of the lithosphere and back-arc dynamics: insights from physical modeling. J. Geophys. Res. 98, 167–185.
Shen, W., Wiens, D.A., Lloyd, A.J., Nyblade, A.A., 2020. A geothermal heat flux map of Antarctica empirically constrained by seismic structure. Geophys. Res. Lett. 47 e2020GL086955.
Shillington, D.J., White, N., Minshull, T.A., Edwards, G.R.H., Jones, S.M., Edwards, R.A., Scott, C.L., 2008. Cenozoic evolution of the eastern Black Sea: a test of depth-dependent stretching models. Earth Planet. Sci. Lett. 265, 360–378.
Shor Jr., G.G., Kiri, H.K., Menard, H.W., 1971. Crustal structure of the Melanesian Area. J. Geophys. Res. 76, 2562–2577.
Shulgin, A., Artemieva, I.M., 2019. Thermochemical heterogeneity and density of continental and oceanic upper mantle in the European-North Atlantic region. J. Geophys. Res. Solid Earth 124. https://doi.org/10.1029/2018JB017025.
Shulgin, A., Faleide, J.I., Mjelde, R., Breivik, A., Huismans, R., 2020. Crustal domains in the western Barents Sea. Geophys. J. Int. 221 (3), 2155–2169.
Sibuet, J.C., Hsu, S.K., Shyu, C.T., Liu, C.S., 1995. Structural and kinematic evolutions of the Okinawa Trough backarc basin. In: Taylor, B. (Ed.), Backarc Basins. Springer, Boston, MA, pp. 343–379. https://doi.org/10.1007/978-1-4615-1843-3_9.
Simpson, R.W., Jachens, R.C., Blakely, R.J., Saltus, R.W., 1986. A new isostatic residual gravity map of the conterminous United States with a discussion on the significance of isostatic residual anomalies. J. Geophys. Res. 91, 8348–8410.
Skogseid, J., Planke, S., Faleide, J.I., et al., 2000. NE Atlantic continental rifting and volcanic margin formation. Geological Society, London, Sp. Publ. 167 (1), 295–326.
Sleep, N., Toksöz, M., 1971. Evolution of marginal basins. Nature 33, 548–550.
Small, C., 1994. A global analysis of mid-ocean ridge axial topography. Geophys. J. Int. 116, 64–84.
Snopek, K., Meier, T., Endrun, B., Bohnhoff, M., Casten, U., 2007. Comparison of gravimetric and seismic constraints on the structure of the Aegean lithosphere in the forearc of the Hellenic subduction zone in the area of Crete. J. Geodynam. https://doi.org/10.1016/j.jog.2007.03.005.
Solari, M.A., Hervé, F., Martinod, J., et al., 2008. Geotectonic evolution of the Bransfield Basin, Antarctic Peninsula: insights from analogue models. Antarct. Sci. 20, 185–196. https://doi.org/10.1017/S095410200800093X.
Sorokhtin, O.G. (Ed.), 1979. Oceanology - Geophysics of the ocean floor. Nauka, Moscow, v. 2, 375 pp. (in Russian).
Spakman, W., Hall, R., 2010. Surface deformation and slab–mantle interaction during Banda arc subduction rollback. Nature Geosci 3, 562–566. https://doi.org/10.1038/ngeo917.
Speed, R.C., Walker, J.A., 1991. Oceanic-crust of the Grenada Basin in the southern Lesser Antilles arc platform. J. Geophys. Res. 96, 3835–3851. https://doi.org/10.1029/90JB02558.
Stachnik, J.C., Abers, G.A., Christensen, D.H., 2004. Seismic attenuation and mantle wedge temperatures in the Alaska subduction zone. J. Geophys. Res. 109, B10. https://doi.org/10.1029/2004JB003018.
Starostenko, V., Buryanov, V., Makarenko, I., et al., 2004. Topography of the crust-mantle boundary beneath the Black Sea Basin. Tectonophysics 381, 211–233.
Stein, C.A., Stein, S., 1992. A model for the global variation in oceanic depth and heat-flow with lithospheric age. Nature 359, 123–129.
Stephenson, R., Schellart, W.P., 2010. The Black Sea back-arc basin: insights to its origin from geodynamic models of modern analogues. In: Sosson, M. (Ed.), Sedimentary Basin Tectonics from the Black Sea and Caucasus to the Arabian Platform. Geol. Soc., London, Sp. Publ., 340, pp. 11–21. https://doi.org/10.1144/SP340.2.
Stephenson, R., Stovba, S., 2021. Review of the main Black Sea rifting phase in the cretaceous and implications for the evolution of the Black Sea lithosphere. J Geodynamics 643, Art. No. 101891. https://doi.org/10.1016/j.jog.2021.101891.
Stern, R.J., 2002. Subduction zones. Rev. Geophys. 40 (4), 1012. https://doi.org/10.1029/2001RG000108.
Stern, R., Dickinson, W.R., 2010. The Gulf of Mexico is a Jurassic backarc basin. Geosphere 6, 739–754. https://doi.org/10.1130/GES00585.1.
Stern, R.J., Barth, G.A., Scheirer, D.S., Scholl, D.W., 2012. the Bering Sea Form as a Cenozoic Backarc Basin? AmGeophys. Union, Fall Meeting 2012. T54A-06.
Stern, R.J., Fouch, M.J., Klemperer, S., 2003. An overview of the Izu-Bonin-Mariana subduction factory. In: Eiler, J., Hirschmann, M. (Eds.), Inside the Subduction Factory: Am. Geophys. Union, Geophys. Monograph 138, pp. 175–222. https://doi.org/10.1029/138GM10.
Studinger, M., Bell, R.E., Finn, C.A., Blankenship, D.D., 2002. Mesozoic and Cenozoic extensional tectonics of the West Antarctic Rift system from high-resolution airborne geophysical mapping. Bull. R. Soc. N. Z. 35, 563–569.
Suyehiro, K., Takahashi, N., Ariie, Y., et al., 1996. Continental crust, crustal underplating, and low-Q Upper Mantle beneath an Oceanic Island Arc. Science 272 (5260), 390–392.
Sychev, P.M., Soinov, V.V., Veselov, O.V., Volkova, N.A., 1983. Heat flow and geodynamics of the transition zone from Asia to the North Pacific. In: Hilde, T.W.C., Uyeda, S. (Eds.), Geodynamics of the Western Pacific-Indonesian Region. Am. Geophys. Union, Geodyn. Ser., 11, pp. 237–247.
Syracuse, E.M., van Keken, P.E., Abers, G.A., 2010. The global range of subduction zone thermal models. Phys. Earth Planet. Inter. 183, 73–90.
Takahashi, N., Kodaira, S., Klemperer, S., et al., 2007. Crustal structure and evolution of the Mariana intra-oceanic island arc. Geology 35, 203–206. https://doi.org/10.1130/G23212A.
Takahashi, N., Kodaira, S., Tatsumi, Y., et al., 2009. Structural variations of arc crusts and rifted margins in the southern Izu-Ogasawara arc-back arc system. Geochem. Geophys. Geosyst. 10, Q09X08 https://doi.org/10.1029/2008GC002146.
Tamaki, K., 1986. Age estimation of the Japan Sea on the basis of stratigraphy, basement depth and heat flow data. J. Geomagn. Geoelectr. 38, 427–446.
Tamaki, K., 1995. Opening Tectonics of the Japan Sea. In: Taylor, B. (Ed.), Backarc Basins: Tectonics and Magmatism. Springer, New York, pp. 407–420.
Tapponnier, P., 1977. Evolution tectonique du système alpin en Méditerranée: Poinçonnement et écrasement rigide-plastique. Bull. Soc. Geol. Fr. 7 (3), 437–460.
Taylor, B. (Ed.), 1995. Backarc Basins: Tectonics and Magmatism. Springer Science + Business Media, New York, p. 524.
Taylor, B., 1979. Bismarck Sea: Evolution of a back-arc basin. Geology 7, 171–174.
Taylor, B., Goodliffe, A., Martinez, F., et al., 1995. Continental rifting and initial sea-floor spreading in the Woodlark basin. Nature 374, 534–537. https://doi.org/10.1038/374534a0.
Taylor, B., Huchon, P., 2002. Active continental extension in the western Woodlark Basin: a synthesis of Leg 180 results. In: Huchon, P., Taylor, B., Klaus, A. (Eds.), Proc. ODP, Sci. Results, 180. http://www-odp.tamu.edu/publications/180_SR/synth/synth.htm.
Taylor, B., Karner, G.D., 1983. On the evolution of marginal basins. Rev. Geophys. 21, 1727–1741.
Taylor, B., Martinez, F., 2003. Back-arc basin basalt systematics. Earth Planet. Sci. Lett. 210, 481–497. https://doi.org/10.1016/S0012-821X(03)00167-5.
Thomas, C., Livermore, R.A., Pollitz, F., 2003. Motion of the Scotia Sea Plates. Geophys. J. Intern. 155, 789–804.
Thybo, H., Artemieva, I.M., 2013. Moho and magmatic underplating in continental lithosphere. Tectonophysics 609, 605–619.
Thybo, H., Nielsen, C.A., 2009. Magma-compensated crustal thinning in continental rift zones. Nature 457, 873–876. https://doi.org/10.1038/nature07688.
Tirel, C., Gueydan, F., Tiberi, C., Brun, J.P., 2004. Aegean crustal thickness inferred from gravity inversion. Geodynamical implications. Earth Planet. Sci. Lett. 228, 267–280.
Tontini, F.C., Bassett, D., de Ronde, C.E.J., et al., 2019. Early evolution of a young back-arc basin in the Havre Trough. Nat. Geosci. 12, 856–862.
Tontini, F.C., Graziano, F., Cocchi, L., et al., 2007. Determining the optimal Bouguer density for a gravity data set: Implications for the isostatic setting of the Mediterranean Sea. Geophys. J. Int. 169, 380–388. https://doi.org/10.1111/j.1365-246X.2007.03340.x.
Trey, H., Cooper, A., Pellis, G., et al., 1999. Transect across the West Antarctic rift system in the Ross Sea, Antarctica. Tectonophysics 301, 61–74.
Tugolessov, D.A., Gorshkov, A.S., Meysner, L.B., Khakhalev, E.M., 1985. Tectonics of Mesozoic and Cenozoic deposits of the Black Sea Basin, Nedra. Moscow, 214 pp. (in Russian).
Turner, I.M., Peirce, C., Sinha, M.C., 1999. Seismic imaging of the axial region of the Valu Fa Ridge, Lau Basin - the accretionary processes of an intermediate back-arc spreading ridge. Geophys. J. Int. 138, 495–519.
Uyeda, S., 1986. Facts, ideas and open problems on trench-arc-backarc systems. In: Wezel, F.C. (Ed.), The Origin of Arc. Elsevier, Amsterdam, pp. 435–460.
Uyeda, S., Kanamori, H., 1979. Back-arc opening and the mode of subduction. J. Geophys. Res. 84, 1049–1061.
Vaes, B., van Hinsbergen, D.J.J., Boschman, L.M., 2019. Reconstruction of subduction and back-arc spreading in the NW Pacific and Aleutian Basin: clues to causes of cretaceous and Eocene plate reorganizations. Tectonics 38, 1367–1413.
Valyashko, G., Chernyavsky, G., Seliverstov, N., Ivanenko, A., 1993. Back-arc spreading in the Komandorsky Basin. Doklady Russian Acad. Sci. 338, 212–216.
Van Horne, A., Sato, H., Ishiyama, T., 2017. Evolution of the Sea of Japan back-arc and some unsolved issues. Tectonophysics 710–711, 6–20.
Van Keken, P.E., Kiefer, B., Peacock, S.M., 2002. High-resolution models of subduction zones: implications for mineral dehydration reactions and the transport of water into the deep mantle. Geochem. Geophys. Geosyst. 3, 1056. https://doi.org/10.1029/2001GC000256.
Volvovsky, I.S., Volvovsky, B.S., 1975. Cross-sections of the earth's crust in the territory of the USSR based on deep seismic sounding data. Moscow, Sovetskoe Radio 268 pp (in Russian).
Wada, I., He, J., Hasegawa, A., Nakajima, J., 2015. Mantle wedge flow pattern and thermal structure in Northeast Japan: effects of oblique subduction and 3-D slab geometry. Earth Planet. Sci. Lett. 426, 76–88.
Wang, T.K., Chen, M.K., Lee, C.S., Xia, K.Y., 2006. Seismic imaging of the transitional crust across the northeastern margin of the South China Sea. Tectonophysics 412, 237–254.

Watanabe, T., Langseth, M.G., Arcs, Island, Trenches, Deep Sea, Anderson, R.N., 1977. Heat flow in back-arc basins of the western Pacific. In: Talwani, M., Pittman III, W.P. (Eds.), Back-Arc Basins. AGU Maurice Ewing Series, vol. 1, pp. 137–161.
Wei, S.S., Wiens, D.A., 2020. High bulk and shear attenuation due to partial melt in the Tonga-Lau back-arc mantle. J. Geophys. Res. 125 (1), 2019JB017527.
Weigelt, E., Jokat, W., 2001. Peculiarities of roughness and thickness of oceanic crust in the Eurasian Basin, Arctic Ocean. GeophysicalJ. Int. 145, 505–516.
Weissel, J.K., 1980. Evidence for Eocene oceanic crust in the Celebes Basin. In: Hayes, D. E. (Ed.), The Tectonic and Geologic Evolution of Southeast Asian Seas and Islands. American Geophysical Union Geophys. Monog. Ser., 23, pp. 37–47.
Werner, R., Baranov, B., Hoernle, K., et al., 2020. Discovery of Ancient Volcanoes in the Okhotsk Sea (Russia): new constraints on the opening history of the Kurile Back Arc Basin. Geosciences 10, 442. https://doi.org/10.3390/geosciences10110442.
White, R.S., McKenzie, D., O'Nions, R.K., 1992. Oceanic crustal thickness from seismic measurements and rare-earth element inversions. J. Geophys. Res. 97, 19683–19715. https://doi.org/10.1029/92JB01749.
White, R.S., Smith, L.K., Roberts, A.W., Christie, P.A.F., Kusznir, N.J., 2008. Lower-crustal intrusion on the North Atlantic continental margin. Nature 452, 460–465.
White, W.M., Klein, E.M., 2014. Composition of the Oceanic Crust. In: Holland, H.D., Turekian, K.K. (Eds.), Treatise on Geochemistry, (Second Edition), v. 4. Elsevier, pp. 457–496. https://doi.org/10.1016/B978-0-08-095975-7.00315-6.
Wilson, M., 2007. Igneous Petrogenesis. Springer, 466 pp.
Wilson, T.J., Bevis, M., Konfal, S., et al., 2015. Understanding glacial isostatic adjustment and ice mass change in Antarctica using integrated GPS and seismology observations. Eur. Geophys. Union Annu. Meet. Suppl. 2015EGUGA.17.7762W.
Winberry, P., Anandakrishnan, S., 2004. Crustal structure of the West Antarctic rift system and Marie Byrd Land hotspot. Geology 32, 977–980. https://doi.org/10.1130/G20768.1.
Wirth, E.A., Korenaga, J., 2012. Small-scale convection in the subduction zone mantle wedge. Earth Planet. Sci. Lett. 357–358, 111–118.
Woodhead, J., Eggins, S., Gamble, J., 1993. High field strength and transition element systematics in island arc and back-arc basin basalts: evidence for multi-phase melt extraction and a depleted mantle wedge. Earth Planet. Sci. Lett. 114, 491–504.
Wright, I., 1993. Pre-spread rifting and heterogeneous volcanism in the Southern Havre Trough back-arc basin. Mar. Geol. 113, 179–200.
Yamazaki, T., Yuasa, M., 1998. Possible Miocene rifting of the Izu-Ogasawara (Bonin) arc deduced from magnetic anomalies. Island Arc 7, 374–382. https://doi.org/10.1111/j.1440-1738.1998.00196.x.
Yan, Q., Shi, X., Yuan, L., Liu, Z., 2022. Tectono-magmatic evolution of the Philippine Sea Plate: a review. Geosyst. Geoenviron. 1 (2), 100018 https://doi.org/10.1016/j.geogeo.2021.100018.
Yang, T.F., Lee, T., Chen, C.H., et al., 1996. A double island arc between Taiwan and Luzon: consequence of ridge subduction. Tectonophysics 258, 85–101.
Yanshin, A.L., Bassenyants, Sh.A., Pilipenko, A.I., Shlezinger, A.E., 1980. New data on the time of formation of the Black Sea deep basin. Dokl. Akad. Nauk SSSR 252 (l), 223–227 (in Russian).
Yegorova, T., Gobarenko, V., 2010. Structure of the Earth's crust and upper mantle of the West-and East-Black Sea Basins revealed from geophysical data and its tectonic implications. Geol. Soc., London, Sp. Publ. 340 (1), 23–42. https://doi.org/10.1144/SP340.3.
Zelt, B.C., Taylor, B., Goodliffe, A., 2001. 3-D crustal velocity structure at the rift tip in the western Woodlark Basin. Geophys. Res. Lett. 28, 3015–3018.
Zhao, M.H., Du, F., Wang, Q., et al., 2018. Current status and challenges for three-dimensional deep seismic survey in the South China Sea. Earth Sci. 43 (10), 3749–3761 (in Chinese with English abstract).
Zhao, M.H., Qiu, X.L., Xia, S.H., et al., 2010. Seismic structure in the northeastern South China Sea: S-wave velocity and Vp/Vs ratios derived from three-component OBS data. Tectonophysics 480, 183–197.
Zhu, L., Mitchell, B.J., Akyol, N., et al., 2006. Crustal thickness variations in the Aegean region and implications for the extension of continental crust. J. Geophys. Res. 111, B01301. https://doi.org/10.1029/2005JB003770.
Zonenshain, L.P., Le Pichon, X., 1986. Deep basins of the Black Sea and Caspian Sea as remnants of Mesozoic back-arc basins. Tectonophysics 123, 181–211.